Vol. 69 • No. 3

March 2026

Microwave Journal

WARNING

RF TEST & MEASUREMENT IN PROGRESS

DO NOT ENTER

SPECIAL FOCUS:
Cables & Connectors

horizon house®

Founded in 1958

mwjournal.com

MILLER MMIC

Advancing RFIC Design Through Human-AI collaboration and competition

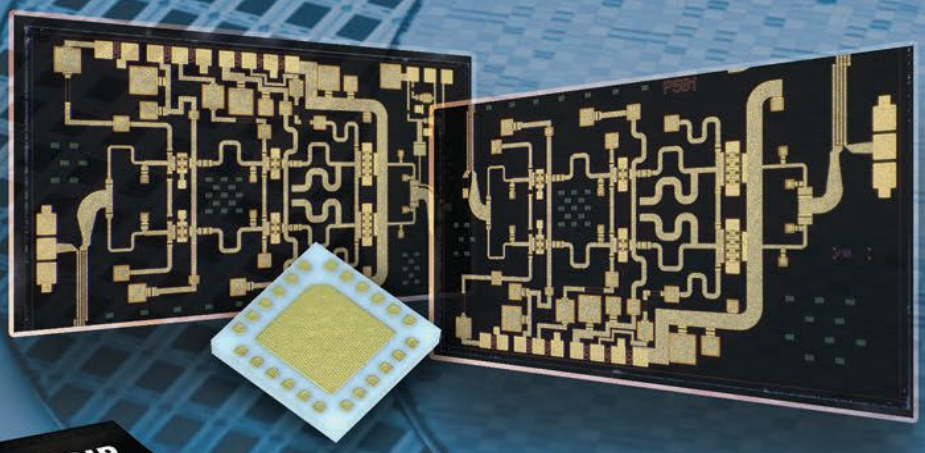

Miller MMIC is a global provider of RF semiconductor solutions with expertise in GaAs and GaN processes. We offer a diverse range of products tailored to various wireless applications. Our product lineup encompasses a wide array of offerings, including Low Noise Amplifiers, Distributed Amplifiers, Power Amplifiers, Driver Amplifiers, RF Switches, RF PIN Diode Switches, and numerous other voltage- and digitally-controllable RF components.

QFN and SiP (System-In-Package) available

RF Distributed Low Noise Amplifiers

PN	Freq Low (GHz)	Freq High (GHz)	Gain (dB)	NF(dB)	P1dB (dBm)	Voltage (VDC)	Current (mA)	Package
MMW001T	DC	20.0	17~19	1~3.5	23 @ 10GHz	8.0	145	die
MMW4FP	DC	50.00	16.00	4.00	24.00	10	200	die
MMW507	0.20	22.0	14.0	4 - 6	28.0	10.0	350	die
MMW508	DC	30.0	14.0	2.5dB @ 15GHz	24.5	10.0	200	die
MMW509	30KHz	45.0	15.0		20.0	6.0	190	die
MMW510	DC	45.0	11.0	4.5	15.5	6.0	100	die
MMW510F	DC	30.00	20.00	2.50	22.00			die
MMW511	0.04	65.0	10.0	9.0	18.0	8.0	250	die
MMW512	DC	65.0	10.0	5.0	14.5	4.5	85	die
MMW5FN	DC	67.00	14.00	2.00	19.00	4.5	81	die
MMW5FP	DC	67.00	14.00	4.00	21.00	8	140	die
MMW011	DC	12.0	14.0		30.5	12.0	350	die

Low Noise Amplifiers

PN	Freq Low (GHz)	Freq High (GHz)	Gain (dB)	NF(dB)	P1dB (dBm)	Voltage (VDC)	Current (mA)	Package
MML040	6.0	18.0	24.0	1.5	14.0	5.0	35	die
MML058	1.0	18.0	15.0	1.7	17.0	5.0	35	die
MML063	18.0	40.0	11.0	2.9	15.0	5.0	52	die
MML080	0.8	18.0	16.5/15.5	1.9/1.7	18/17.5	5.0	65/40	die
MML081	2.0	18.0	25/23	1.0/1.0	16/9.5	5.0	37/24	die
MML083	0.1	20.0	23.0	1.6	11.0	5.0	58	die

RF Driver Amplifier

PN	Freq Low (GHz)	Freq High (GHz)	Gain (dB)	NF(dB)	P1dB (dBm)	Voltage (VDC)	Current (mA)	Package
MM3006	2.0	20.0	19.5	2.5	22.0	7.0	130	die
MM3014	6.0	20.0	15.0	-	19.5	5.0	107	die
MM3017T	17.0	43.0	25.0		22.0	5.0	140	die
MM3031T	20.0	43.0	20.0		24.0	5.0	480	die
MM3051	17.0	24.0	25.0	-	25.0	5.0	220	die
MM3058	18.0	40.0	20/19.5	2.5/2.3	16/14	5/4	69/52	die
MM3059	18.0	40.0	16/16	2.5/2.3	16/15	5/4	67/50	die

GaAs Medium Power Amplifier

PN	Freq Low (GHz)	Freq High (GHz)	Gain (dB)	P1dB (dBm)	Psat (dBm)	Voltage (VDC)	Current (mA)	Package
MMP107	17.0	21.0	19.0	30.0	30.0	6.0	400	die
MMP108	18.0	28.0	14.0	31.5	31.0	6.0	650	die
MMP111	26.0	34.0	25.5	33.5	33.5	6.0	1300	die
MMP112	2.0	6.0	20.0	31.5	32.0	8.0	365	die
MMP501	20.0	44.0	15.0	27 -- 32	29 - 34	5.0	1200	die
MMP502	18.0	47.0	14.0	28.0	30.0	5.0	1500	die

PN: MMW5FP

RF GaAs MMIC DC-67GHz

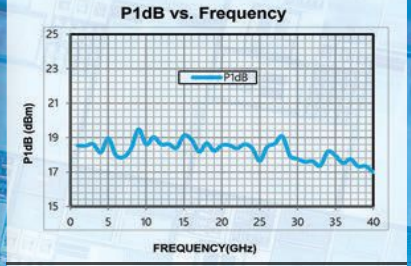

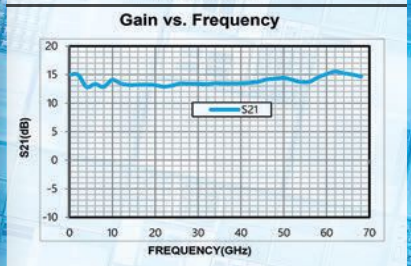

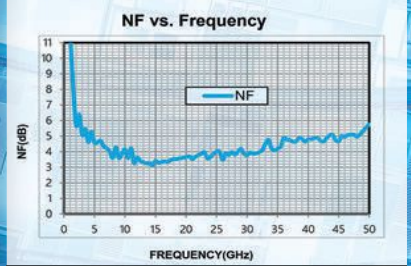

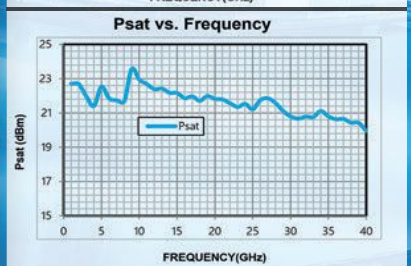

CALL US 1-833-2MILLER(264-5537)
WWW.MILLERMMIC.COM

MILLER MMIC

sales@millermmic.com
support@millermmic.com

ADVANCED TECHNOLOGY & INNOVATIVE SOLUTIONS FOR MISSION CRITICAL APPLICATIONS

DORADO JQL FERROCOM

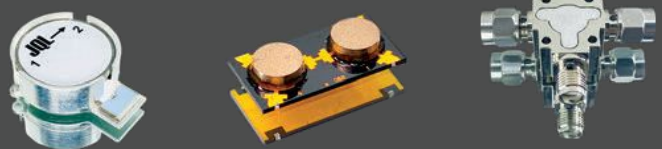

ISOLATORS & CIRCULATORS

SURFACE MOUNT, MICROSTRIP, DROP-IN, COAXIAL & WAVEGUIDES

EMS

DESIGN & ASSEMBLY OF ELECTRONIC BOARDS

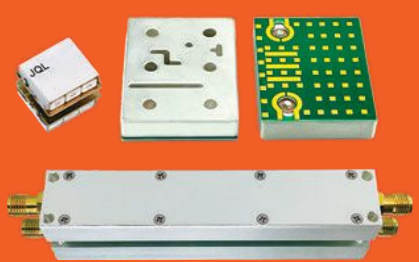

FILTERS & MULTIPLEXERS

**CERAMIC,
CERAMIC WAVEGUIDE,
CAVITY & DISCRETE**

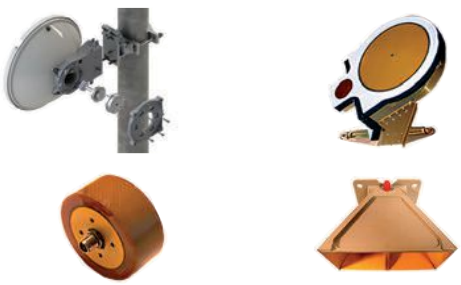

ANTENNA

**MICROWAVE ANTENNA:
SINGLE & DUAL POLARIZATION, 6 TO 80 GHZ**

**SPIRAL, HORN & BICONICAL ANTENNA:
500 MHZ TO 40 GHZ**

MADE IN USA

+1-(888) 236-9828 (US)
+1-(630) 246-7833 (INTL)

FOR MORE PRODUCT INFORMATION
GET IN TOUCH WITH US

US Operations
1255 Armour Blvd.,
Mundelein, IL 60060
USA

JQLTECHNOLOGIES.COM
DORADO-INTL.COM
FERROCOMRF.COM
SALES@JQLTECHNOLOGIES.COM

European Operations
Via Palazetti, 22
40068 San Lazzaro di Savena BO
ITALY

DC TO 50 GHz

MMIC Amplifiers

300+ Models Designed in House

- Wide selection of GaAs HBT and E-pHEMT designs
- Noise figure as low as 0.38 dB
- OIP3 up to +50 dBm
- Industry-leading phase noise performance
- In-house packaging assembly
- Surface mount and bare die formats
- Upscreening available

LEARN MORE

Options for Every Requirement

CATV (75Ω)

Supporting DOCSIS® 3.1 and 4.0 requirements

Dual Matched

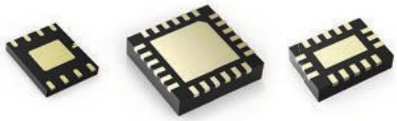

Save space in balanced and push-pull configurations

Hi-Rel

Rugged ceramic package meets MIL requirements for harsh operating conditions

High Linearity

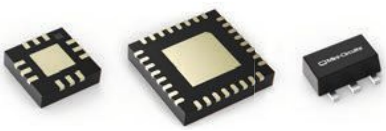

High dynamic range over wide bandwidths up to 45 GHz

Low Noise

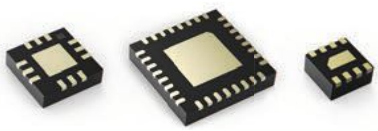

NF as low as 0.38 dB for sensitive receiver applications

Low Additive Phase Noise

As low as -173 dBc/Hz @ 10 kHz offset

RF Transistors

<1 dB NF with footprints as small as 1.18 x 1.42mm

Variable Gain

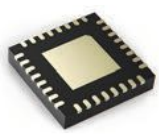

Up to 31.5 dB digital gain control

Wideband Gain Blocks

Flat gain for broadband and multi-band use

Mini-Circuits®

RF-LAMBDA

THE LEADER OF RF BROADBAND SOLUTIONS

BROADBAND SSPA / EMC BENCHTOP

SOLID STATE POWER AMPLIFIER

0.1-22GHZ ULTRA BROADBAND SSPA

RFLUPA01M22GA
4W 0.1-22GHZ

RFLUPA0218GB
20W 1-19GHZ

MADE IN USA

0.1-6GHZ VHZ, UHF, L, S, C BAND

RFLUPA02G06GC
100W 2-6GHZ

RFLUPA0706GD
30W 0.7-6GHZ

6-18GHZ C, X, KU BAND

RFLUPA08G11GA
50W 8-11GHZ

RFLUPA0618GD
60W 6-18GHZ

RFLUPA06G12GB
25W 6-12GHZ

18-50GHZ K, KA, V BAND

RFLUPA18G47GC
2W 18-47GHZ

RFLUPA27G34GB
15W 27-34GHZ

RFLUPA47G53GA2
10W 47-53GHZ

RFLUPA27G34GB
30W 18-40GHZ

BENCHTOP RF MICROWAVE SYSTEM POWER AMPLIFIER

REMC02G06GE
600W 2-6GHZ

REMC18G40GC2
40W 18-40GHZ

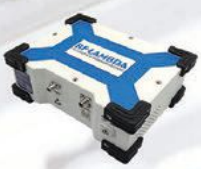

RAMP30G65GG
8W 30-65GHZ

RAMP06G18GA
10W 6-18GHZ

RAMP00M65GA
DC-65GHZ

www.rflambda.com 1-888-976-8880 San Diego, CA, US Ottawa, ONT, Canada
sales@rflambda.com 1-972-767-5998 Carrollton, TX, US Frankfurt, Germany

WE STAND AMONG GIANTS

Innovation that cuts giants down to size.

Miniature. Modular. Intelligent.

SPECTRUM CONTROL™

spectrumcontrol.com/sci-blocks

Power that has stood the test of time

For over 50 years, Infineon IR HiRel has made history by powering countless space missions that continue to unlock the secrets of our universe.

At the core of our success is our diverse portfolio of industry-leading radiation hardened MOSFETs. From our R4 and R5 generations that continue to power Voyager 1 for over 48 years to our new R9 superjunction MOSFETs that will support the next generation of history making missions like Artemis 2 and beyond.

Explore our extensive portfolio of rad hard MOSFETS, which include N-channel (20V to 650V) and P-channel (-30V to -200V) product options available in hermetic and plastic packages.

You can design with complete confidence, knowing you are using the best radiation hardened MOSFETs designed, manufactured and tested to the highest industry standards possible and backed by a global technology leader.

www.infineon.com/hirel

Rad hard power MOSFET technologies

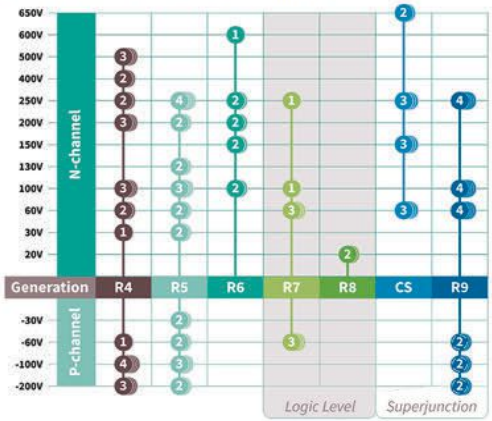

IOR HiRel
An Infineon Technologies Company

PMI
PLANAR MONOLITHICS

Components & Modules

to 70 GHz

- Modern hybrid MIC/MMIC design
- 4,500+ Hi-Rel Commercial, Off-the-shelf (COTS) Models
- Industry-leading customer and applications support
- Form, fit, function and custom package designs
- Hermetic sealing, military or aerospace screening

Planar Monolithics (PMI) designs and manufactures a full range of solutions for your most demanding RF and Microwave challenges.

Get a complete list of our components and module portfolio, available options, and download product features and other technical data at **pmi-rf.com**

Or contact us at **1-877-752-6271** or **sales@pmi-rf.com**

CORRY MICRONICS

Elevating the Brand. Keeping the Legacy.

Obsolete Filters?

We cross reference.

Match. Modify. Manufacture.

CONTACT US

corrymicronics.com

Microwave Journal
CONTENTS

March 2026
Vol. 69 • No. 3
Test & Measurement
+ Cable & Connectors
mwjournal.com

Time Travel

Cover Feature

Technical Features

SPECIAL FOCUS: Cables & Connectors 81

RapidRF

World's 1st AI Driven RFIC DESIGN PLATFORM

A PUSH-BUTTON GDS TAPE-OUT READY SOLUTION

END APPLICATIONS CUSTOMERS

PERFORMANCE-DRIVEN FOCUS
EXPANDED DESIGN CHOICES
ENHANCED SECURITY AND CONFIDENTIALITY
REDUCED DEPENDENCE ON IC VENDORS
SIGNIFICANT COST SAVINGS

SEMICONDUCTOR COMPANIES

HUGE DESIGN COST REDUCTION
TAILORED TO CUSTOMER NEEDS
100X, 1000X FASTER
SUCCESSFUL RATE INCREASE

RapidRF

TRULY ENABLES A "DIRECT INTERACTION" MODEL FOR THE RFIC INDUSTRY ACROSS EVERY SECTOR.

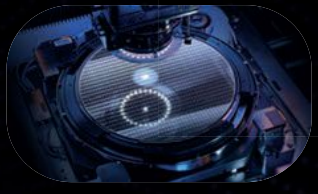

FOUNDRIES

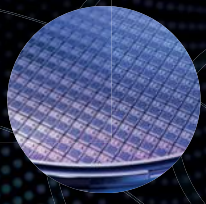

HIGHER REVENUE GREATER DESIGN VOLUME
EXPANDED CUSTOMER BASE LOWERING DESIGN ENTRY BARRIERS
ACCELERATED PRODUCT ITERATION

SIMPLE 3 STEPS

- LOGIN WWW.RAPIDRF.AI
- ENTER DESIGN TARGET
- PRESS "GENERATE"

A TAPE-OUT-READY GDS FILE WILL BE GENERATED AND **AVAILABLE FOR DOWNLOAD.**

Microwave Journal

CONTENTS

mwjournal.com

Product Features

Tech Brief

Departments

Microwave Journal (USPS 396-250) (ISSN 0192-6225) is published monthly by Horizon House Publications Inc., 685 Canton St., Norwood, MA 02062. Periodicals postage paid at Norwood, MA 02062 and additional mailing offices.

POSTMASTER: Email address corrections to mwj@e-circ.net.com. Subscription information: (978) 671-0446. This journal is issued without charge upon written request to qualified persons working in the RF & microwave industry. Other subscriptions are: domestic, $130.00 per year, two-year subscriptions, $200.00; foreign, $225.00 per year, two-year subscriptions, $400.00; back issues (if available) and single copies, $20.00 domestic and $30.00 foreign. Claims for missing issues must be filed within 90 days of date of issue for complimentary replacement.

Posted under Canadian international publications mail agreement #PM40612608

STAFF

EXECUTIVE EDITORIAL OFFICE
685 Canton Street, Norwood, MA 02062
Tel: (781) 769-9750
FAX: (781) 769-5037
e-mail: mwj@mwjournal.com

EUROPEAN EDITORIAL OFFICE
16 Sussex Street, London SW1V 4RW, England
Tel: Editorial: +44 207 596 8730 Sales: +44 207 596 8740
FAX: +44 207 596 8749

SUBSCRIPTION SERVICES
Send subscription inquiries and address changes to:
Tel: (978) 671-0446
e-mail: mwj@e-circ.net

www.mwjournal.com

Printed in the USA

From Introduction to Production

RFMW®

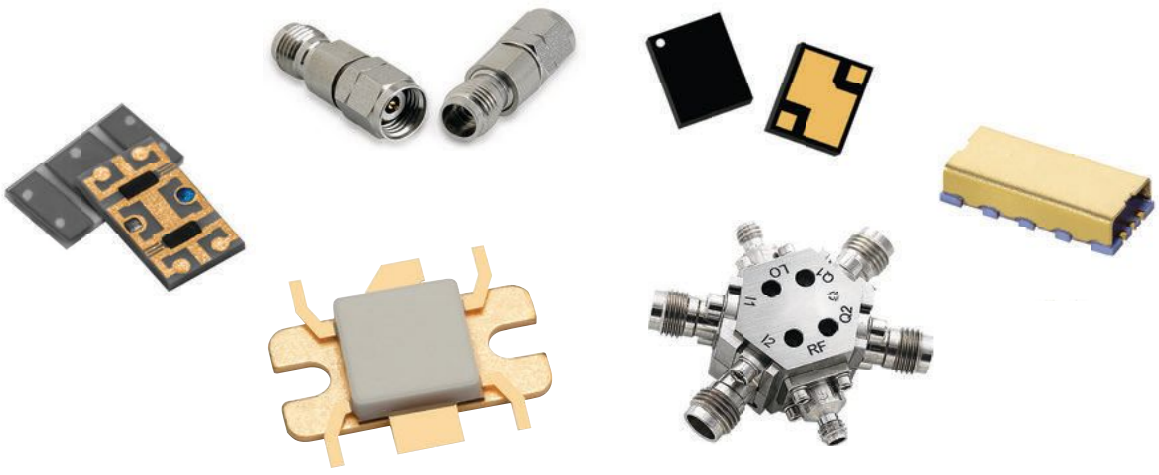

Highly Skilled, Experienced, Technical Sales

World-leading Manufacturers of RF, Microwave, and Power
Best-in-class Logistics and Supply Chain Solutions

Amplifiers | Antennas | Attenuators | Beamformers | Cable Assemblies | Couplers
Combiners & Splitters | Diodes | Filters | Interconnect | Mixers | MMICs & RFICs
Resistors & Terminations | Switches | Test & Measurement | Transistors | Oscillators & Timing

Ask the Experts
www.RFMW.com

Sales@RFMW.com | Toll Free: +1-877-367-7369
188 Martinvale Lane, San Jose, CA 95119 U.S.A.

Microwave Journal ONLINE .COM

LEARNING CENTER

Webinars
Practical insights from industry leaders

White Papers
New technologies, design and test techniques

eBooks
Curated technical articles and design guidance

Looking for a specific RF or microwave topic?

Need a quick refresher on a design challenge?

Our AI-powered search tool helps you quickly find relevant articles, technical resources and industry insights from our trusted database. Simply type your question or topic in natural language and get results in seconds. Use it to:

- Research technologies and applications
- Explore past technical articles
- Find solutions and design insights faster
- Discover content you may have missed

Alan Mond, President and CEO of **East Coast Microwave**, shares his professional journey to ECM, his solutions to the hardships brought by the changing economy and his keys to a successful RF distribution company.

Executive Interview

Join Us Online

Follow us @Pathindle @MWJEditor

Join us at the RF and Microwave Community

Become a fan at facebook.com/microwavejournal

Microwave Journal podcasts include the RF/microwave update series, Frequency Matters, plus interviews with industry experts and executives.

Catch *Frequency Matters*, the industry update from *Microwave Journal*, microwavejournal.com/FrequencyMatters

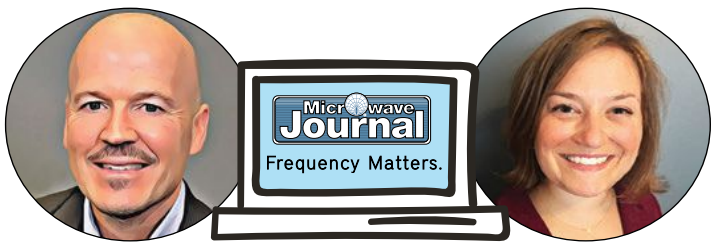

Visit us @ mwjournal.com

ENGINEERED FOR EXCELLENCE, PROVEN BY PERFORMANCE

LC • CERAMIC • CAVITY • PRINTED • MULTIPLEXERS • SWITCHED FILTER BANKS • MULTI-FUNCTION ASSEMBLIES

3H Comunication Systems offers high quality, cost-effective solutions for RF and microwave filter products and other front-end solutions for multiple markets including military defense, commercial, public safety, aerospace and medical industries - all with a 5-year warranty.

3H Communication Systems

AS9100 & ISO9001:2015 CERTIFIED

949.529.1583 | sales@3hcomm.com

3HCommunicationSystems.com

LOVE AT FIRST SPEC

Not Flowers

When Compatibility Really Matters, Choose the Perfect Cable

LEARN MORE

Key Features

- 400+ models in stock (custom lengths & configurations available)
- Cable construction options from jumpers to VNA cables & more
- Wide range of connector types, genders, orientations and mounts
- Rugged construction for high reliability & long life

Mini-Circuits

MARK YOUR CALENDAR

STAY CONNECTED TO COMING EVENTS

MARCH

23-26
Satellite x GovMilSpace
Washington, DC
www.SATShow.com

24-26
EMV
Cologne, Germany
https://emv.mesago.com

25-26
FutureG for Defense Summit
Washington, DC
https://futureg.dsigroup.org/

APRIL

13-16
IEEE WCNC
Kuala Lumpur, Malaysia
https://wcnc2026.ieee-wcnc.org

15-16
IEEE Texas Symposium
Waco, Texas
https://texassymposium.org/

19-24
EuCAP
Dublin, Ireland
www.eucap2026.org

20-21
IEEE WAMICON
Clearwater, Fla.
www.ieeewamicon.org

20-22
IC-MAM
Barcelona, Spain
https://icmam-ieee.org

20-22
CS International
Brussels, Belgium
https://csinternational.net

20-22
PIC International
Brussels, Belgium
https://picinternational.net

MAY

5-7
Sensors Converge
Santa Clara, Calif.
www.sensorsconverge.com

11-15
2026 IEEE Radar Conference
Phoenix, Ariz.
https://2026.ieee-radarconf.org/

18-21
CS Mantech
Portland, Ore.
https://csmantech.org

19-21
AOC Europe
Helsinki, Finland
www.aoceurope.org/

Call for Papers Deadlines

3/27
EuMW

5/1
IEEE RFID-TA 2026

FOR DETAILS VISIT MWJOURNAL.COM/EVENTS

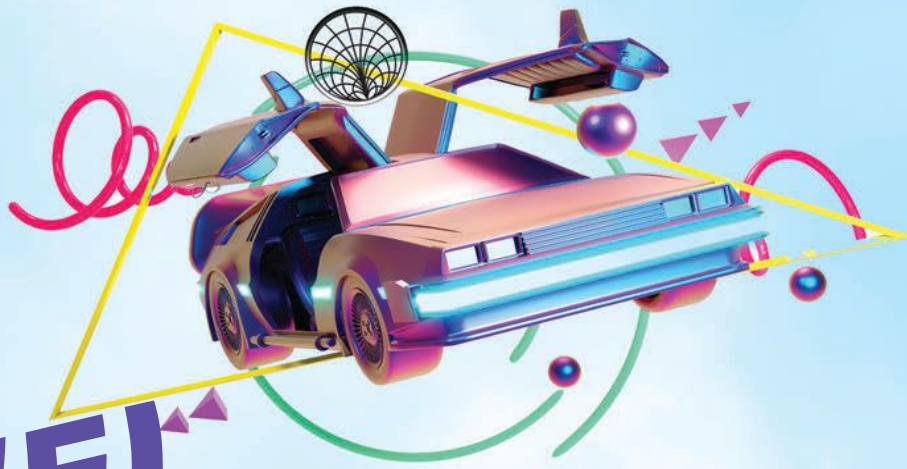

TIME TRAVEL

Stefano Selleri and Massimo Mazzoni
University of Florence, Florence, Italy

Diamonds Are (Not) Forever*

The RF and microwave community is well acquainted with the work of Michael Faraday (1791-1867) on electricity and magnetism and, most famously, with his discovery of induction in 1831. It is less well known, however, that he also contributed to chemistry, a field that was his first interest. Notably, in his late years, he gave a series of elementary lectures still enchanting today.[1] These became renowned as the "Christmas Lectures," very appropriate for Londoners' eagerness to learn about applied science when popular scientific outreach did not yet exist.

In his early years, Faraday attracted the attention of Sir Humphry Davy (1778-1829), the famous chemist and director of the Royal Institution, which supported carrying out public scientific experiments. Davy chose Faraday as an assistant in 1813, and in the same year, a 22-year-old Faraday left England with Davy, enrolled both as an assistant and a valet for a "Grand Tour" in Europe, which eventually lasted to 1815.[2]

In Florence, Faraday and Davy used a large lens pair, the "Bregans lenses," owned by the Grand Duke of Tuscany and currently exhibited at the Science Museum in Florence,[3] to set up an experiment. In the experiment, a diamond was stored in a glass enclosure with pure oxygen and ignited via concentrated solar rays. No ashes were left, and among the gases, only carbon dioxide was present, proving that no other elements were present in the diamond.

Scientists long knew diamonds could be burned; that same lens had been used by two Florentine experimentalists, Averani and Targioni, from 1694 to 1695, trying to burn various gemstones. They burned diamonds but could not determine their composition. In contrast, Davy's careful setup proved the composition, and a young Faraday learned in his youth from Davy how to devise accurate and inarguable experiments. He then mastered this art and became one of the greatest experimental physicists in the following years.

On November 14, 2025, to celebrate the two hundredth anniversary of Faraday's visit to Florence, the experiment was repeated in Florence in front of a vast audience in the chemistry laboratories of the National Research Council.

This modern-day celebration of fundamental scientific discoveries reminds us that RF and microwave technology is not a standalone field, but a convergence of applications of foundational scientific principles.

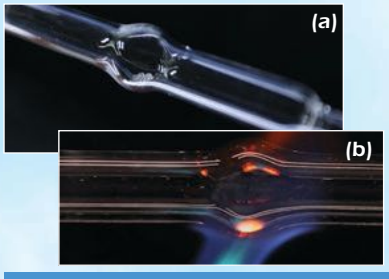

(a) The diamond fragments in the quartz tube and (b) the same fragments glowing, in a flux of pure oxygen, as they are almost completely combusted.

The gas, flowing from right to left in the image, reacts with the heated diamonds and the resulting carbon dioxide is revealed by reaction with the barium hydroxide in the two middle flasks.

References

*Read the title on the notes "Diamonds are Forever," 1971, music: John Barry, lyrics: Don Black, voice: Shirley Bassey

1. M. Faraday, Chemical History of a Candle, London: Griffin, Bohn & Co., 1861.
2. G. Pelosi and S. Selleri, "Michael Faraday and James Clerk Maxwell: The Florentine days," Il Colle di Galileo, 9(2), 2020, pp. 27-37, Online DOI: 10.36253/cdg-12062.
3. "Chemical "Affinities," Museo Galileo - Institute and Museum of the History of Science, https://catalogo.museogalileo.it/oggetto/Lente.html.

VECTOR NETWORK ANALYZER EXTENSION MODULES (VNAX)

- Banded modules from WR-28 (26-40 GHz) to WM-164 (1.1-1.5 THz)
- High Test Port Power (+13dBm at WR-6.5, +1dBm at WR-3.4)
- High Dynamic Range (120dB typical for most bands)
- Dual Source option (for IMD measurements) available
- Small form factor
- Higher power modules are available upon request

SPECTRUM ANALYZER EXTENSION MODULES (SAX)

- Banded modules from WR-28 (26-40 GHz) to WM-164 (1.1-1.5 THz)
- High Sensitivity (-150dBm/Hz DANL for most bands)
- Low Conversion Loss
- High IF Bandwidth for Block Down-Conversion (up to 40 GHz)
- Up-Conversion option available
- Small form factor

SIGNAL GENERATOR EXTENSION MODULES (SGX)

- Banded modules from WR-28 (26-40 GHz) to WM-164 (1.1-1.5 THz)
- High Test Port Power (+18dBm at WR6.5, +6dBm at WR-3.4)
- Small form factor

COMPACT CONVERTERS (CCU/CCD)

- Banded modules from WR-19 (40-60 GHz) to WM-570 (330-500 GHz)
- For wideband up-conversion and down-conversion
- Low conversion loss
- High P1dB
- External filters and amplifiers available
- Small form factor

mmWave & THz solutions

VIRGINIA DIODES

Virginia Diodes, Inc.
979 2nd St. SE, Suite 309
Charlottesville, VA 22902
434.297.3257
vadiodes.com

Why the Future of High-Power Test Benches Must Be Fully Integrated and Automated

Florian Pivit
Milexia, Heilbronn, Germany

Jaafar Saied
Milexia, Saint-Aubin, France

The business of testing and measuring is stepping up a gear. Today's digitally-driven global economy expects high levels of performance and accuracy from its technology. This has helped to drive record growth in the test and measurement (T&M) market, valued at USD 34.11 billion in 2024 and set to reach USD 43.95 billion by 2030, according to Grand View Research.

The need for reliable testing is now paramount in a number of different industries. From aerospace electronics to modern defence systems, from communications infrastructure to energy and medicine, a low tolerance for failure requires testing and measurement that can function powerfully and at scale. What all these verticals have in common is that a single undetected technical weakness can escalate into expensive operational downtime, failed regulatory compliance and life-threatening disaster.

T&M is not just in hot demand; it is also clearly evolving to meet modern needs. Tools such as high-power RF and microwave test benches are still used, but these are now being transformed to work in a more automated and integrated fashion. Integrated test facilities are not new; they have existed for years in defence laboratories and aerospace qualification centres. But what were once bespoke, static installations are being replaced by software-driven platforms that combine high-power capabilities with automation, analytics and lifecycle traceability.

FROM HARDWARE-CENTRIC TO SOFTWARE-DEFINED

Testing of infrastructure in sectors such as telecom networks and energy has historically relied heavily on rigid modelling and operational monitoring within decentralised systems. Networks were designed to tolerate faults through redundancy, with distributed elements continuously evaluating abnormal conditions and rerouting traffic when required. In the energy sector, as renewable sources such as wind and solar were connected to the grid, ensuring stability became a distributed problem.

These instances reveal a common lesson: as systems decentralise and integrate, testing must anticipate interaction effects, not just component-level performance. In both cases, there has been a need to scale back reliance on early integrated test benches with their hardware-centric design.

This design has several limitations:

- **Rigidity:** Benches were designed for specific programmes and were difficult to adapt as requirements changed.
- **Limited scalability:** Approaches suitable for qualification testing did not translate easily to pro-

The only QPL Certified **MECHANICAL SWITCH** House!

Quick Turn **RF FILTER** Prototypes are in our DNA!

Huge Library of **PASSIVES** with Best in Show **HIGH POWER COUPLER** offering!

RUGGED & RELIABLE

AGILE & ADAPTIVE

HIGH POWER & VARIETY

RF MECHANICAL SWITCHES, RF FILTERS & RF PASSIVES

AS9100 CERTIFIED, MADE IN USA

High Performance Precision Microwave Components
Serving the world-wide aerospace & defense community since 1959

Robust Catalog Portfolio - no hassle, quick turn, custom solutions our specialty

RLC Electronics | 83 Radio Circle, Mt. Kisco, NY 10549 | 914-241-1334 | sales@rlcelectronics.com | www.rlcelectronics.com

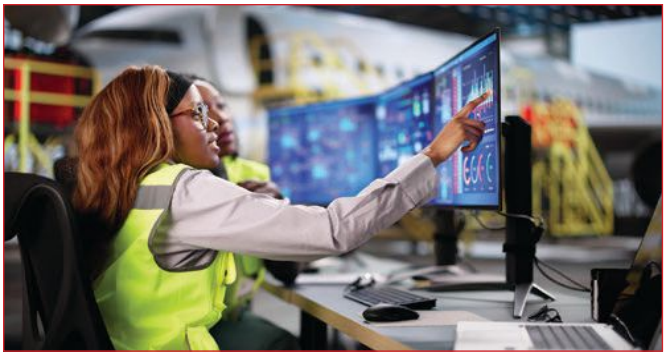

Fig. 1 **Aircraft mechanics performing safety checks.** ***Source:*** **Getty Images.**

duction or long-term maintenance.

- **Human dependency:** Even integrated systems depended heavily on expert operators, increasing risk and variability.

The modern shift is toward software-defined test architectures, as demonstrated in ***Figure 1***. Hardware remains critical, but intelligence increasingly resides in control layers that manage configuration, sequencing, safety and data handling. Modular instrumentation, networked control and abstraction layers allow benches to be reconfigured rapidly without physical rewiring.

This transition mirrors developments in the systems being tested. As radios, power electronics and control units become software-driven, their validation environments must evolve in parallel.

COMBINING HIGH-POWER AND AUTOMATION

Automation has long been associated with low-power laboratory testing, where risks are manageable and margins forgiving. High-power RF and microwave testing, by contrast, introduces non-linear effects and failure modes that fundamentally alter how test systems must be engineered.

At elevated power levels, several factors dominate:

- **Thermal stress:** Components under test and within the bench experience significant heating, affecting performance and longevity.
- **Non-linear behaviour:** Amplifiers, mixers and passive components exhibit compression, harmonics and intermodulation.
- **Reflected power risks:** Impedance mismatches can generate standing waves capable of damaging equipment within microseconds.
- **Electromagnetic coupling:** High field strengths can interfere with control electronics and compromise measurement integrity.

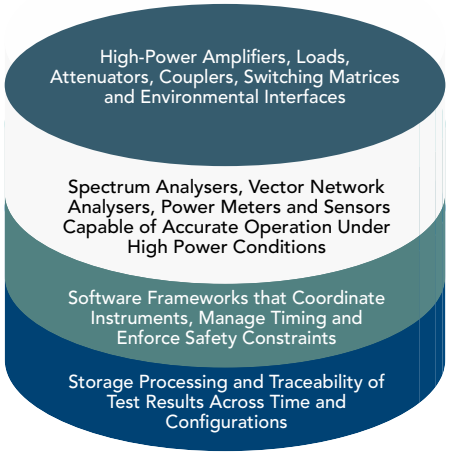

Fig. 2 **Pictogram displaying multi-layer integrated automation.**

In such environments, manual intervention is not just inefficient; it is risky. Automation becomes a safety mechanism as much as a productivity tool. Automated interlocks, continuous monitoring of forward and reflected power and real-time shutdown logic are essential to protect both equipment and personnel.

The critical analytical point is that high-power and automation were historically treated as separate concerns. Today, they must be designed together, from the earliest architectural decisions.

Has Amplifier Performance or Delivery Stalled Your Program?

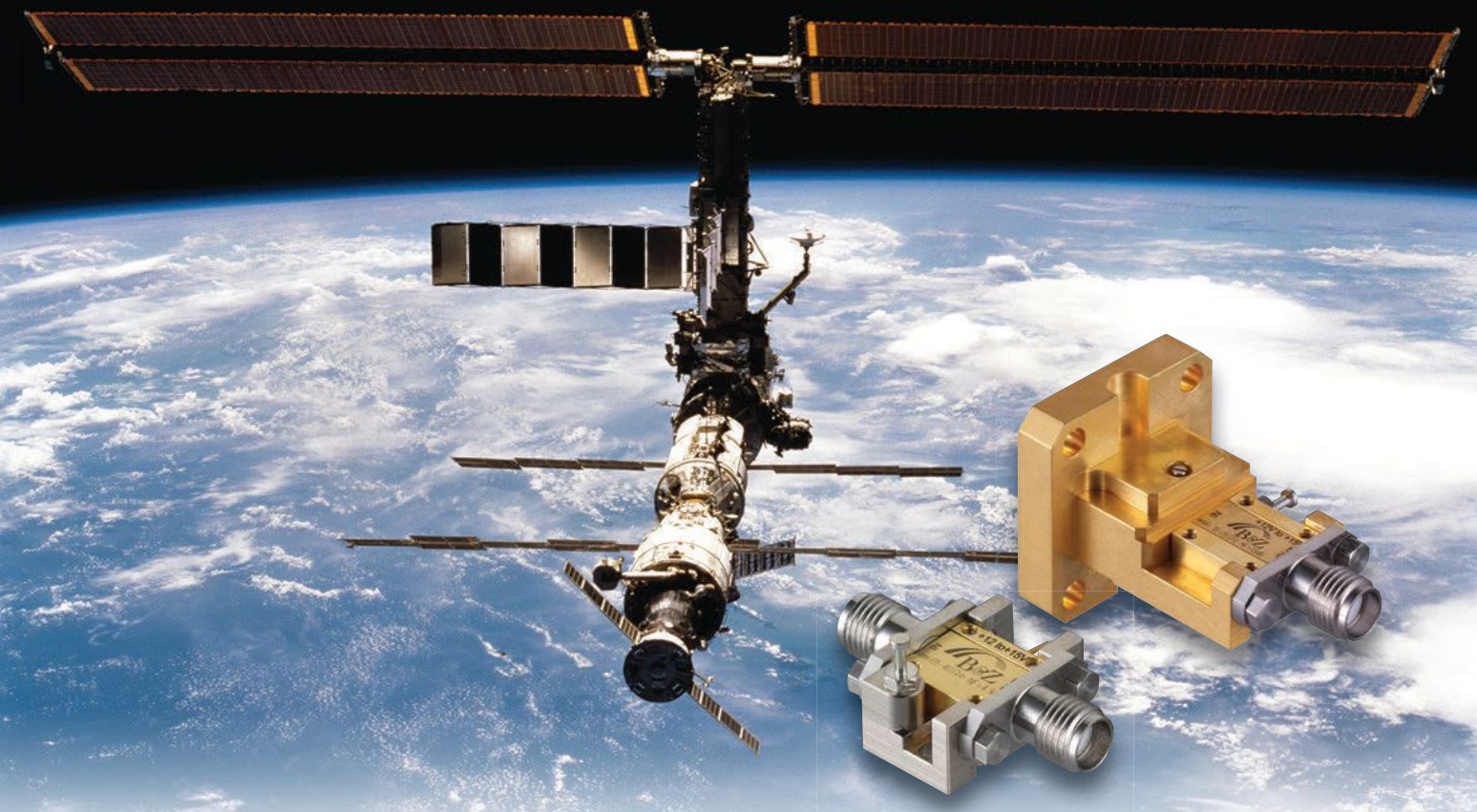

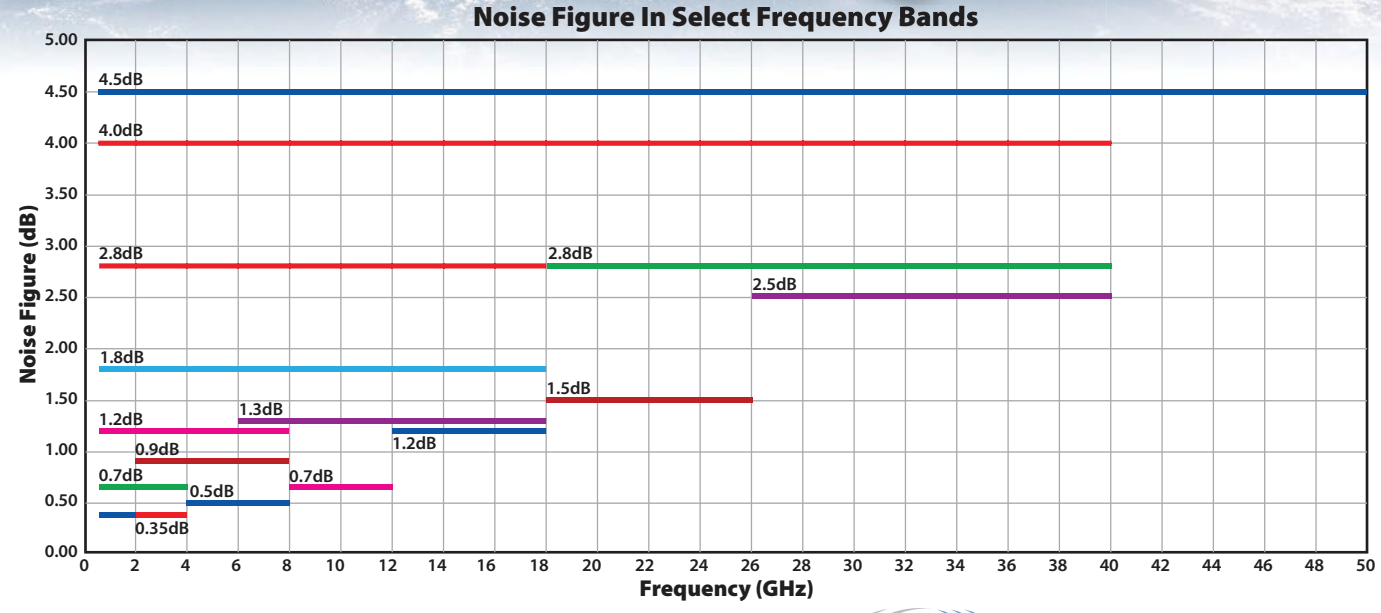

B&Z TECHNOLOGIES
Innovating to Excel

www.bnztech.com

MULTI-LAYER INTEGRATED AUTOMATION

Fully integrated high-power test benches are best understood as systems-of-systems. They combine RF and microwave signal chains, power electronics, thermal management, control software and data infrastructure into a unified whole.

From a technical perspective, this integration operates across several layers, as shown in ***Figure 2***.

1. **Physical layer**: High-power amplifiers, loads, attenuators, couplers, switching matrices and environmental interfaces.
2. **Measurement layer**: Spectrum analysers, vector network analysers, power meters and sensors capable of accurate operation under high-power conditions.
3. **Control layer**: Software frameworks that coordinate instruments, manage timing and enforce safety constraints.
4. **Data layer**: Storage, processing and traceability of test results across time and configurations.

Automation ties these layers together. Test sequences evolve from simple scripts into structured workflows that adapt dynamically to real-time conditions. If reflected power exceeds a threshold, the system responds instantly. If thermal drift is detected, parameters are adjusted or testing pauses automatically. This level of integration fundamentally changes the role of the test bench. It becomes an active participant in validation rather than a passive measurement tool.

INDUSTRY APPLICATIONS UNDER THE SPOTLIGHT

Aerospace and Defence: Testing at the Edge of Physics

Aerospace and defence systems exemplify why integrated, automated high-power test benches are essential, as exemplified in ***Figure 3***. Radar systems, satellite transponders, electronic warfare payloads and secure communications must operate across wide frequency ranges, often at very high peak powers and under extreme environmental conditions.

Fig. 3 **Digital pulse generator. *Source:* Getty Images.**

A modern fighter aircraft, for example, may experience ground temperatures exceeding 50°C in the desert, followed by sub-zero conditions at altitude within minutes. RF performance must remain stable through these rapid thermal transitions. Automated benches capable of synchronising RF excitation with aggressive thermal cycling are essential. Thermo-mechanical life cycles are not merely reliability concerns; they are mission- and life-critical.

In addition, defence systems must withstand deliberate countermeasures. Jamming, spoofing and high-power interference are operational realities. Integrated test benches can emulate hostile RF environments, injecting jamming signals while monitoring system resilience, recovery behaviour and degradation thresholds. This level of validation is impractical with manual or loosely coupled setups.

The analytical value lies not only in efficiency, but in confidence. When test procedures are encoded in software and executed consistently, results become comparable across time, facilities and programmes.

ERAVANT

FORMERLY SAGE MILLIMETER

INTEGRATED

SUBASSEMBLIES

UP TO 330 GHz

- **Comprehensive Support:** End-to-end assistance from initial concept through production
- **Rapid Prototyping:** Accelerated development cycles to meet tight project timelines
- **Engineered to Your Specifications**

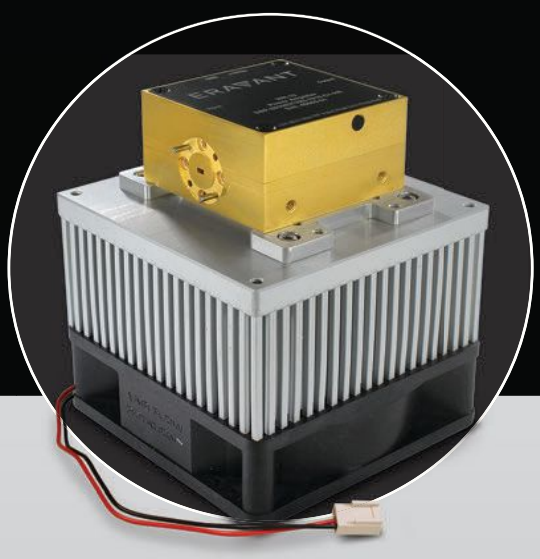

2 Watt High Power Amplifiers available off-the-shelf

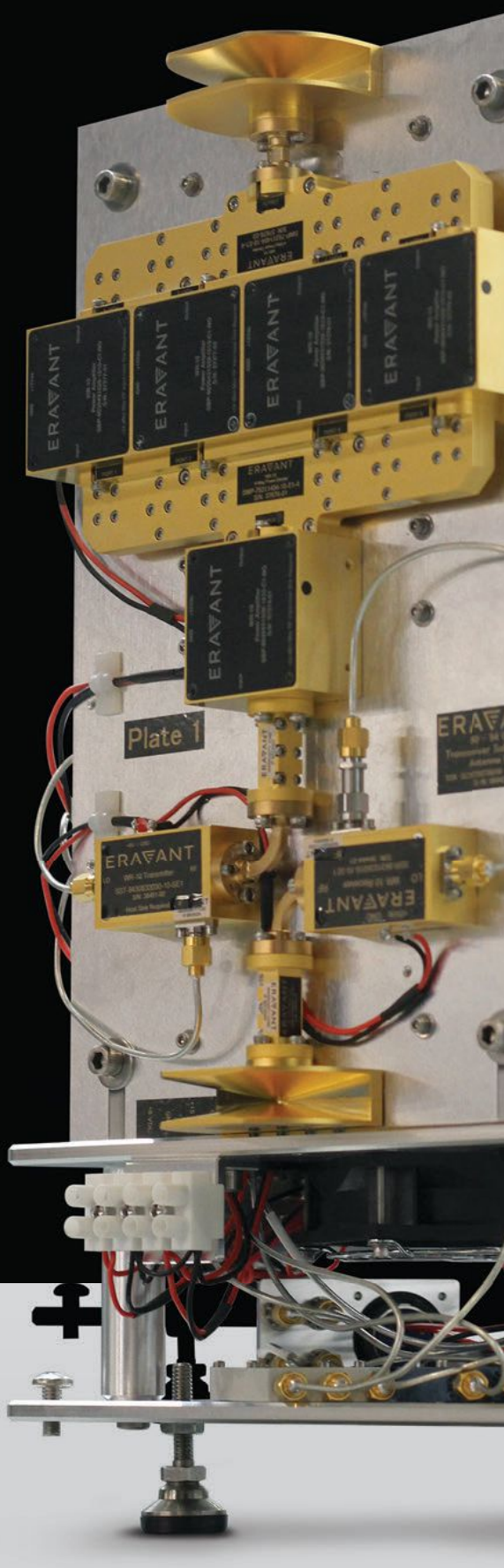

WWW.ERAVANT.COM

www.eravant.com 501 Amapola Avenue Torrance, CA 90501
T: 424-757-0168 F: 424-757-0188 support@eravant.com

Adapters • Amplifiers • Antenna Feeds • Antennas • Attenuators • Bias Tees • Cable Assemblies • Corner Reflectors • Couplers • DC Blocks • Detectors • Ferrite Devices • Filters • Frequency Converters • Frequency Multipliers • Limiters • Magic Tees • Mixers • Noise Sources • Oscillators • Phase Shifters • Power Dividers • Radar Sensors • Subassemblies • Switches • Termination Loads • Test Equipment • Test Hardware & Accessories • TX/RX Modules • Uni-Guide™ • Waveguide Sections

Communications Infrastructure: Complexity at Scale

In telecommunications, complexity manifests through scale and integration rather than extreme environments. Technologies such as massive MIMO, beamforming and wideband modulation require simultaneous characterisation of many RF paths, often under high-power conditions.

Massive MIMO radio systems used in 5G networks represent investments of millions of dollars and demand engineering precision. Testing must verify not only individual transmit and receive chains, but also collective behaviour, such as beam patterns, phase coherence and power distribution under dynamic traffic loads. Automated, integrated benches make this feasible.

Satellite communications further illustrate the stakes. Components such as oscillators and high-power amplifiers undergo burn-in tests lasting thousands of hours. Once deployed, repair is impossible. A failure in orbit is catastrophic. Automated high-power benches enable long-duration, unattended testing with continuous monitoring, ensuring latent defects are identified before launch. Here, automation enables a shift from static compliance testing to dynamic performance evaluation that reflects real network behaviour.

Energy, Transport and Industrial Systems: Converging Domains

High-power RF testing increasingly intersects with power electronics in energy and transport systems. Renewable energy converters, rail signalling equipment and industrial wireless controls operate in electrically noisy environments where RF performance and power integrity are tightly coupled, as exemplified in ***Figure 4***.

Integrated benches that combine RF testing with high-voltage and high-current validation allow engineers to observe interactions that isolated tests miss. Switching noise from power converters can degrade communication links, while RF emissions may interfere with control electronics.

Fig. 4 **Graphic illustration of tightly configured data streams.** ***Source:*** **Getty Images.**

Looking ahead to automated and driverless vehicles, this convergence intensifies. Autonomous systems rely on radar, communications, sensors and control electronics operating in real-time. Failures are not merely inconvenient; they carry direct safety implications. Automation, AI and digital twins become essential tools to validate these interactions reliably and repeatedly.

Medical Technology: Precision, Safety and Traceability

Medical technology provides a compelling illustration of why integration and automation matter. Devices employing RF and microwave energy, such as MRI systems, RF ablation equipment, neurostimulators and implantable electronics, operate under uniquely stringent constraints.

Implantable cardiac pacemakers, for example, must function flawlessly for decades inside the human body. RF emissions must remain within strict exposure limits, and immunity to external RF interference must be guaranteed. Automated high-power test benches enable exhaustive, repeatable testing across operating conditions while ensuring comprehensive documentation.

Regulatory scrutiny is intense. Every test configuration, parameter and result must be traceable. Auto-

RF-LAMBDA

MADE IN USA

THE LEADER OF RF BROADBAND SOLUTIONS

EMC Broadband RF Power Amplifier

High Power Solid State

HUNDREDS IN STOCK

FAST SHIPPING

FREQUENCY UP TO 90GHZ

POWER UP TO 2KW CW

BENCHTOP AND RACKMOUNT

REMC06G18GG 6-18GHZ 400W

- AUTOMATIC BUILT IN SELF CALIBRATION AND BIAS ADJUSTMENT.
- OVER TEMPERATURE, CURRENT, INPUT POWER PROTECTION.
- VSWR MEASUREMENT AND OPEN CIRCUIT PROTECTION.
- USER FRIENDLY CONTROL INTERFACE.
- REMOTE ETHERNET CONTROL AND FIRMWARE UPDATE.
- HIGH POWER EFFICIENCY AND LIGHTWEIGHT.

RAMP42G47GA 42-47GHZ 8W

REMC02G06GE 2-6GHZ 500W

RAMP18G40GB-U 18-40G 20W

RAMP05M80GC 0.5-80GHZ

REMC18G40GQ 18-40GHZ 200W CW

mation ensures repeatability, while integrated data management supports long-term compliance. Digital twins and AI analytics further enhance confidence by enabling predictive assessment of ageing and degradation without restarting full approval cycles.

From Automated Testing to Intelligent Validation

Automation, while transformative, represents only an intermediate stage in the evolution of high-power RF and microwave test benches. As systems continue to grow in complexity, automation alone is insufficient to capture the full range of behaviours that define real-world performance. The next phase is characterised by intelligence, modelling and lifecycle integration, in which test benches no longer simply execute predefined procedures but actively contribute to design understanding and long-term system assurance.

This shift is driven by a fundamental change in how engineering risk is managed. Rather than treating testing as a gate at the end of the development lifecycle, emerging approaches embed validation throughout the lifecycle, supported by digital models, advanced analytics and distributed collaboration frameworks.

AI-Driven Analytics: From Data Collection to Insight Generation

Modern automated test benches generate vast volumes of data: time-domain waveforms, spectral content, thermal profiles, power metrics and environmental parameters. Historically, much of this data was underutilised, stored for compliance rather than insight.

AI and machine learning techniques are beginning to change this dynamic. In high-power RF and microwave testing, AI-driven analytics can support:

- **Anomaly detection:** Identifying subtle deviations in behaviour that may indicate early-stage degradation long before conventional limits are exceeded.
- **Pattern recognition:** Correlating performance drift with specific operating conditions, duty cycles or thermal histories.
- **Design feedback:** Highlighting recurring weaknesses across test populations, therefore informing future design iterations.

Importantly, these techniques do not replace engineering judgement. Instead, they act as force multipliers, allowing engineers to focus attention where it matters most. In complex systems with thousands of parameters, AI helps surface relationships that would otherwise remain hidden.

From an analytical perspective, the value of AI lies in its ability to transform test benches from pass/fail instruments into learning systems, continuously refining understanding of how high-power RF systems behave over time.

Cloud Integration and Distributed Collaboration

As engineering teams become more geographically distributed, test environments must support collabora-

Talent Microwave

www.talentmw.com/en/

Wide Band High Power Amplifier

8-12GHz 1KW CW Solid State Power Amplifier

Features

- Ultra Wide Band: 8-12GHz
- Gain:60dB Min·
- Output Power: 60dBm Min
- Low power consumption
- Low spurious signal

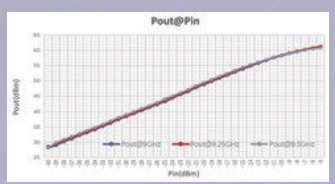

- High-efficiency GaN technology
- Forward/reverse power monitoring
- Over voltage,over temperature, over VSWR protection

EMC RS103 10kHz-40GHz 200V/M Amplifier

RS103 200V/M 0.7-40GHz PA
One Rackmount Solution

- 26-40GHz 50W PA
- 18-26GHz 50W PA
- 6-18GHz 200W PA
- 0.7-6GHz 250W PA

Solid State Power Amplfier Modules

Fast Delivery

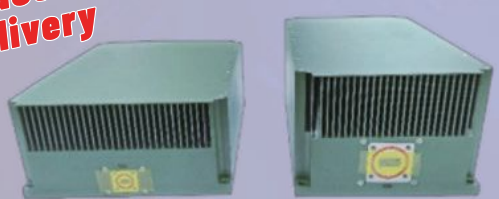

- 26.5-40GHz
- Output Psat: 47dBm
- Model: TLPA26.5G40G-47-47

- 6-18GHz
- Output Psat:48dBm
- Model: TLPA6G18G-47-48

AC Type Benchtop Power Amplifier Up to 100KW

3 Years Warranty

- RS103 EMC 200V/M Amplifier
- 8-12GHz 1KW CW SSPA
- 0.5-6GHz 500W CW SSPA
- C band 10KW CW SSPA
- 1-4GHz 20KW Pulse SSPA
- 4-8GHz 2000W CW SSPA
- 6-18GHz 1000W CW SSPA
- 8-18GHz 2500W Pulse SSPA
- 26-40GHz 500W CW SSPA
- 40-60GHz 100W CW SSPA
- 75-110GHz 10W CW SSPA

Web: www.talentmw.com/en Mail: sales@talentmw.com Add: Suzhou. China

tion without compromising data integrity or security. Cloud integration is emerging as a key enabler in this regard.

For automated high-power test benches, cloud-connected architectures allow:

- **Centralised data repositories:** Test results from multiple sites are aggregated and analysed consistently.
- **Remote access and oversight:** Experts can review test execution and results without being physically present.
- **Cross-functional collaboration:** Design, test, quality and regulatory teams working from a shared data foundation.

In regulated industries, this capability must be implemented carefully, with strict controls over access, versioning and traceability. When done correctly, however, cloud integration reduces duplication of effort and accelerates decision-making across the product lifecycle.

Lifecycle Confidence: Testing Beyond Initial Qualification

A defining feature of future test strategies is the emphasis on lifecycle confidence. For many high-power RF and microwave systems, particularly in aerospace, energy and healthcare, operational lifetimes span decades. Initial qualification, while essential, cannot guarantee long-term reliability.

Automated, integrated test benches increasingly support:

- **Production consistency:** Ensuring that systems leaving the factory remain aligned with qualified performance.
- **Field return analysis:** Comparing failed or degraded units against baseline test data to identify root causes.
- **Upgrade validation:** Retesting modified systems against original benchmarks to manage obsolescence and enhancements.

This lifecycle perspective reframes the role of the test bench. It becomes a persistent reference point, a technical memory of the system, rather than a one-time hurdle.

Yet, technology alone is insufficient. Process, skills development and collaboration are equally critical. Integrating RF, high-power electronics, software and safety systems requires multidisciplinary expertise. Engineers must understand automation frameworks and data analysis alongside traditional RF theory. Effective test systems increasingly depend on close cooperation between system designers, test engineers and technology providers.

The central question facing the industry is no longer whether to adopt integrated and automated high-power test benches, but how to implement them effectively. As electronic systems become more complex and the stakes rise, testing must evolve from a downstream activity to a strategic enabler. ■

Scalable VNAs for Cable and Component Manufacturers

from Copper Mountain Technologies

VALUE

- 9 kHz to 18 GHz coverage supporting validation of RF cables, connectors, and assemblies
- 24 µs measurement speed and 130+ dB dynamic range to reduce test time while maintaining precise pass/fail accuracy
- High measurement stability and accuracy for repeatable S-parameter characterization, production testing, and quality assurance
- Low unit cost with volume discount opportunities for scalable deployment

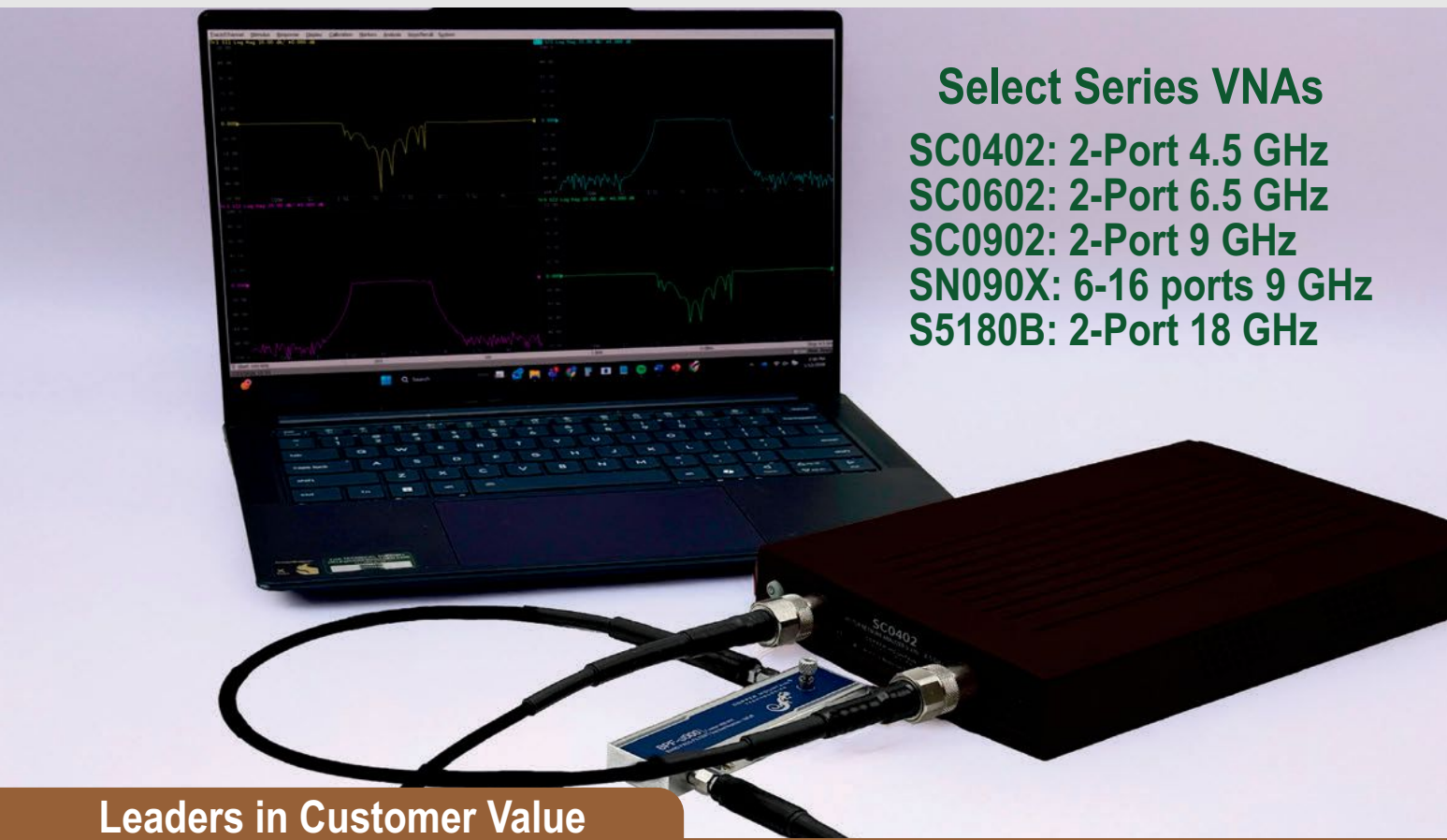

Select Series VNAs

SC0402: 2-Port 4.5 GHz
SC0602: 2-Port 6.5 GHz
SC0902: 2-Port 9 GHz
SN090X: 6-16 ports 9 GHz
S5180B: 2-Port 18 GHz

Leaders in Customer Value

- Metrology-grade performance backed by CMT's **ISO/IEC 17025 (2017) accredited labs**
- License-Free **Software for Windows and Linux** | Time domain included at no additional cost
- Direct access to **automation and applications engineers** to optimize fixtures, limits, and test sequences
- Made in the **EU and USA**

EXTEND YOUR REACH®

WWW.COPPERMOUNTAINTECH.COM

COPPER MOUNTAIN TECHNOLOGIES

RF Amplifiers and Sub-Assemblies for Every Application

Delivery from Stock to 2 Weeks ARO from the catalog or built to your specifications!

- Competitive Pricing & Fast Delivery
- Military Reliability & Qualification
- Various Options: Temperature Compensation, Input Limiter Protection, Detectors/TTL & More
- Unconditionally Stable (100% tested)

ISO 9001:2000 and AS9100B CERTIFIED

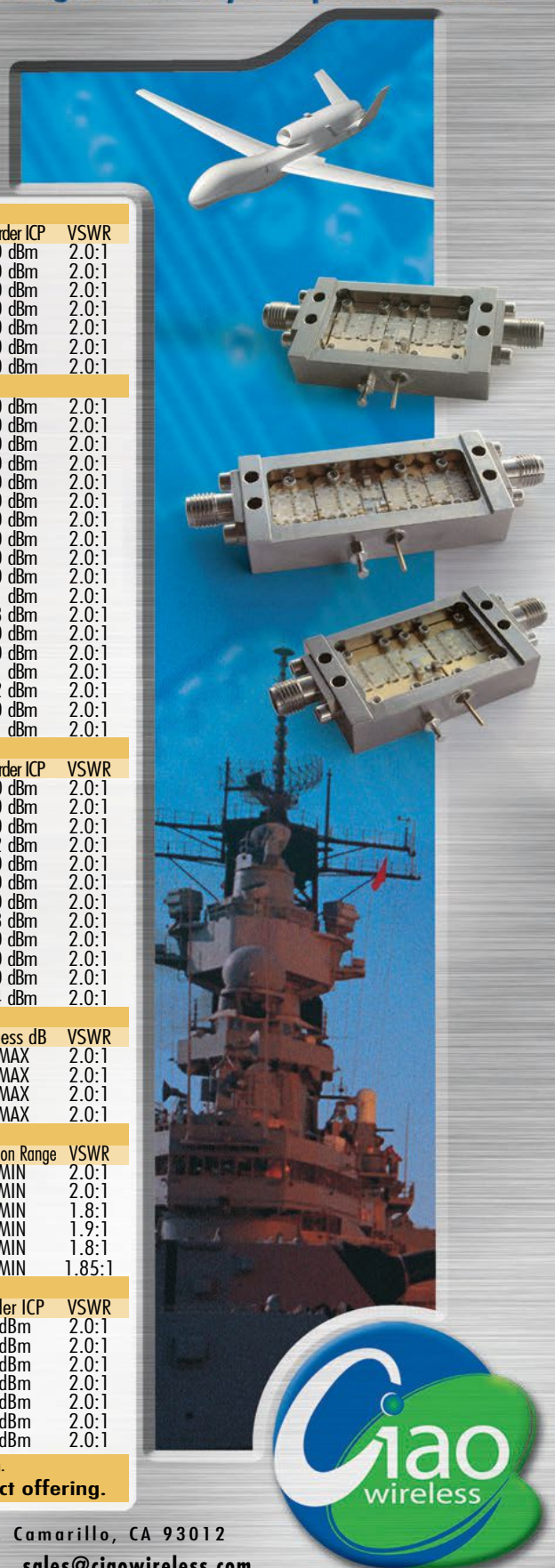

OCTAVE BAND LOW NOISE AMPLIFIERS

Model No.	Freq (GHz)	Gain (dB) MIN	Noise Figure (dB)	Power-out @ P1-dB	3rd Order ICP	VSWR
CA01-2110	0.5-1.0	28	1.0 MAX, 0.7 TYP	+10 MIN	+20 dBm	2.0:1
CA12-2110	1.0-2.0	30	1.0 MAX, 0.7 TYP	+10 MIN	+20 dBm	2.0:1
CA24-2111	2.0-4.0	29	1.1 MAX, 0.95 TYP	+10 MIN	+20 dBm	2.0:1
CA48-2111	4.0-8.0	29	1.3 MAX, 1.0 TYP	+10 MIN	+20 dBm	2.0:1
CA812-3111	8.0-12.0	27	1.6 MAX, 1.4 TYP	+10 MIN	+20 dBm	2.0:1
CA1218-4111	12.0-18.0	25	1.9 MAX, 1.7 TYP	+10 MIN	+20 dBm	2.0:1
CA1826-2110	18.0-26.5	32	3.0 MAX, 2.5 TYP	+10 MIN	+20 dBm	2.0:1

NARROW BAND LOW NOISE AND MEDIUM POWER AMPLIFIERS

Model No.	Freq (GHz)	Gain (dB) MIN	Noise Figure (dB)	Power-out @ P1-dB	3rd Order ICP	VSWR
CA01-2111	0.4 - 0.5	28	0.6 MAX, 0.4 TYP	+10 MIN	+20 dBm	2.0:1
CA01-2113	0.8 - 1.0	28	0.6 MAX, 0.4 TYP	+10 MIN	+20 dBm	2.0:1
CA12-3117	1.2 - 1.6	25	0.6 MAX, 0.4 TYP	+10 MIN	+20 dBm	2.0:1
CA23-3111	2.2 - 2.4	30	0.6 MAX, 0.45 TYP	+10 MIN	+20 dBm	2.0:1
CA23-3116	2.7 - 2.9	29	0.7 MAX, 0.5 TYP	+10 MIN	+20 dBm	2.0:1
CA34-2110	3.7 - 4.2	28	1.0 MAX, 0.5 TYP	+10 MIN	+20 dBm	2.0:1
CA56-3110	5.4 - 5.9	40	1.0 MAX, 0.5 TYP	+10 MIN	+20 dBm	2.0:1
CA78-4110	7.25 - 7.75	32	1.2 MAX, 1.0 TYP	+10 MIN	+20 dBm	2.0:1
CA910-3110	9.0 - 10.6	25	1.4 MAX, 1.2 TYP	+10 MIN	+20 dBm	2.0:1
CA1315-3110	13.75 - 15.4	25	1.6 MAX, 1.4 TYP	+10 MIN	+20 dBm	2.0:1
CA12-3114	1.35 - 1.85	30	4.0 MAX, 3.0 TYP	+33 MIN	+41 dBm	2.0:1
CA34-6116	3.1 - 3.5	40	4.5 MAX, 3.5 TYP	+35 MIN	+43 dBm	2.0:1
CA56-5114	5.9 - 6.4	30	5.0 MAX, 4.0 TYP	+30 MIN	+40 dBm	2.0:1
CA812-6115	8.0 - 12.0	30	4.5 MAX, 3.5 TYP	+30 MIN	+40 dBm	2.0:1
CA812-6116	8.0 - 12.0	30	5.0 MAX, 4.0 TYP	+33 MIN	+41 dBm	2.0:1
CA1213-7110	12.2 - 13.25	28	6.0 MAX, 5.5 TYP	+33 MIN	+42 dBm	2.0:1
CA1415-7110	14.0 - 15.0	30	5.0 MAX, 4.0 TYP	+30 MIN	+40 dBm	2.0:1
CA1722-4110	17.0 - 22.0	25	3.5 MAX, 2.8 TYP	+21 MIN	+31 dBm	2.0:1

ULTRA-BROADBAND & MULTI-OCTAVE BAND AMPLIFIERS

Model No.	Freq (GHz)	Gain (dB) MIN	Noise Figure (dB)	Power-out @ P1-dB	3rd Order ICP	VSWR
CA0102-3111	0.1-2.0	28	1.6 Max, 1.2 TYP	+10 MIN	+20 dBm	2.0:1
CA0106-3111	0.1-6.0	28	1.9 Max, 1.5 TYP	+10 MIN	+20 dBm	2.0:1
CA0108-3110	0.1-8.0	26	2.2 Max, 1.8 TYP	+10 MIN	+20 dBm	2.0:1
CA0108-4112	0.1-8.0	32	3.0 MAX, 1.8 TYP	+22 MIN	+32 dBm	2.0:1
CA02-3112	0.5-2.0	36	4.5 MAX, 2.5 TYP	+30 MIN	+40 dBm	2.0:1
CA26-3110	2.0-6.0	26	2.0 MAX, 1.5 TYP	+10 MIN	+20 dBm	2.0:1
CA26-4114	2.0-6.0	22	5.0 MAX, 3.5 TYP	+30 MIN	+40 dBm	2.0:1
CA618-4112	6.0-18.0	25	5.0 MAX, 3.5 TYP	+23 MIN	+33 dBm	2.0:1
CA618-6114	6.0-18.0	35	5.0 MAX, 3.5 TYP	+30 MIN	+40 dBm	2.0:1
CA218-4116	2.0-18.0	30	3.5 MAX, 2.8 TYP	+10 MIN	+20 dBm	2.0:1
CA218-4110	2.0-18.0	30	5.0 MAX, 3.5 TYP	+20 MIN	+30 dBm	2.0:1
CA218-4112	2.0-18.0	29	5.0 MAX, 3.5 TYP	+24 MIN	+34 dBm	2.0:1

LIMITING AMPLIFIERS

Model No.	Freq (GHz)	Input Dynamic Range	Output Power Range Psat	Power Flatness dB	VSWR
CLA24-4001	2.0 - 4.0	-28 to +10 dBm	+7 to +11 dBm	+/- 1.5 MAX	2.0:1
CLA26-8001	2.0 - 6.0	-50 to +20 dBm	+14 to +18 dBm	+/- 1.5 MAX	2.0:1
CLA712-5001	7.0 - 12.4	-21 to +10 dBm	+14 to +19 dBm	+/- 1.5 MAX	2.0:1
CLA618-1201	6.0 - 18.0	-50 to +20 dBm	+14 to +19 dBm	+/- 1.5 MAX	2.0:1

AMPLIFIERS WITH INTEGRATED GAIN ATTENUATION

Model No.	Freq (GHz)	Gain (dB) MIN	Noise Figure (dB)	Power-out @ P1-dB	Gain Attenuation Range	VSWR
CA001-2511A	0.025-0.150	21	5.0 MAX, 3.5 TYP	+12 MIN	30 dB MIN	2.0:1
CA05-3110A	0.5-5.5	23	2.5 MAX, 1.5 TYP	+18 MIN	20 dB MIN	2.0:1
CA56-3110A	5.85-6.425	28	2.5 MAX, 1.5 TYP	+16 MIN	22 dB MIN	1.8:1
CA612-4110A	6.0-12.0	24	2.5 MAX, 1.5 TYP	+12 MIN	15 dB MIN	1.9:1
CA1315-4110A	13.75-15.4	25	2.2 MAX, 1.6 TYP	+16 MIN	20 dB MIN	1.8:1
CA1518-4110A	15.0-18.0	30	3.0 MAX, 2.0 TYP	+18 MIN	20 dB MIN	1.85:1

LOW FREQUENCY AMPLIFIERS

Model No.	Freq (GHz)	Gain (dB) MIN	Noise Figure dB	Power-out @ P1-dB	3rd Order ICP	VSWR
CA001-2110	0.01-0.10	18	4.0 MAX, 2.2 TYP	+10 MIN	+20 dBm	2.0:1
CA001-2211	0.04-0.15	24	3.5 MAX, 2.2 TYP	+13 MIN	+23 dBm	2.0:1
CA001-2215	0.04-0.15	23	4.0 MAX, 2.2 TYP	+23 MIN	+33 dBm	2.0:1
CA001-3113	0.01-1.0	28	4.0 MAX, 2.8 TYP	+17 MIN	+27 dBm	2.0:1
CA002-3114	0.01-2.0	27	4.0 MAX, 2.8 TYP	+20 MIN	+30 dBm	2.0:1
CA003-3116	0.01-3.0	18	4.0 MAX, 2.8 TYP	+25 MIN	+35 dBm	2.0:1
CA004-3112	0.01-4.0	32	4.0 MAX, 2.8 TYP	+15 MIN	+25 dBm	2.0:1

CIAO Wireless can easily modify any of its standard models to meet your "exact" requirements at the Catalog Pricing.

Visit our web site at www.ciaowireless.com for our complete product offering.

Ciao Wireless, Inc. 4000 Via Pescador, Camarillo, CA 93012
Tel (805) 389-3224 Fax (805) 389-3629 sales@ciaowireless.com

RTX's Raytheon Selected by DARPA to Develop Advanced Maritime Defense Technologies

Raytheon, an RTX business, has been selected by the Defense Advanced Research Projects Agency (DARPA) to develop an advanced sensing and targeting system that will help defend vulnerable commercial shipping and naval logistics vessels against emerging threats such as unmanned surface vehicles (USVs).

Under the contract, Raytheon's Advanced Technology team will design, build and demonstrate a system that consists of electro-optical/infrared (EO/IR) sensors, advanced detection software and robust command-and-control capabilities to enhance situational awareness and threat response.

The system, which is being developed for DARPA's Pulling Guard program, will deploy the sensors via a tethered drone connected to a semi-autonomous unmanned platform that is towed by commercial and naval logistics vessels. The sensors will provide real-time target tracking data to remote operators, enabling them to make rapid, informed engagement decisions.

Phase one of the program will focus on simulated engagements to evaluate system performance and operator workflows. In phase two, the system will transition to integrating operational launchers and effectors for live operations.

"Through this development, we are advancing critical security technologies for commercial shipping in regions like the Red Sea," said Colin Whelan, president of Advanced Technology at Raytheon. "By integrating our proven expertise in command-and-control, high performance sensing and effectors, we will deliver a scalable, cost-effective solution that minimizes risks to both cargo and naval assets."

Beyond its primary focus on vulnerable ship protection, the technology Raytheon is developing has the potential to deliver broader capabilities across a wide range of naval and security operations, including automated overwatch for medium and large USVs and manned combatants operating in multiple theaters.

Pulling Guard Program (Source: DARPA)

First EW-Based Counter-UAS Technology to Demonstrate Effects Against Fiber-Optic Guided Drones

Epirus recently released video footage of the company's Leonidas VehicleKit high-power microwave (HPM) platform successfully disabling a fiber-optic-guided unmanned aerial system (UAS) during a December 2025 live-fire technology demonstration at a U.S. government testing site. The event marks the first known instance of electromagnetic interference being weaponized to defeat a fiber-optic guided drone.

Fiber-optic first-person view (FPV) drones have emerged as a game-changing tactic in contested environments, particularly in Ukraine, where they are employed daily for one-way attacks and intelligence, surveillance and reconnaissance missions. Unlike conventional UAS that rely on RF links for pilot control, fiber-optic-guided FPV drones connect to their pilots via spools of long, thin fiber-optic cable. These fiber-optic guided FPV drones operate without an RF command-and-control link, rendering them immune to jamming, spoofing and other legacy electronic warfare (EW) counter-UAS measures.

The Leonidas HPM platform defeats fiber-optic guided drones by delivering precise, software-defined weaponized electromagnetic interference to induce full kill within critical onboard electronics rather than relying on kinetic destruction or RF disruption. The Leonidas HPM platform uses non-ionizing radiation, making it inherently safe for humans when used as intended and its software-defined, highly directional phased array antennas focus energy on identified target areas only. Its near-instantaneous effects enable operators to influence the target's drop zone to minimize collateral damage.

Ukrainian Deputy Prime Minister and Digital Transformation Minister Mykhailo Fedorov has publicly stated that Russian forces are now fielding fiber-optic FPV drones with 31 miles of range and that these drones represent "a very considerable threat to logistics and personnel."

"The proliferation of fiber-optic guided UAS represents a major shift in drone warfare and exposes a growing operational gap for counter-UAS defenses — one that Leonidas is designed to address and close," said Andy Lowery, Epirus CEO. "Leonidas' ability to defeat this new class of threat represents an important breakthrough in safe, non-kinetic defense against emerging drone tactics and reinforces Epirus' leadership in scalable, one-to-many counter-UAS platform development."

For More Information

Visit mwjournal.com for more defense news.

HAVELSAN Showcases Autonomous Swarm Drone Capabilities Under Its "Digital Troops" Concept

HAVELSAN recently demonstrated its autonomous swarm drone capabilities through a live field activity conducted with a swarm of POYRAZ quadcopter drones, showcasing kamikaze and multi-target engagement capabilities within a realistic operational scenario. The demonstration attracted strong interest from senior civilian and military officials.

The activity validated the end-to-end performance of HAVELSAN's distributed swarm architecture, which operates without the need for a central decision maker. Despite simulated communication disruptions and network losses during the mission, the swarm maintained operational continuity throughout the scenario.

As part of the demonstration, the swarm autonomously divided into sub-swarms assigned to different targets. Each sub-swarm executed synchronized dive maneuvers toward its designated target. The system's self-reconfiguring and fault-tolerant structure was confirmed when malfunctioning elements autonomously disengaged from the swarm, while the remaining units continued the mission without interruption.

The activity also demonstrated that swarm operations can be integrated with other unmanned and sensor systems, enabling autonomous targeting and mission execution based on data gathered from multiple platforms. This demonstration once again highlighted HAVELSAN's approach to delivering platform-independent, scalable and mission-oriented solutions in the field of autonomous and unmanned systems.

> Self-reconfiguring and Fault Tolerant Structure Operates Without the Need for a Central Decision Maker

Target data obtained from surveillance UAVs and other sensors were autonomously processed by the swarm intelligence. Throughout the mission, approach, formation keeping and engagement processes were executed without the need for operator intervention. Munitions were activated only when predefined mission rules and safety conditions were met, and mission completion data were automatically shared across the swarm and transmitted to higher-level mission management systems.

The activity also featured BULUT, HAVELSAN's autonomous UAV with vertical takeoff and landing capability. Equipped with the GIMBAL 275 electro-optical system, BULUT provided real-time imagery, successfully demonstrating multi-platform integration.

Reactel, Inc.

Reacting First to All Your Filter Needs.

Filter Solutions For Mission Critical Applications

High Performance, Rugged Packaging, Small Size and Weight

Great things *can* come in small packages. Reactel filters are ideally suited for the demanding environments that unmanned vehicles encounter.

Many manufacturers rely on Reactel to provide units which are:
High performance - Lightweight - Low profile

Contact a Reactel engineer with your filter or multiplexer requirements. We can create a unit which will be the perfect fit for your applications.

RF & Microwave Filters - Multiplexers - Multifunction Assemblies

8031 Cessna Avenue • Gaithersburg, Maryland 20879 • (301) 519-3660 • reactel@reactel.com • reactel.com

Intertek

RoHS Compliant 2002/95/EC

MADE IN MD
Since 1979

µCeramIQ®

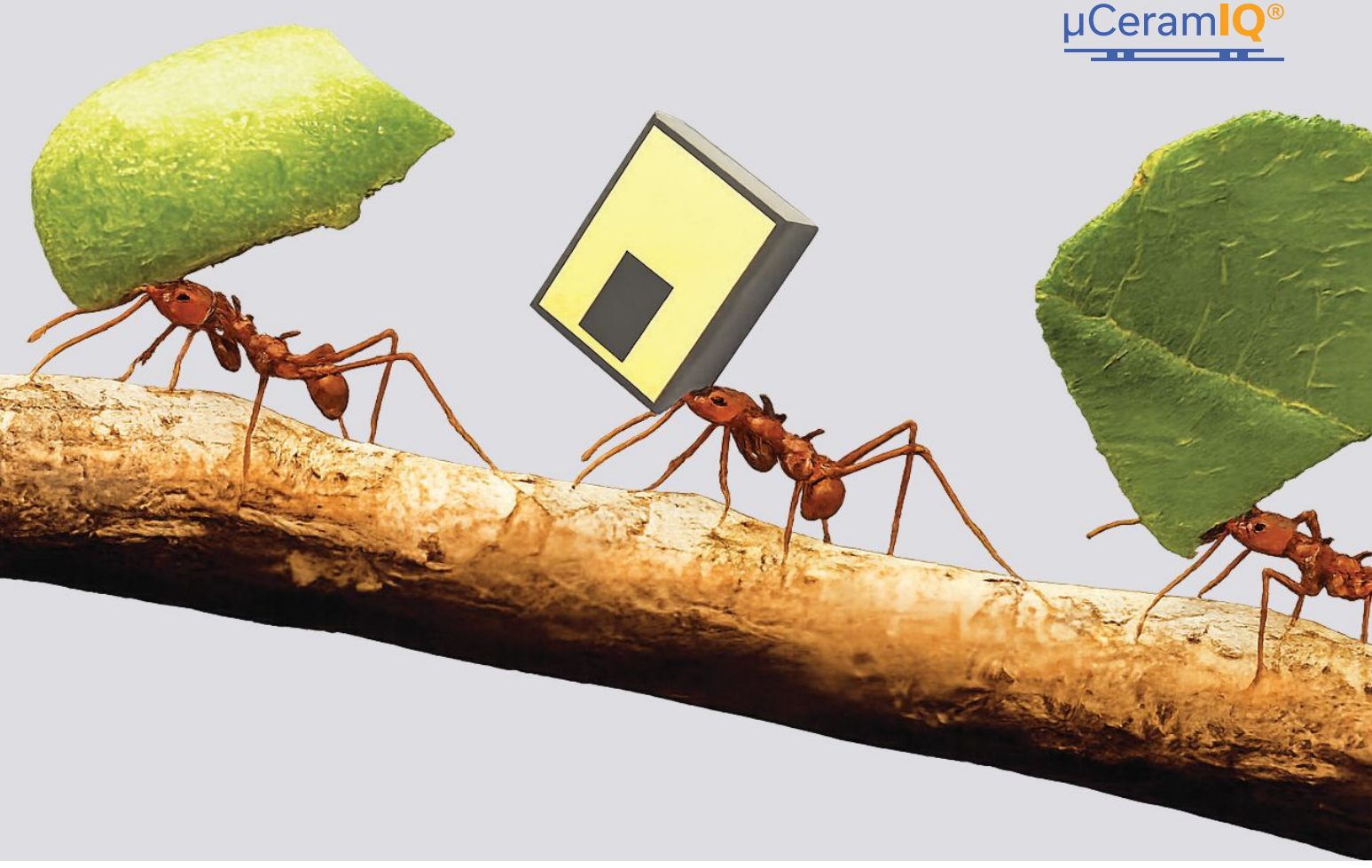

LFHK / BFHK / HFHK SERIES

Small but Mighty

Carrying the Load for High-Rejection and SWAP-C

LEARN MORE

- High pass, low pass & band pass models
- Passbands from DC to 36 GHz
- Stopbands up to 67 GHz
- Rejection up to ≥90+ dB
- Footprint as small as 1008

Protected by US Patents 11,638,370 and 11,744,057

Mini-Circuits®

RF GaN: Geopolitics Fuel Sustained Growth

According to Yole Group's recent report on the RF GaN market, GaN devices play a critical role in high-power RF signal generation and amplification, with growing adoption across telecom infrastructure, defense and satellite communications. The market is expected to reach $2.4 billion by 2031, growing at an 11 percent compound annual growth rate (CAGR) between 2025 and 2031, up from about $1.3 billion in 2025. After a downturn starting in 2023 due to weaker demand for telecom infrastructure, the market is now rebounding, driven by rising defense spending and supported by renewed momentum in satcom applications. In today's geopolitical climate, it is defense demand in particular that is accelerating RF GaN adoption, positioning the sector as the market's primary growth engine.

Yole Group's report analyzes market dynamics in the context of 5G network evolution, growing defense requirements and long-term preparation for 6G systems. As telecom architectures shift toward active antenna systems and defense platforms continue to transition to solid-state RF solutions, GaN is gaining share over legacy technologies. GaN-on-SiC remains the dominant platform, while GaN-on-Si is being increasingly adopted in specific applications.

Defense and aerospace represent the second major pillar of the RF GaN market, characterized by high performance requirements, long qualification cycles and stable demand. In parallel, satcom increasingly relies on GaN for high-power uplinks in ground gateways and satellite terminals as operating frequencies expand from K/Ka-Band up to E/W-Band applications.

GaN RF is now a core technology in defense, enabling higher performance AESA radar, compact electronic warfare (EW) systems and high-power military satellite communications. The RF GaN defense market, valued at U.S. $592 million in 2025, is expected to reach U.S. $1 billion by 2031, growing at a 10 percent CAGR. Growth is driven by the increasing deployment of GaN-based solid-state RF technologies across radar, EW and military satcom, with the U.S. remaining the leading adopter.

Packaged RF GaN Device - Forecast 2025-2031
Split by Application
Source: RF GaN 2025 Report, Yole Group

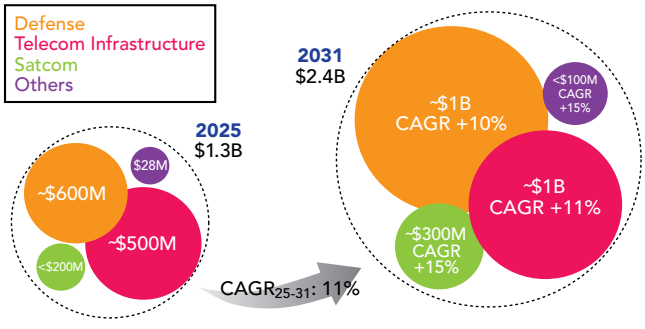

RF GaN Forecast (Source: Yole Group)

In radar systems, GaN RF technology has become a core enabler of AESA architecture operating across the S- to X-Bands. Airborne radar represents the largest application segment, supported by the transition from traveling-wave tube technologies to GaN-based transmit/receive modules that deliver higher output power, improved resolution, reduced weight and greater scalability. Adoption of GaN has also increased significantly in ground-based radar systems, while naval radar modernization is progressing more gradually as innovation efforts focus on sensor integration and multifunction apertures.

Beyond radar, EW is among the fastest-growing RF GaN segments, as wideband, high-efficiency GaN power amplifiers enable compact jamming systems for counter-UAS applications, next-generation tactical radios and high-data-rate military communications.

5G Mobile Core Network Market Revised up to 12 Percent CAGR

According to a recently published report from Dell'Oro Group, the global 5G mobile core network (MCN) market five-year forecast has been revised upward to 12 percent CAGR from 2025 to 2030, as the 5G Standalone (SA) market reaches an inflection point. Likewise, the multi-access edge computing (MEC) market forecast has been raised to 22 percent CAGR as demand for lower-latency AI applications continues to grow.

"The key inflection point is the acceleration in 5G SA network subscriber growth as these networks mature and expand coverage to more cities, including rural and indoor areas, encouraging more 4G subscribers to upgrade," said Dave Bolan, research director at Dell'Oro Group. "Additionally, the introduction of Reduced Capability (RedCap) 5G SA chips for smartwatches and lower-cost 5G SA IoT devices is making 5G SA more appealing to consumers and enterprises, especially for private networks compared to LTE. Also, new mobile network operators (MNOs) are preparing to launch more 5G SA networks."

"Other factors include the launch of 5G-Advanced by a dozen MNOs, introducing new capabilities, including dynamic network slicing, which will drive new consumer and enterprise low-latency applications, also driving demand for more MEC nodes throughout MNOs' networks and on-premises for enterprises. The increasing adoption of agentic AI will increase the demand for more MCN capacity and MEC nodes, fueling growth," Bolan added.

Additional highlights from the MCN and MEC 5-Year

For More Information Visit mwjournal.com for more commercial market news.

Forecast January 2026 Report include:

- The modernization of the IP Multimedia Subsystem (IMS) Core to a cloud-native architecture, the retirement of more 3G networks and 5G Voice over New Radio with new immersive and interactive calling features are accelerating growth.
- The rank order of the regions for the 5G MCN market based on five-year cumulative revenue is as follows: Europe, Middle East and Africa, Asia Pacific excluding China, China, North America and Caribbean and Latin America (CALA).
- The 4G MCN market will continue to decline. However, 4G will be significant in the Middle East and Africa, parts of Southeast Asia and CALA, accounting for the vast majority of the market.

FWA Infrastructure and CPE Spending to Remain Above $10 Billion Annually Through 2029

According to a recently published report from Dell'Oro Group, fixed wireless access (FWA) continues to surge, supporting both residential and enterprise connectivity due to its ease of deployment along with the more widespread availability of 4G LTE and 5G sub-6 GHz networks. Preliminary findings suggest total FWA revenues, including RAN equipment, residential CPE and enterprise router and gateway revenue remain on track to advance 10 percent in 2025, as mobile operators continue to expand the availability of FWA services in more markets to steal away more disaffected DSL and cable broadband subscribers.

"In the U.S., we continue to see the largest mobile operators expand their availability of FWA services in both existing and new markets, especially as FWA service revenue has boosted overall earnings," said Jeff Heynen, vice president with the Dell'Oro Group. "Mobile operators in India, Southeast Asia, Europe and the Middle East are taking a page from the U.S. operators' book and are quickly expanding their own FWA offerings, especially with the imminent threat of Starlink, Amazon, OneWeb and other LEO satellite broadband providers," added Heynen.

Additional highlights from the report:

- Total FWA subscriptions, which include residential, SMB and large enterprises, are expected to grow steadily, surpassing 191 million by 2029.
- 5G sub-6 GHz and mmWave units will dominate the global residential CPE market.

Ku/ Ka/ V/ E-Band Power Amplifier MMICs

Maximized performance for linear power applications

Ku/Ka-Band MMIC Die and Packaged MMICs

MMIC Die:

NPA1020-DE	12.5 - 14.5 GHz	15 W
NPA2020-DE	23.0 - 25.0 GHz	10 W
NPA2001-DE	26.5 - 29.5 GHz	35 W
NPA2002-DE	27.0 - 30.0 GHz	35 W
NPA2003-DE	27.5 - 31.0 GHz	35 W
NPA2004-DE	25.0 - 27.5 GHz	40 W
NPA2030-DE	27.5 - 31.0 GHz	20 W
NPA2040-DE	27.5 - 31.0 GHz	10 W

QFN Packaged MMICs:

NPQ2101-SM	27.5 - 31.0 GHz	5 W
NPQ2103-SM	27.5 - 31.0 GHz	8 W
NPQ2105-SM	27.5 - 31.0 GHz	12 W
NPQ2107-SM	27.5 - 31.0 GHz	17 W

Contact Nxbeam for Flange Packaged Options

V-Band MMICs

MMIC Die:

NPA4000-DE	47.0 - 52.0 GHz	1.5 W
NPA4010-DE	47.0 - 52.0 GHz	3.0 W

E-Band MMICs

MMIC Die:

NPA7000-DE	65.0 - 76.0 GHz	1.0 W

Around the **Circuit**

Barbara Walsh, Multimedia Staff Editor

IN MEMORIAM

Professor André Vander Vorst passed away peacefully on December 25, 2025, after a long and distinguished life devoted to science, education and service to the international microwave community. Vander Vorst was an electrical and mechanical engineer who made contributions to microwave science and engineering. He was widely respected for his scientific vision, his commitment to education and his dedication to European and international professional organisations. Professor Vander Vorst played a pivotal role in shaping the European microwave community. He was a corresponding member of the Organising Committee of the first European Microwave Conference (EuMC) in London in 1969, chaired the EuMC Technical Programme Committee in Brussels in 1971 and served as general chair of EuMC 1984 in Liège, Belgium. He acted as a reviewer for every EuMC since 1969. He was one of the founder members of the European Microwave Association (EuMA) when it was established in 1998 and served the Association with exceptional dedication as secretary-general and treasurer for 18 years. During this period, he was instrumental in establishing the EuMA headquarters and creating the organisational framework that continues to support EuMA and European Microwave Week today.

MERGERS & ACQUISITIONS

Anywaves and **EmTroniX** announced a strategic alliance through a merger under a unified industrial group. Brought together into a single entity, the two companies are combining their expertise to become a leading global player in space RF and payload subsystem technologies. This merger aims to deliver integrated and competitive solutions to meet the demanding requirements of the European, U.S. and international space market in electronic systems, antennas and advanced RF technologies for telecom, Earth and space observation. Building on an already successful operational collaboration to deliver advanced programs, the merger between Anywaves and EmTroniX reflects a shared commitment to accelerate the technical and industrial development of advanced telecommunication solutions, from antennas and electronics to fully integrated payloads.

NEW STARTS

ICsense, a TDK Group company and fab-independent European design group with expertise in analog, digital, mixed signal and high voltage integrated circuit design, has opened a new electronic wafer sort (EWS) cleanroom as part of its latest strategic investment program. With the application-specific integrated circuit (ASIC) market growing significantly, expected to reach an estimated $41.68 billion by 2034 at a CAGR of 7 percent from 2026 to 2034, ICsense has not only ramped up its in-house production capabilities to provide a complete turnkey EWS and final-test ASIC solution, but its fab independence also means customers benefit from flexibility in foundry selection, process technologies and scalable large volume production.

ACHIEVEMENTS

The Broadcast Engineering Society (India) (BES) has recognized and honored individuals who have made exemplary contributions in advancing the objectives for which the BES was established. In this regard, the BES has awarded **Ulrich L. Rohde** the Lifetime Achievement Award along with the Honorary Fellowship of BES (India) for his work with software-defined radios. The BES presented this award at the International Conference & Exhibition Broadcast & Media Technology – BES EXPO 2026 in New Delhi, India.

Eviden, the Atos Group product brand in advanced computing, cybersecurity products, mission-critical systems and Vision AI, announced that it has been selected by the **NATO Support and Procurement Agency** (NSPA) to modernize the ground-to-air-to-ground communication systems of the Spanish Air and Space Force. The €12 million contract includes the supply, installation and maintenance of next-generation communication systems that will enhance operations at air traffic control towers across various air bases, Air Force airfields, and Air Surveillance Squadron bases of the Spanish Air and Space Force.

MatrixSpace is the winner in the **U.S. Army's** xTech-Counter Strike competition, part of Operation Flytrap 4.5. MatrixSpace was the only active sensing provider selected among 15 finalists, highlighting the company's breakthrough capabilities in rapidly deployable airspace awareness. Operation Flytrap is the U.S. Army's key initiative to accelerate innovative, scalable C-UAS technologies through live soldier experimentation, rapid acquisition pathways and transition to operational units. MatrixSpace showcased its Expeditionary AI Radar and 360 AI Radar, powered by AiEdge software, demonstrating fast setup, seamless integration into Army FAAD-C2 via the NATO-standard SAPIENT protocol and real-time situational awareness at the tactical edge.

NTT DOCOMO, Inc. announced that they have successfully conducted the world's first outdoor demonstration using real-time transceiver systems with AI-powered wireless technology for 6G mobile communications. The demonstration was carried out in collaboration with NTT, Inc., Nokia Bell Labs and SK Telecom Co., Ltd. Field trials took place at three locations in Yokosuka City, Kanagawa Prefecture, and confirmed that the use of AI improved throughput (transmission speed) by up to 100 percent compared with conventional non-AI-based methods under the same environmental conditions, effectively doubling the communication speed.

For More Information

For up-to-date news briefs, visit mwjournal.com

GOLD STANDARD

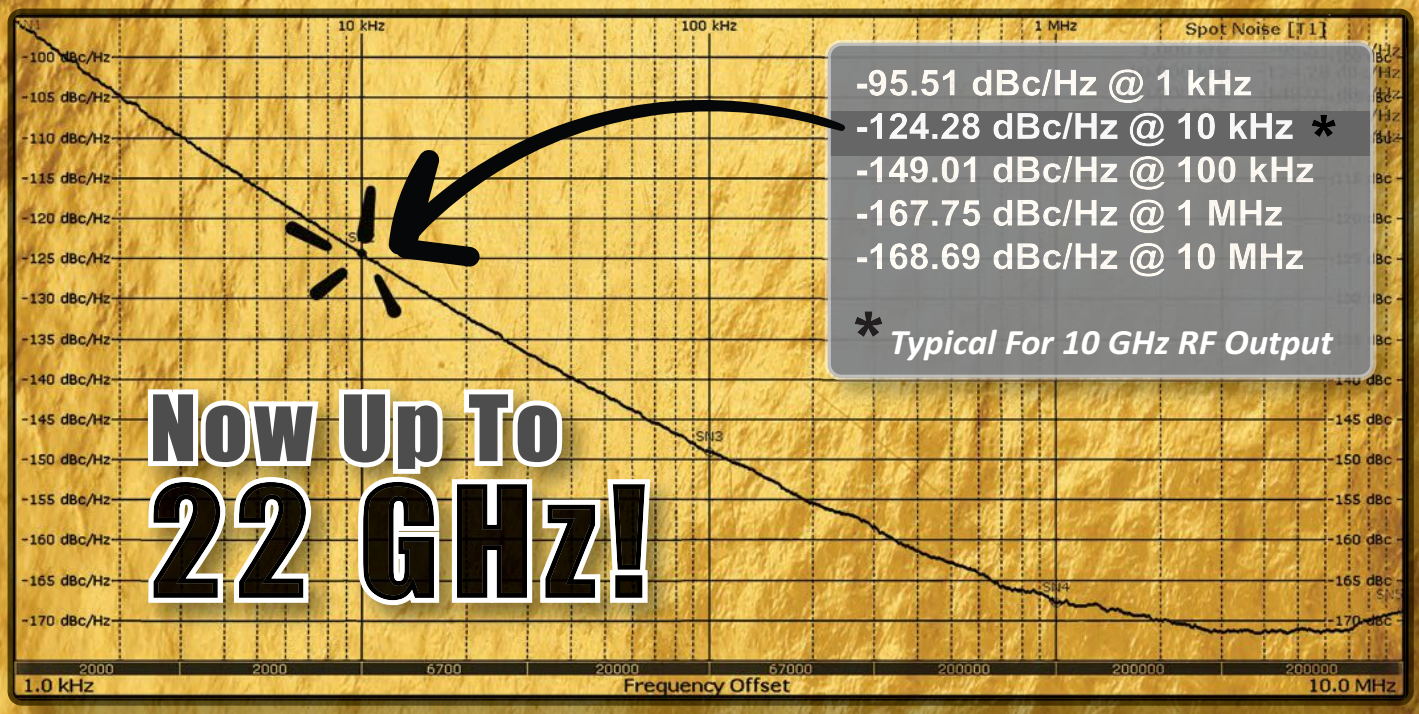

GSDRO + GKDRO SERIES

FEATURES:

- Exceptional Phase Noise
- Lead Free RoHS Compliant
- Patented Technology
- Field Replacement SMA connectors for pc board soldering pin contact mounting. Contact us for more info

Applications:

Radar, Test Equipment, 5G, Phase Locked Oscillators

Talk To Us About Your Custom Requirements.

SYNERGY® MICROWAVE CORPORATION

Phone: (973) 881-8800 | Fax: (973) 881-8361
E-mail: sales@synergymwave.com | Web: www.synergymwave.com
Mail: 201 McLean Boulevard, Paterson, NJ 07504

Around the **Circuit**

Altum RF announced the successful renewal of its ISO 9001:2015 certification. Valid through 2029, this renewal highlights Altum RF's ongoing commitment to quality, reliability and excellence across its global operations — including its headquarters and design center in Eindhoven, the Netherlands, and the design center in Sydney, Australia. The certification was awarded by TÜV Nord Nederland, part of the internationally recognized TÜV NORD GROUP, a leader in quality system certification with over a century of experience. Operating in more than 70 countries, TÜV NORD is known for its rigorous standards and commitment to excellence.

CONTRACTS

Elma Electronic announced it was awarded a contract for the **Missile Defense Agency** Scalable Homeland Innovative Enterprise Layered Defense (SHIELD) indefinite delivery/indefinite quantity contract with a ceiling of $151 billion. This contract encompasses a broad range of work areas that allows for the rapid delivery of innovative capabilities to the warfighter with increased speed and agility. The SHIELD contract leverages AI and machine learning-enabled applications where pertinent and maximizes the use of digital engineering, open systems architectures, model-based systems engineering and agile processes in the acquisition, development, fielding and sustainment of these capabilities.

Mercury Systems Inc. announced contract awards totaling more than $60 million for work associated with two critical U.S. space and strategic weapons programs. In December, Mercury was awarded a development contract extension in support of a large strategic weapons program that leverages the company's expertise in strategic radiation-hardened data and signal processing. Initially awarded in 2023, Mercury's development work on the program will now continue through 2031 and include the delivery of additional flight-testing units. In December, Mercury was also awarded a new contract from an innovative space systems prime contractor to produce subsystems for a U.S. national security space program.

Frequency Electronics Inc. (FEI), a provider of precision timing and frequency control products for space and terrestrial applications, announced the follow-on award of several contracts from a major aerospace company for precision "g" (acceleration) compensated oven-controlled quartz oscillators for ultimate application in U.S. government software-defined radio systems. These precision oscillators incorporate FEI's state-of-the-art patented technology for operating in high dynamic environments and generate precise frequencies that are critical to the overall performance of the Link 16 system. The contracts are valued at approximately $6 million. Follow-on contracts for additional units valued at over $2 million are anticipated within three months.

Verus® Research has been awarded a four-year, $6 million effort to support the **Naval Surface Warfare Center Dahlgren Division (NSWCDD)** via the **Naval Surface Technology & Innovation Consortium (NSTIC)**. Under this award, Verus Research will implement its novel concept referred to as Adaptive Radio Frequency Chamber and Hardware in the loop for Integrated Missile Subsystem Evaluation and Assessments (ARCHIMES). This endeavor begins with test and data analysis support for the Navy's DEFEND and METEOR programs and is a follow-on effort to Verus Research's Airborne High Power Microwave Instrumentation (AirHI) project.

Applied Physical Electronics, L.C. (APELC) has been awarded a $1.73 million Small Business Innovation Research Phase II contract by the **U.S. Air Force** to develop a transportable array structure to support high-power RF and high-altitude electromagnetic pulse (HEMP) sources. This two-year project focuses on solving a key structural challenge within EMP array development. As multiple organizations race to advance EMP technologies, APELC's award aims to fill a significant interest — designing a reconfigurable, transportable array frame capable of supporting large, heavy pulsed power systems in a variety of field environments.

European Engineering Consultancy Ltd. (EECL) has been awarded a £1.5 million contract by the **European Space Agency** to deliver ground support equipment and environmental and space-qualification testing for a next-generation digital satellite payload. Thanks to a strategic introduction by Space South Central, EECL will provide end-to-end qualification services, including thermal-vacuum cycling, vibration and mechanical testing, EMC assessment and comprehensive payload validation. The company will also design and supply automated ground support equipment and test systems to streamline qualification and integration processes. The new payload introduces a more complex and software-defined digital processing system, positioning EECL's automation-driven approach as a critical component in achieving rapid and repeatable test cycles.

PEOPLE

▲ *John Baylouny*

Leonardo DRS Inc. announced that **John Baylouny** has officially assumed the role of president and CEO, effective January 1, 2026. Baylouny is deeply rooted in the organization, bringing more than 35 years of experience across senior leadership, engineering, design, operations and P&L leadership roles. As COO, he oversaw the company's workforce across both operating segments and drove enterprise strategy for next-generation capability development. Backed by his deep experience, relentless drive for excellence and unwavering commitment to our warfighters. Baylouny's leadership marks a bold new chapter for Leonardo DRS, one that he believes will be defined by speed and innovation.

Design with Confidence. Source with Speed.

Fixed attenuators from the Spectrum Control brands you trust. Available at RFMW.

Powerfilm™

Chip Attenuators

Attenuation: up to 30 dB
Frequency: up to 40 GHz
Power: up to 250W
Cryo models also available

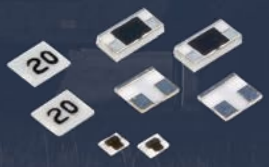

Inmet & Weinschel™

Coaxial Attenuators

Attenuation: up to 60 dB
Frequency: up to 50 GHz
Power: up to 500W
Cryo models also available

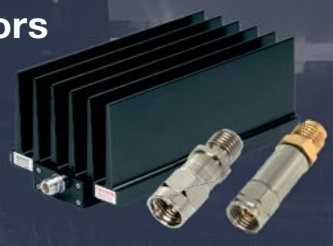

Model	Frequency	Power	DB Values in Stock
PCAAF Wrap around terminal & ground	DC-8 GHz	0.75 - 5W	1 - 12
PCAAW Wrap around ground	DC-18 GHz	0.75 - 4W	0 - 20
PCAA No wrap	DC-18 GHz	0.75 - 5W	1 - 8
PCAL Tabbed	DC-12.4 GHz	1.5W	1, 3, 12
PCAF Wrap around terminal & ground	DC-4 GHz	1.5W	0 - 5

Model	Frequency	Power	DB Values in Stock
18A - SMA *Hex connector available	DC-18 GHz	2W	0 - 40
40A – 2.9mm *Hex connector available	DC-40 GHz	0.5W	2, 11, 30
53 – Type N Conduction/ Convection Cooled	DC-2.5Gz	500W	3, 20, 30
50EH – 2.4mm (Hex)	DC-50 GHz	0.5W	3, 10, 30
86 – 3.5mm Conduction Cooled/ Bi-directional	DC-22 GHz	50W	3, 6, 10

Quick Links To In-Stock Attenuators

spectrumcontrol.com/rfmw-att

SPECTRUM CONTROL™

RFMW®

Around the **Circuit**

Richardson Electronics, Ltd. announced that **Rainer Bornwasser** has been appointed vice president of Global Sales for Canvys – Visual Technology Solutions, a division of Richardson Electronics, effective February 1, 2026. The appointment underscores Richardson Electronics' commitment to accelerating global growth, expanding strategic OEM partnerships and strengthening its position in high-value medical and industrial display markets through its Canvys division. Bornwasser brings more than 30 years of international sales and leadership experience across the medical technology and industrial display sectors.

▲ *Rainer Bornwasser*

▲ *Tom Kelly*

dBm Technical Sales announced that **Tom Kelly**, an accomplished RF and microwave engineering professional, has joined the company as a field sales engineer. Kelly brings over two decades of hands-on technical experience across design, testing, systems engineering and applications development within the defense and high performance semiconductor sectors. Kelly earned both his B.S.E.E. and M.S.E.E. degrees in microwave engineering from the University of Massachusetts, Lowell. Throughout his career, Kelly has held key engineering roles at Raytheon, NXP Semiconductors, MACOM and Mini Circuits, where he specialized in LDMOS and GaN RF power design. His work has supported mission-critical programs across radar, electronic warfare and next-generation communications, giving him deep insight into the challenges and requirements of defense-grade RF systems.

REP APPOINTMENTS

Insight SIP has appointed **Core Staff** as an authorized distributor for Japan, effective from the beginning of 2026. Core Staff is a major Japanese distributor, with both an online webshop service and a traditional field sales and support operation. This allows Core Staff to serve customers of all sizes across Japan effectively, offering the best of fast online service and in-person human contact. Headquartered in Tokyo, CoreStaff has seven offices across Japan, together with international subsidiaries in Hong Kong, China and Taiwan, as well as Thailand, U.S. and Germany. The international offices primarily support Japanese customers, either in the case of overseas manufacturing or sourcing of overseas components not readily available in Japan.

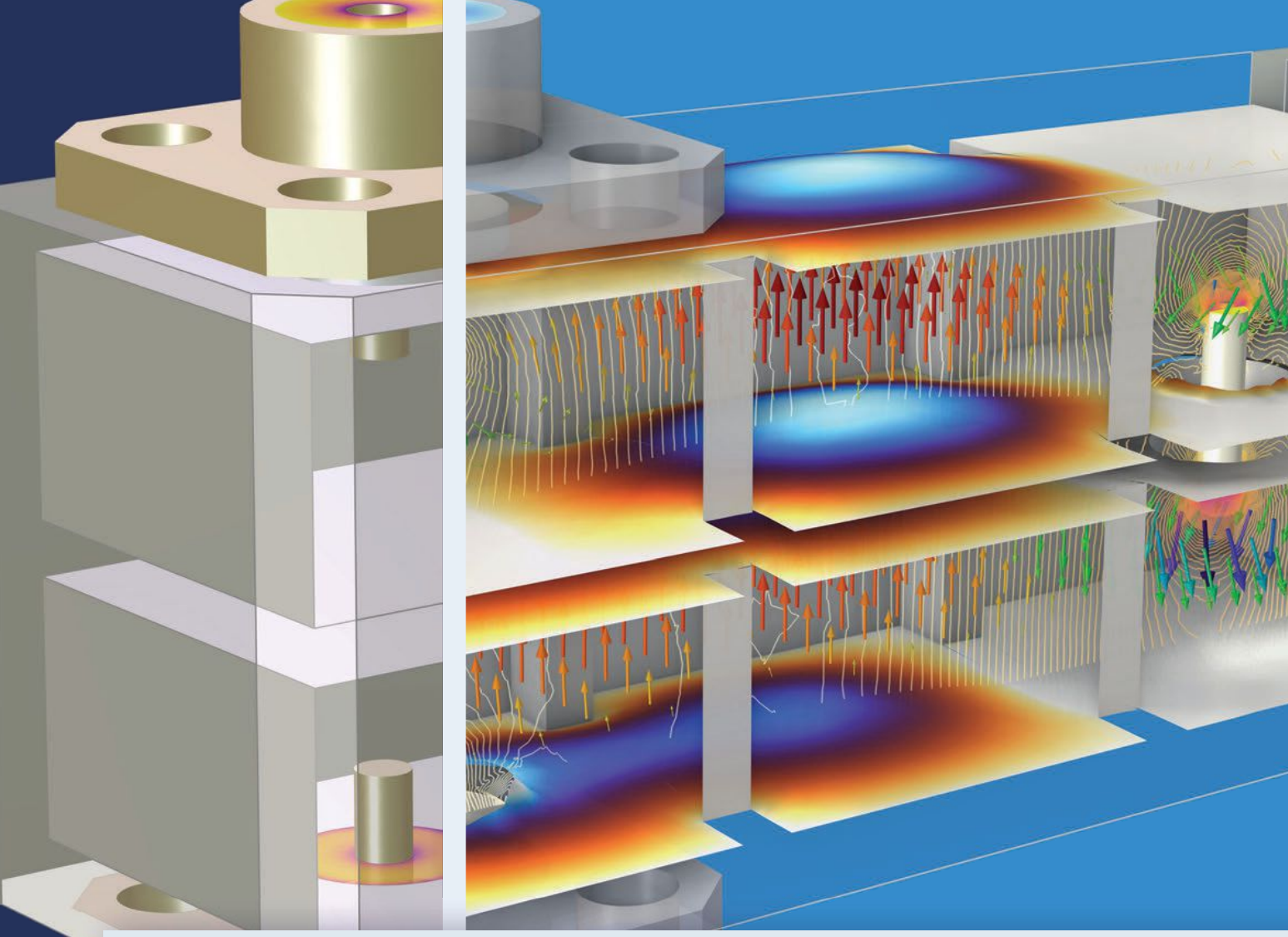

Take the Lead in RF Design

with COMSOL Multiphysics®

Multiphysics simulation is expanding the scope of RF analysis to higher frequencies and data rates. Accurate models of microwave, mmWave, and photonic designs are obtained by accounting for coupled physics effects, material property variation, and geometry deformation. Ultimately, this helps you more quickly see how a design will perform in the real world.

» *comsol.com/feature/rf-innovation*

COMSOL

INVITED PAPER

High Dynamic Range Low Noise Active Down-Conversion SiGe HBT Mixer with Dual-Feedback Linearization

Trusha Kared and Ulrich L. Rohde
Brandenburg University of Technology, Cottbus, Germany
Synergy Microwave Corporation, Paterson, N.J., USA

The increasing complexity of wireless communication systems necessitates careful optimization of noise performance, linearity and power efficiency in RF front-end designs. Among various silicon technologies, SiGe heterojunction bipolar transistors (HBTs) have emerged as the most compelling choice due to their superior high speed characteristics and well-controlled base parasitics. Their high transition frequency f_T and inherently low base resistance enable excellent noise behavior, making them particularly suitable for low noise, high-linearity applications. Owing to these advantages and their scalability, bipolar devices continue to serve as key building blocks in silicon-based RF front ends.

The proposed high performance SiGe HBT double-balanced down-conversion mixer integrates several advanced design techniques to enhance overall performance. A transformer-free single-ended-to-differential conversion network is employed to improve efficiency and eliminate bulky passive components at the RF input. To further enhance linearity, a dual-feedback linearization strategy is implemented, simultaneously optimizing impedance matching and minimizing harmonic distortion. In addition, a symmetric device layout combined with multilayer PCB technology effectively suppresses LO-to-RF feedthrough, reducing crosstalk and improving port isolation. Collectively, these design strategies yield a highly linear, low noise and power-efficient mixer architecture, establishing a new performance benchmark for SiGe HBT-based mixer implementations and offering a robust alternative to conventional CMOS-based solutions.

INTRODUCTION AND CIRCUIT ANALYSIS

The active mixer uses a differential transistor as a current switch. The base voltage controls DC current flow from the collector to the emitter. By switching the base voltage at the LO frequency, while the small-signal RF is present in the inverted DC signal, the two signals will multiply. Gain is achieved by amplifying the RF signal (voltage-to-current conversion) before switching. The pre-amplification of the RF signal improves the signal-to-noise ratio (SNR), reduces the impact of noise and distortions introduced by switch losses and simplifies the input voltage-to-current conversion.

The proposed circuit is shown in ***Figure 1***. The double-balanced mixer combines RF and LO signals while minimizing LO leakage at the IF output. This is achieved using two cross-coupled single-balanced networks that cancel in-phase and out-of-phase LO com-

RF-LAMBDA

THE LEADER OF RF BROADBAND SOLUTIONS

EUROPE DEUTSCHLAND

RF SWITCHES

MM / MICROWAVE DC-90GHz

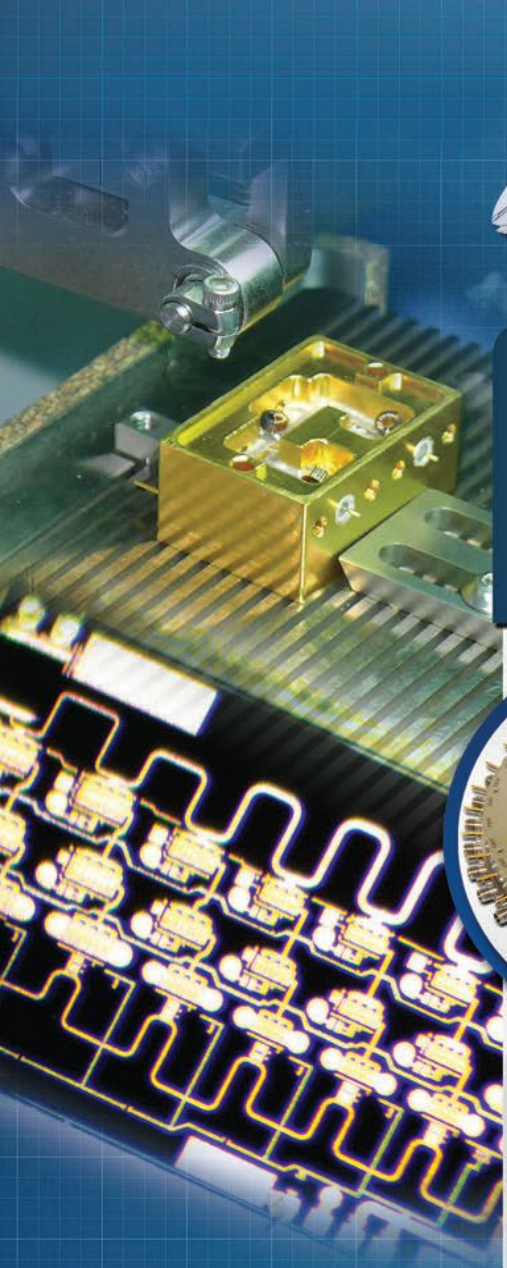

160 CHANNELS
mm/Microwave

0.05-20GHz
Filter Bank Switch Matrix
For Phase Array Radar Application Satellite communication.

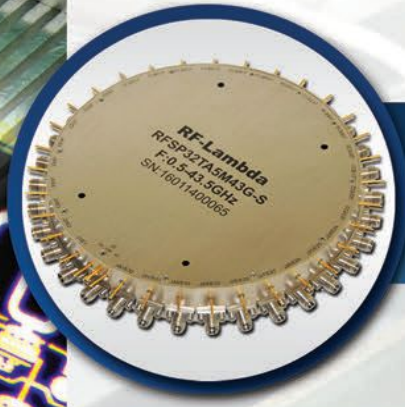

PN: RFSP32TA5M43G
SP32T SWITCH 0.5-43.5GHz

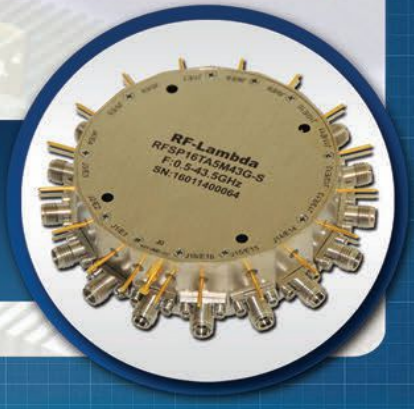

PN: RFSP16TA5M43G
SP16T SWITCH 0.5-43.5GHz

www.rflambda.com
sales@rflambda.com

1-888-976-8880
1-972-767-5998

San Diego, CA, US
Plano, TX, US
Ottawa, ONT, Canada
Frankfurt, Germany

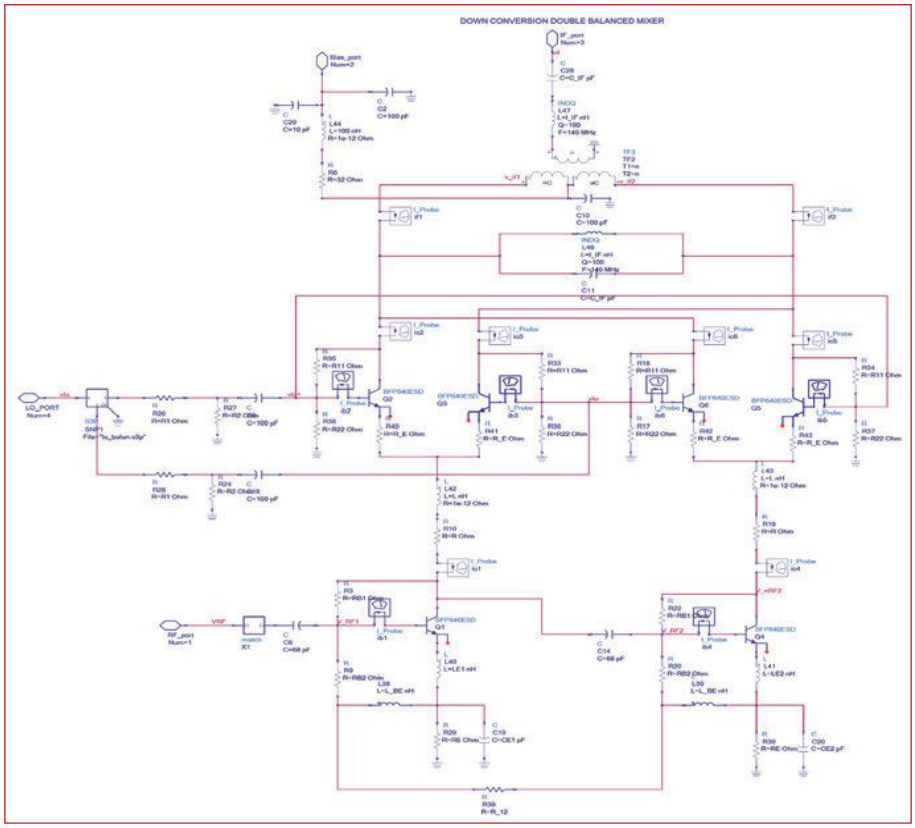

Fig. 1 **The architecture of a wideband double-balanced down-conversion mixer.**

ponents before the current-to-voltage conversion stage. For analysis purposes, we can divide the circuit into two halves, each representing an identical single-balanced mixer network. The first left-half circuit consists of Q1 at the RF stage, with Q2 and Q3 serving as the switching cores. In the second half circuit, Q4 is at the RF stage and Q5 and Q6 are LO switching cores.

The single-balanced bipolar transistor (BJT) mixer utilizes transistor nonlinearities to perform frequency conversion by mixing an RF signal (v_{RF}) with a local oscillator (v_{LO}). In this circuit (Figure 1), transistor Q1 modulates its collector current based on the RF input. The LO signal drives the differential pair (Q2 and Q3) in a push-pull configuration, alternately steering the modulated collector current of Q1 between the two branches. This produces a differential output current (i_2-i_3) that comprises the sum and difference frequency components ($f_{LO} \pm f_{RF}$). The differential output current i_{out} is expressed in ***Equation 1***.

$$i_{out} = \frac{(i_m - i_n)}{2} = i_{RF} \tanh\left(\frac{v_{LO}}{2V_T}\right) \quad (1)$$

Here, the tanh term captures the saturating behavior of the LO differential pair. The large signal component, i_{RF}, does not affect the output current. The double-balanced mixer effectively rejects the DC bias current component at the IF port, depending on current matching in the branches, load matching and the common-mode rejection of subsequent stages.

A down-conversion double-balanced Gilbert Cell Mixer with single-ended RF input and a fixed IF-tuned circuit with differential output at 145 MHz is presented in this work. The LO frequency sweep is from 355 to 1855 MHz and is fed differentially to the four LO transistors. The mixer is designed for a frequency range of 500 to 2000 MHz, and the RF signal is fed differentially (single-ended-to-differential conversion) to the RF transistor, as shown in Figure 1. This circuit consumes roughly 80 mW of power (supply voltage 4 V and total current 20 mA). The LO mixing core and RF stages are designed using Infineon high-linearity NPN SiGe BFP640 transistors and low noise NPN SiGe BFP840 transistors, respectively.

EXODUS ADVANCED COMMUNICATIONS

BUILT FOR SPEED.
ENGINEERED FOR POWER.

FINISH STRONG

AMP20102 / 2.0-8.0 GHz, 400W

RF & Microwave Amplifiers CW & Pulse

10 kHz-75 GHz

EXODUS

AMP10125
2.0-8.0 GHz, 70W

AMP20189
2.0-8.0 GHz, 20W

AMP20199
2.0-8.0 GHz, 40W

AMP20098
2.0-8.0 GHz, 120W

AMP20100
2.0-8.0 GHz, 200W

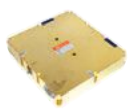

AMP10062
6.0-18.0 GHz, 40W

3674 E. Sunset Road, Suite 100, Las Vegas, Nevada 89120 USA
Tel : 1-702-534-6564 Email : sales@exoduscomm.com

At the output, a fixed IF frequency of 145 MHz, a parallel-tuned circuit is used as a load between the differential outputs. Due to the high impedance, the mixer's gain is maximum at its resonant frequency. The load impedance R_L of the tuned circuit is computed by determining the real part of R_L at resonance. Therefore, ***Equation 2*** is true.

$$R_L = (SL \parallel \frac{1}{SC}) \quad (2)$$

So, the total real part of the load can be expressed as ***Equation 3***.

$$\mathrm{Re}\{R_L\} = \sqrt{\frac{L}{C}} \quad (3)$$

A step-down transformer is used to combine the differential output at the IF port and match it to the 50 Ω output.

Each RF stage comprises multiple feedback loops to adjust for transistor nonlinearity. In addition, series feedback from the second stage to the first stage corrects the phase shift between the two RF currents, thereby improving the mixer's dynamic range. Each RF stage uses "dual-feedback linearization" to stabilize the current, with series inductive feedback at the input port and shunt resistive feedback at the output port controlling the output voltage, improving the transistor's nonlinear transfer characteristics and reducing voltage distortion.[1,2]

Because of series feedback, the mixing circuit is less affected by source impedance. It enhances input impedance matching, reducing RF stage noise and increasing the input SNR. The shunt feedback minimizes noise at the output and lowers the output impedance, making it easier for the circuit to match the load. Enhanced linearity, a higher distortion-free dynamic range and a low noise figure were the outcomes of the combination effect of series and shunt feedback. The design optimizes conversion gain, noise figure, linearity and dynamic range at 1000 MHz RF frequency and 145 MHz fixed IF frequency.

RF port differential driver optimization is the most important tradeoff. Here, a complex workaround is utilized in place of costly, potentially asymmetrical transformers like those found in diode mixers. The proposed approach involves a pre-driver stage that converts a single-ended line to a balanced line. As shown in Figure 1, the circuit employs a 180-degree phase shift in the first RF stage transistor to drive the second transistor. In ideal theory, the first RF common-emitter stage introduces a 180-degree phase shift between the base and collector. At the second step, the base-collector phase shift will be reset to zero degrees. However, the phase shift between two transistors is never completely optimal.

The gain of the second RF stage is g_m times higher than that of the first RF stage. Balanced differential signal pairs convey signals with the same amplitude but a 180-degree phase change. If differential signaling is not properly balanced, it can cause interference or crosstalk,[3] resulting in common-mode noise or voltage at the IF port. As a result, the gain at the second RF stage must be reduced to match the first stage's performance. This can be accomplished by emitter degeneration in the second RF stage. With the specified impedance, both RF stages are emitter-degenerated, enhancing input stage linearity while also providing noise and power matching.

A: CONVERSION GAIN

Figure 1 shows that the double-balanced mixer uses two voltage-dependent current sources. Moreover, both current sources have equal bias currents; the IF port current switches between $g_m V_{RF}$ and $-g_m V_{RF}$. The DC biasing current I_{bias} is balanced because it always flows through both loads. As a result, the differential output voltage V_{IF} is unaffected by the biasing current. The IF port current can be described in ***Equation 4***.

$$I_{IF} = g_m V_{RF} \left\{ \begin{array}{l} \frac{2}{\pi}\cos(\omega_{RF} - \omega_{LO}) + \\ \frac{2}{\pi}\cos(\omega_{RF} + \omega_{LO}) + \\ \frac{2}{3\pi}\cos(\omega_{RF} - 3\omega_{LO}) + \\ \frac{2}{3\pi}\cos(\omega_{RF} + 3\omega_{LO}) + \\ \ldots \end{array} \right. \quad (4)$$

The voltage conversion gain of a double-balanced down-conversion mixer is the ratio of the output am-

ATEK MIDAS

DC to 100 GHz MMICs
Custom Silicon RFICs & Mixed-Signal ASICs

Advanced Switched & Tunable MMIC Filters to 18 GHz

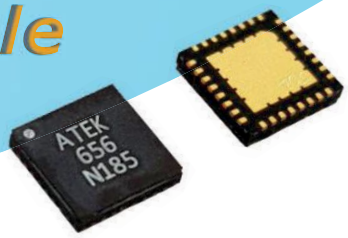

Fast, High Rejection, Compact Filters from Stock

Filter Topology	Part #	Frequency Range	Filter Bands	Loss (dB)	Rejection (dBc)	IIP3 (dBm)	Tuning Speed (nS)	Supply	Package (mm)
Tunable BPF + Dual Bypass	ATEK884P5	1 – 7.5 GHz	32	9	40	+40	260	+5V @ 7 mA	5×5 QFN
Tunable BPF	ATEK873N4	8 – 18.5 GHz	Analog	7	50	+28	100	0 to +8V	4×4 QFN
Tunable LPF	ATEK821P4	1 – 2.5 GHz	15	2.5	50	+45	130	+5V @ 0.5 mA	4×4 QFN
Tunable LPF	ATEK822P4	0.35 – 1.1 GHz	15	2.5	40	+45	150	+5V @ 0.5 mA	4×4 QFN
Tunable LPF	ATEK889P4	1.5 – 3.35 GHz	16	3	60	+40	130	+5V @ 1.5 mA	4×4 QFN
Tunable LPF	ATEK888P5	20 – 530 MHz	32	2	45	+44	250	+5V @ 8 mA	5×5 QFN
Tunable HPF	ATEK890P4	1 – 1.95 GHz	16	2	55	+52	130	+5V @ 2 mA	4×4 QFN
Switchable Sub-Octave BPF Bank	ATEK656N5	2 - 18 GHz	6	6.5	45	+33	150	+5V @ 12 mA	5×5 QFN
Switchable Sub-Octave BPF Bank + Bypass	ATEK950P6	485 – 8000 MHz	7	6	45	+43	150	+5V @ 15 mA	6×6 QFN

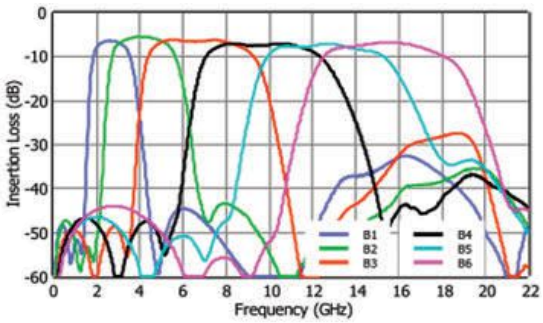

ATEK656N5 2-18GHz Switchable BPF

- *150nS Tuning Speed*
- *+33dBm Input IP3*
- *45dBc Rejection*
- *Ideal for SDRs & AESAs*

Specializing in Custom Filter Solutions Including EOL Replacements

We offer a wide range of catalog MMIC products

- ✓ Driver Amps, LNAs, Power Amps,
- ✓ Switches, Attenuators, Phase Shifters,
- ✓ Mixers, Passives, Equalizers,
- ✓ Die, SMT & Connectorized Modules

ATEK Midas applies novel expertise, creativity, and passion to design high performance analog, mixed-signal silicon ASICs & RFICs, advanced GaAs & GaN MMICs, RF Modules, & Integrated Microwave Assemblies for communication & sensor applications to 100 GHz.

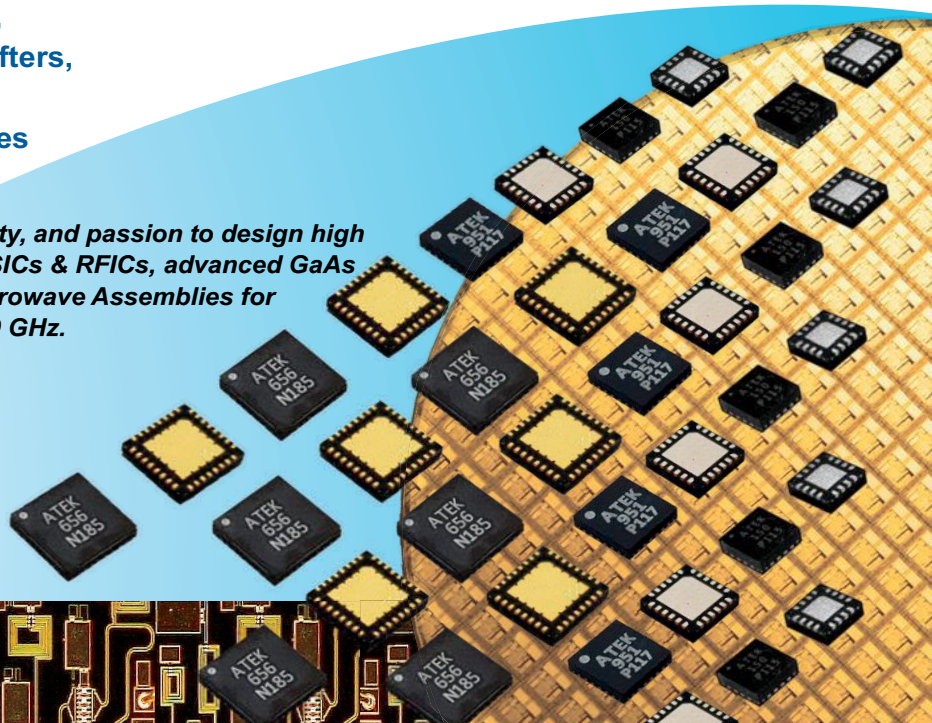

sales@atekmidas.com

www.ATEKMIDAS.com

plitude to the input amplitude and can be written as ***Equation 5***:

$$GC = \frac{2}{\pi} g_m R_L = \frac{2}{\pi} \frac{I_{tail}}{2V_T} R_L \qquad (5)$$

For the emitter degeneration case, the effective transconductance g_m can be written as shown in ***Equation 6***.

$$g_{m\_eff} = \frac{g_m}{1 + g_m Z_E} \qquad (6)$$

while emitter degenerating impedance Z_E can be found using ***Equation 7***.

$$Z_E \approx \left(SL_E + \left(R_E \parallel \frac{1}{SC_E} \right) \right) \qquad (7)$$

with the calculated value of $Z_E \approx 21.983+j19.577$ and $|Z_E| \approx 29.436\ \Omega$.

From Equations 2 and 3 the total real part of

$$R_e\{R_L\} = \sqrt{\frac{L}{C}} \approx \sqrt{\frac{560\,nH}{2.2\,pF}} \approx 503.94\ \Omega \approx 227\ \Omega$$

(connected to ground)

The input impedance Z_{in} of the double balance mixer at RF frequency, looking into the base of the RF transistor Q1, is determined by the feedback element R_{B1} and the degenerative impedance Z_E. Therefore, ***Equation 8*** is true,

$$re\{Z_{in}\} \approx R_{B1} \parallel (r_b + \frac{\beta}{g_m} + Z_E) \qquad (8)$$

and the effective transconductance g_{m_eff} at the mixing frequency of 145 MHz is 0.182 S and is shown in ***Figure 2***.

So, the voltage conversion gain can be expressed by ***Equation 9***.

$$A_v = \frac{2}{\pi} g_{m\_eff} R_L = \frac{2}{\pi} \frac{g_m}{1 + g_m R_E} R_L = \frac{2}{\pi} \frac{0.182 * 227}{1 + (0.182 * 29.436)} \approx 12.338\ dB \qquad (9)$$

The measured value was about 12.64 dB.

B: TOTAL MIXER NOISE DOWN-CONVERTED TO THE IF PORT

The presence of noise in nonlinear circuits presents a complex challenge that requires careful analysis.

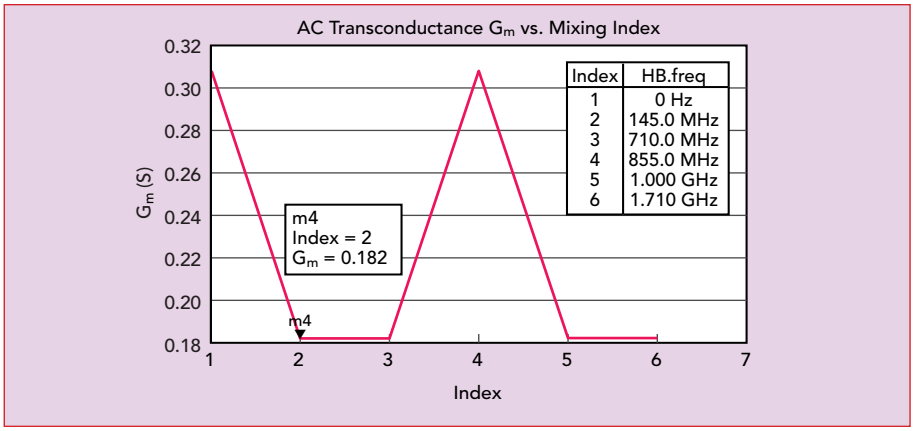

Fig. 2 **AC transconductance of the BJT Mixer.**

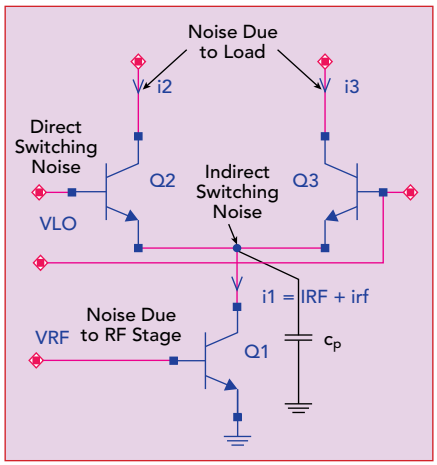

Fig. 3 **The primary noise sources in the single-balanced mixer.**

Noise sources are typically considered to be stationary in linear circuits.[4,5] The noise produced by a mixer exhibits periodic variation. The resulting noise processes are classified as cyclo-stationary,[6,7] in which the dominant noise sources are switched on and off by the local oscillator. ***Figure 3*** depicts the key mechanisms that contribute to noise, emphasizing the principal sources and outlining a basic approach for calculating noise spectral densities in a single-balanced mixer. The overall noise figure is determined by aggregating both linear noise sources and those influenced by the circuit's periodic and time-varying characteristics.[8,9]

In a double-double-balanced mixer, the noise contribution at the intermediate frequency (IF) port is doubled as a result of the presence of two transconductance stages and switches. An in-depth examination of the mixer noise sources and their contributions to the IF port is presented by T. Kared.[1] The total noise at the mixer output can be expressed as ***Equation 10***.

Therefore, the input referred noise of the given mixer is shown in ***Equation 11***.

$$\overline{V_{ni,total}^2} = \frac{1}{(gain)^2} \overline{V_{n0,total}^2} \qquad (11)$$

$$\overline{V_{n0,total}^2} = \overline{V_{n,R_L}^2} + 2\left(\overline{I_{n0,s}^2}\right) R_L^2 + \overline{V_{n,o\_RF}^2}$$

$$\overline{V_{n0,total}^2} = 4KTR_L^2 \left[\frac{2}{R_L} + 2\left((2r_{b2} g_m + 1) \left(\frac{I_{RF}}{\pi V_{LO}} \right) \right) + 2\left(g_m^2 \left(r_{b1} + \frac{1}{2g_m} \right) \right) \right] \qquad (10)$$

Where: K = Boltzmann constant
T = Temperature in Kelvin (290 K)
I_{RF} = DC bias current or tail current
r_{b1} = Internal base resistance of RF stage
r_{b2} = Internal base resistance of switching stage
g_m = Transconductance of mixer, in this case, it is g_{m_eff}
V_{LO} = Amplitude of the LO signal

Dalicap
DALICAP TECH. CORPORATION

Microwave / RF Ceramic Capacitor

DLC75 Series
Ultra-Low ESR,RF/Microwave MLCC

Product Features:

Ultra-low ESR value,high working voltage, high RF power,high self-resonant frequency.

Product Application:

VHF/LHF/Microwave communication system,communication base station, repeater station,WiMAX.

Size:

0201, 0402,0603, 0805, 0708, 1111

DLc75P capacitance List

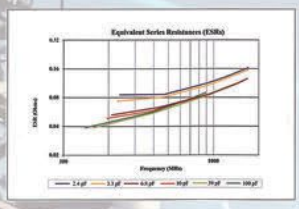

Equivalent Series Resistances (ESRs)

Horizontal & Vertical First Parallel Resonances

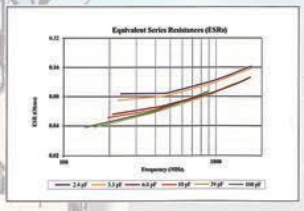

Horizontal & Vertical First Series Resonances (FSRs)

Ceramic Circuit Board

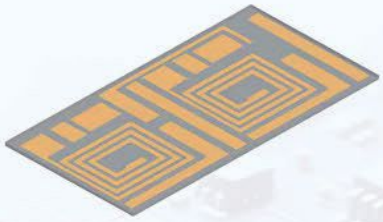

Product Features:

- Excellent heat dissipation performance
- High mechanical strength
- Superior reliability
- Compatible with RF high-power loads

Product Application:

High-power semiconductor equipment, new energy, LED, microwave communication, lasersystem and other fields.

Size:

Custom size is available

Dalicap

Dalicap Tech. Corporation is a global leader in Precision RF/Microwave Solutions. As the No.1 leader in China’s RF capacitor niche market and ranked among the top globally, Dalicap is a trusted strategic partner for Tier-1 international market leaders in medical MRI and semiconductor RF power sectors.

We provide high-performance solutions through a fully self-controlled manufacturing process, offering a comprehensive portfolio including High Q MLCCs, SLCCs,Power Capacitor Assemblies (Modules),Bracket Capacitors,Thin Film circuits and DPC ceramic PCBs for high-power RF modules.

Our veteran R&D teams ensure rapid response to customized requests, leveraging a unique RF lab and specialized testing to guarantee superior product realization in the world’s most demanding RF environments.

www.dalicap.com dalicap@dalicap.com +86-411-87632359

Substituting Equation 10 into 11, we get ***Equations 12*** and ***13***.

$$\overline{V_{ni,total}^2} = \frac{4KTR_L^2\left[\frac{2}{R_L}+2\left(\left(2r_{b2}g_m+1\right)\left(\frac{I_{RF}}{\pi V_{LO}}\right)\right)+2\left(g_m^2\left(r_{b1}+\frac{1}{2g_m}\right)\right)\right]}{\left(\frac{2g_{m1}R_L}{\pi}\right)^2} \quad (12)$$

$$\overline{V_{ni,total}^2} = \pi^2 KT\left[\frac{2}{g_m^2 R_L}+2\left(r_{b1}+\frac{1}{2g_m}\right)+\left(\frac{2}{g_m^2}\left(2r_{b2}g_m+1\right)\left(\frac{I_{RF}}{nV_{LO}}\right)\right)\right] \quad (13)$$

So, the single-sideband noise figure SSB[10] can be given as ***Equation 14***.

$$NF_{SSB} = 1+\frac{\overline{V_{ni,total}^2}}{4KTR_S} \quad (14)$$

The IF spectrum will not contain any image frequencies due to the selectivity of the 145 MHz IF filter at the IF port. The resulting noise figure is single-sideband (SSB), not double-sideband (DSB). ***Figure 4*** shows the simulated and measured conversion gain and noise figure as functions of RF frequency. The measured results exhibit a conversion gain of 12 dB ± 1 dB and a noise figure of 7 dB ± 0.4 dB over the frequency range of 600 MHz to 1.8 GHz, while the simulated results show a conversion gain of 11.4 dB ± 0.5 dB and a noise figure of 8 dB ± 0.2 dB across 500 MHz to 2 GHz. The IF frequency is down-converted to 145 MHz. Thus, the LO frequency is 145 MHz below the RF frequency. The LO balun frequency response determines the LO bandwidth. The LO and RF signals are AC-coupled via a coupling capacitor, which determines the lower frequency limit. At higher frequencies, parasitics (primarily substrate capacitance) from the board layout are prevalent and cannot be accurately modeled. This is the main reason the measured gain and noise figure bandwidth are lower than the simulated values.

From Figure 4, the measured noise figure of the mixer is lower than the simulated value. According to Friis' formula, the input stage dominates the overall noise figure, with later stages contributing less. The mixer's total noise mainly depends on each transistor's internal base resistance and transconductance of each device; higher base resistance increases thermal noise and degrades SNR. Lower base resistance thus improves noise performance. The discrepancy between measured and simulated results likely arises from modeling inaccuracies and conservative SPICE parameter data in the ADS simulator, which limit simulation accuracy.

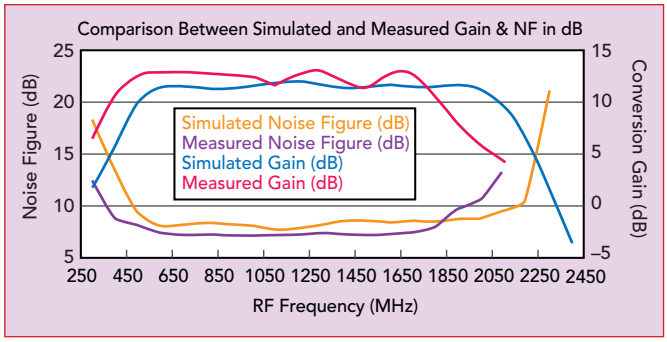

▲ **Fig. 4 Comparison between simulated and measured data as a function of the RF frequency.**

C: LINEARITY

The dynamic range of the mixer limits most communication systems. The linearity of the mixer relies on the RF transconductance stages, the LO switches and the tail current source. If the LO switches are ideal, the impedance observed at the emitters of Q2 and Q3 corresponds to that of the common-base stage, i.e., $1/g_{m2,3}$.[11] The voltage gain at the collector terminal of Q1 is minimal, i.e, $g_{m1}/(g_{m2,3})$; therefore, the input third-order intercept point (IIP_3) of the mixer is governed by the RF transconductance stage Q1, rather than the LO switching core.[11] Since only the RF signal should be fed back to linearize the RF stage, the LO and IF signals should be minimized at the RF port to maintain port-to-port isolation. The collector currents of Q2, Q3, Q5 and Q6 are combined such that the RF and LO signals cancel at the IF ports. Applied feedback exclusively linearizes the RF stages; however, it does not affect the mixing stages. Concurrently, shunt-voltage feedback (Figure 1) is established between the collector of Q1 and the RF signal port node via resistor R_{B1}. The analysis uses a large signal and the Ebers-Moll equation.

$$I_f = \frac{\left(\left(\alpha_F \cdot \frac{\alpha_F \cdot I_{bias}}{\left(e^{\frac{-((V_{RF^+})-(V_{RF^-}))}{V_T}}+1\right)}\right)\right)}{\frac{(R+sL)-V_{\_RF1}}{R_{B1}}} \quad (15)$$

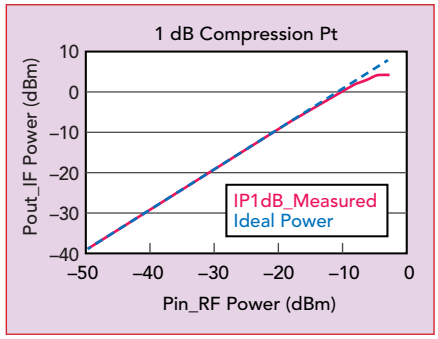

▲ **Fig. 5 Measured compression characteristic of the down-conversion double-balanced mixer prototype.**

Equation 15 indicates that there are no terms involving the LO and IF signals. As a result, this current can be fed back to the input RF to help linearize the RF stage. The subsequent derivation shows that undesired signals are canceled at the IF port, as expected from the series feedback equation. Therefore, dual-feedback can be employed to improve circuit linearization. The detailed derivation of Equation 15 is provided by T. Kared.[1]

Figure 5 shows the measured compression characteristic of the down-conversion double-balanced mixer as a function of RF input power. Here, f_{LO}=855 MHz and f_{RF}=1000 MHz, and the RF power increases in each measurement. The mixer exhibits an uncompressed gain of about 10.79 dB, which drops by 1 dB at an input power of -8 dBm.

Figure 6 illustrates the two-tone intermodulation test results used to determine the IIP_3 and output third-order intercept point (OIP_3) of the down-conversion double-balanced mixer prototype. The x-axis represents the applied RF input power (dBm), while the y-axis shows the corresponding IF output power (dBm). The red curve denotes the

MCV MICROWAVE + TELONIC BERKELEY

ITAR Compliant International Traffic in Arms Regulations

AS 9120B REGISTERED COMPANY

ISO 9001:2015 CERTIFIED COMPANY

MCV Microwave and Telonic Berkeley have merged and operating as sister companies. Together, we design and manufacture custom RF components, value-added sub-assemblies and complete system solutions including:

- Switches
- Resonators
- Antennas
- Connectors
- Fixed & tunable filters
- Multichip modules
- Switched filter banks
- High-power cables
- Waveguide adapters
- Power amplifiers (SSPAs)
- Ultra-high-Q dielectrics

Design and manufacturing available on both the East and West Coasts.

Fixed & Tunable Filters

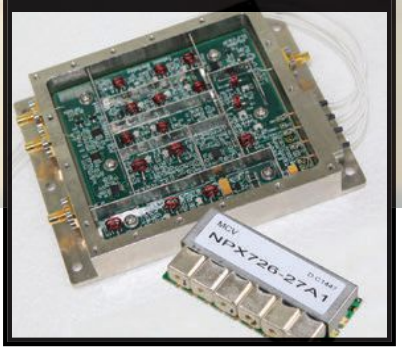

Broadband Couplers up to 67GHz

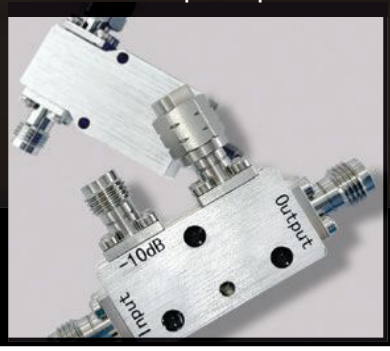

Manual / Digital Step Attenuators

LNA / SSPA Amplifiers

RF Switches up to 110GHz

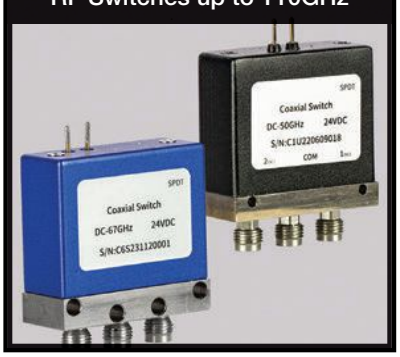

RF / mmWave Sub Assemblies

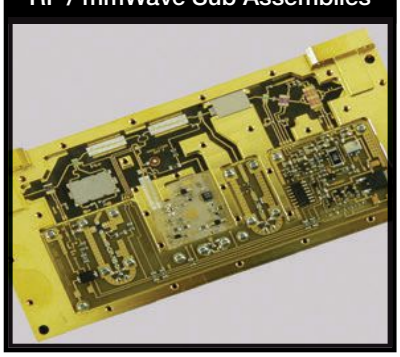

WEST COAST:
Telonic Berkeley Inc.
(760) 473-4811
info@telonicberkeley.com

Made in USA

EAST COAST:
MCV Microwave
(302) 877-8079
sales@mcv-microwave.com

fundamental IF output power, which increases linearly with the RF input up to the compression region. The orange curve represents the third-order intermodulation (IM_3) products, which rise at approximately 3x the rate of the fundamental tone. The linear extrapolations of both lines intersect at the IIP_3 point, marked on the plot.

To determine the mixer's IIP_3, two input tones at 999.95 and 1000.05 MHz, each with a power level of -30 dBm, were applied. A 3 dB power divider separated two RF tones, producing IF outputs at 144.95 and 145.05 MHz, with third-order intermodulation products at 144.85 and 145.15 MHz. The third-order intercept point can be calculated using ***Equation 16***.

$$IIP_3 = P_{in} + \frac{\Delta P}{2} \quad (16)$$

Where P_{in}=-30 dBm and $\Delta P = P_{out} - P_{IM3}$

Now, for a lower sideband tone, $\Delta P = P_{out} - P_{IM3}$=-21.93-(-90.11)=68.18, therefore IIP_{3_LSB}=4.09 dBm. For the upper sideband tone, $\Delta P = P_{out} - P_{IM3}$=-21.73-(-91.13)=69.40, so IIP_{3_USB} =4.7 dBm. The OIP_3 point is simply IIP_3+Gain, which results in an approximate calculated OIP_3 point of about 15 dBm.

The noise floor of the circuit is about -166 dBm. The IP3 and 1 dB compression points are roughly 5 dBm and -8 dBm, respectively, so the available dynamic range can be calculated as (-174 dBm - 1 dB compression point + NF). This yields approximately 159 dBm/Hz for the available dynamic range. ***Table 1*** compares the simulated and

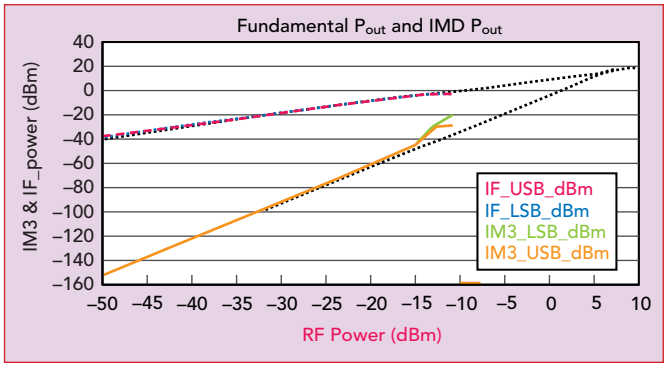

▲ Fig. 6 **Extrapolation of the IP3 point at an RF frequency of 1 GHz.**

TABLE 1

COMPARISON BETWEEN SIMULATED AND MEASURED RESULTS AFTER OPTIMIZATION[1]

Parameter Metrics	*Simulated Performance*	*Measured Performance*	*Calculated Performance*
RF Frequency	1 GHz	1 GHz	1 GHz
LO Frequency	855 MHz	855 MHz	855 MHz
Mixer Bandwidth	0.5 to 2.1 GHz constant IF of 145 MHz	0.5 to 1.8 GHz constant IF of 145 MHz	-
Conversion Gain Bandwidth	11.4 ± 0.5 dB	12 ± 1 dB	12.338 dB (predicted conversion gain)
Noise Figure	8 dB	7.03 dB	7.96 dB (predicted)
1 dB Compression Point	-6.9 dBm	Between -9 and -8 dBm	-
IIP_3 Measurement	6.716 dBm	4.7 dBm	-
OIP_3 Measurement	17.9 dBm	15 dBm	
L-I Isolation	-65 dB	-58 dB	-
L-R Isolation	-65 dB	-70 dB	-
RF Port Return Loss	Better than -12 dB	Better than -8 dB	-
LO Port Return Loss	Better than -10 dB	Better than -8 dB	-
IF Port Return Loss	-26 dB at 145 MHz	-20 dB at 145 MHz	-

Next-generation Coaxial Components to 110 GHz

Metrology-grade solutions with robust MIL-202F environmental ratings

Components for Passive and Active Measurements

Anritsu offers the largest line of W1 coaxial components that provides direct connect millimeter-wave (mmWave) applications from EW testing to optical correction and device characterization. With coverage from nearly DC to 110 GHz, these components provide a substantial benefit to customers as most test systems now feature a coaxial interface that provides a direct-connect operation and avoids the use of adapters.

- Operable from low frequency to 110 GHz, allowing for broadband frequency scalability
- Direct connection 1.0 mm test port
- Saves setup time and complexity by having a common interface between DUT, test ports, and components
- Offers flexibility for measurements by providing new component types where limited or non-existent component solutions exist
- True parameter performance through guaranteed electrical performance

W255MF
Bias Tee

41W Series
Fixed Attenuators

W241A
Power Splitter

W240A
Power Divider

MN25110A
Directional Coupler

W252FM
Kelvin Bias Tee

Anritsu
Advancing beyond

Discover how you can achieve measurement confidence with Anritsu.
Learn more at **www.anritsu.com/en-us/components-accessories**

measured parametric performance of the down-conversion double-balanced mixer.

CONCLUSION

A new approach to designing a double-balanced mixer without the need for a bulky transformer at the RF stage is presented in this work. By implementing the dual-feedback linearization technique here, the voltage and current at the RF stages can be linearized, improving the nonlinear transfer characteristics and increasing IIP_3 and the 1 dB compression point while maintaining a noise of about 7 dB and a gain of about 12 dB. ■

ACKNOWLEDGMENTS

This research, conducted as part of Trusha Kared's Ph.D. dissertation, was carried out under the distinguished supervision of Prof. Dr.-Ing. habil., Ulrich L. Rohde, Prof. Dr.-Ing. Matthias Rudolph and Prof. Dr.-Ing. Ignaz Eisele (EMFT-Fraunhofer München, UniBW), in collaboration with Synergy Microwave Corporation and the Brandenburg University of Technology. The dissertation embodies a rigorous integration of theoretical development and experimental innovation in high frequency circuit design. Its significance was further recognized through a presentation at the Massachusetts Institute of Technology (MIT) Microsystems Technology Laboratories (MTL), highlighting its contribution to advancing state-of-the-art RF and microwave engineering research.

References

1. T. Kared, "Mathematical Analysis, Design, and Validation of a High Dynamic Range, Low Noise Differential Mixer using SiGe Microwave Transistors," 2025, Web: https://doi.org/10.26127/BTUOpen-712.
2. T. Kared, H. Silaghi, M. Rudolph, A. Silaghi and U. L. Rohde, "Design of a Fixed IF Down-Conversion Double-Balanced Mixer for UHF Band Applications," *Sensors 2025*, 25, 608, Web: https://doi.org/10.3390/s25030608.
3. "The Advantages of Differential Signaling," Cadence, Web: https://resources.system-analysis.cadence.com/blog/msa2021-the-advantages-of-differential-signaling.
4. U. L. Rohde and M. Rudolph, "RF/Microwave Circuit Design for Wireless Applications," John Wiley & Sons, Hoboken, N.J., Second Edition, 2012.
5. G. D. Vendelin, A. M. Pavio and U. L. Rohde, "Microwave Circuit Design Using Linear and Non-Linear Techniques," John Wiley & Sons Inc., Second Edition.
6. J. Roychowdhury, D. Long and P. Feldmann, "Cyclostationary Noise Analysis of Large RF Circuits with Multitone Excitations," *IEEE Journal of Solid-State Circuits*, 33(3):324-336, March 1998.
7. W. A. Gardner, "Cyclostationary in Communication and Signal Processing," *IEEE*, Piscataway, N.J., 1993.
8. C. D. Hull and R. G. Meyer, " A systematic Approach to the analysis of Noise in Mixers," *IEEE Transactions on Circuits and Systems*, 40(12), December 1993.
9. H. Darabi and A. A. Abidi, "Noise in RF-CMOS Miners: A Simple Physical Model," *IEEE Transactions on Solid-State Circuits*, Vol. 35, No. 1. January 2000, pp. 15-25.
10. B. Razavi, "RF Microelectronics," Prentice Hall Inc., New Jersey, 1998.
11. R. G. Meyer, "Intermodulation in High-Frequency Bipolar Transistor Integrated-Circuits Mixers," *IEEE Journal of Solid-State Circuits*, SC-21(4):534-537, August 1986.

Ultra-Flex 110 GHz Low-Loss Cables

Precision 1.0mm | 12" Test Solutions
in Male-Male & Male - Female

VSWR
1.35:1 max

INSERTION LOSS
5.2dB max

SPEED GUARANTEE
Ships in 24 hours

STARTING FROM
$1,328 /piece

INVENTORY READY IN
U.S. & Canada

PRODUCT ASSURANCE
4 months warranty

LEARN MORE

URF

INVITED PAPER

Accelerating Antenna Design Exploration with Neural Network Surrogate Models

Daniel Smith
PhysAI, LLC, Newport, R.I.

Modern antenna development often involves balancing electrical performance, manufacturability, material constraints, cost and thermal management. Rigorous full-wave simulation of parameterized antenna geometries can be computationally intensive, given the fact that there can be up to a dozen geometrical parameters, making design exploration and antenna performance studies difficult. PhysAI has developed a workflow using COMSOL Multiphysics to generate high-fidelity surrogate models that learn the mapping between geometric design parameters and antenna S-parameters over a set frequency range. Once trained, these neural-network-based surrogate models evaluate in milliseconds, enabling real-time design iteration and interactive performance visualization.

This approach allows product managers and RF engineers to jointly explore the design space, assess tradeoffs and identify solutions that balance performance with practical constraints, rather than relying solely on global optimization. Designs that offer near-optimal performance, but improved manufacturability, become easier to identify and robustness analyses can be performed rapidly by sampling around nominal solutions. A real-world antenna test case is studied in the field of RFID tag localization, where antenna impedance matching, gain and far-field pattern are crucial to overall performance. The workflow demonstrates how surrogate modeling accelerates early-stage design and reduces the number of full numerical simulations required. The outcome is a faster, more transparent antenna development process, one where performance and product constraints can be balanced dynamically as opposed to being discovered late in the design cycle.

INTRODUCTION

Antennas are fundamental components in wireless communication systems, ranging from mobile devices and IoT sensors to satellite communications and radar systems. As wireless technologies advance, particularly with the proliferation of 5G/6G networks, RFID systems and autonomous vehicles, the demands on antenna performance have intensified. Modern antennas must deliver high gain, wide bandwidth, specific radiation patterns and efficient impedance matching while adhering to strict constraints on size, cost, materials, manufacturability and thermal dissipation.

Traditional antenna design relies heavily on full-wave electromagnetic (EM) solvers such as COMSOL Multiphysics, ANSYS HFSS or CST Microwave Studio. These tools provide high-fidelity predictions of antenna behavior through finite element method (FEM), method of moments (MoM) or finite-difference time-domain (FDTD) techniques. However, each simulation can take minutes to hours, depending on geometry complexity and frequency resolution. When

SMASHING Performance BARRIERS

ATTENUATORS

FILTERS

EQUALIZERS

HLM-67ABH

DC to 67 GHz Limiter

MULTIPLIERS

LIMITERS

Packaged to PERFORM

Marki Microwave's connectorized bullet housing is a cost-effective packaging solution for 2-port passive products, delivering industry-leading performance from DC to 67 GHz. Customizable across Marki Microwave's extensive bare-die portfolio, the technology supports attenuators, equalizers, filters, multipliers and limiters – including Marki Microwave's new HLM-67ABH, a DC to 67 GHz limiter featuring low 1.35 dB Typical Insertion Loss, +7 dBm Flat Leakage and +24 dBm Input IP3.

- **DC-67 GHz Operation**
- **High-Performance, Low-Loss, Inline housing**
- **Supports 2-Port Products**
- **Customizable across Marki Microwave's bare die catalog**

RFMW®

Global Distribution Partner

Contact: sales@rfmw.com

Marki® microwave

The Trusted Leader When Performance Matters

www.markimicrowave.com

optimizing or exploring designs with 10 to 15 geometric parameters, (e.g., patch dimensions, feed positions, substrate thickness, slot lengths) the computational burden becomes prohibitive. A large parametric sweep might require thousands of simulations, consuming days or weeks of compute time.

This bottleneck limits early-stage design exploration, where engineers and product stakeholders need to evaluate trade-offs collaboratively. Global optimization algorithms can identify theoretical optima, but they often yield designs that are difficult to manufacture or sensitive to tolerances. Late discovery of these practical issues leads to costly iterations.

Machine learning (ML)-based surrogate models offer a powerful solution. By training neural networks on data from a manageable number of high-fidelity simulations, surrogates can approximate EM responses in milliseconds. This enables interactive exploration, rapid sensitivity analysis and multi-objective trade-off visualization.

PhysAI has developed an end-to-end workflow leveraging COMSOL Multiphysics for training data generation and neural networks for surrogate modeling. The following sections describe the approach, workflow details and a practical case study in RFID tag localization.

CHALLENGES IN CONTEMPORARY ANTENNA DESIGN

Antenna design is inherently multi-objective. Key electrical metrics include return loss (S_{11}) for impedance matching, bandwidth, gain and directivity and radiation pattern shape (e.g., omnidirectional versus directional). These must be balanced against practical constraints, such as size and form factor (especially for mobile/IoT), material availability and cost, manufacturing tolerances (e.g., etching precision, dielectric variability), thermal management in high-power applications and integration with other components.

In traditional workflows, RF engineers perform iterative simulations, often guided by experience or single-objective optimization. Product managers enter later, assessing feasibility only after significant design investment. This sequential process risks "perfect" designs that fail in production.

SURROGATE MODELING APPROACH

Surrogate models approximate expensive simulations using data-driven techniques. In EM design, neural networks excel at learning complex mappings from geometric parameters to frequency-dependent outputs like S-parameters.

The PhysAI workflow uses fully connected deep neural networks (DNNs) trained on S-parameter values across a frequency range. Inputs are normalized geometric parameters or material properties; outputs are vectorized S-parameter responses. This formulation captures broadband behavior accurately.

Once trained, the surrogate enables:

- Real-time prediction (milliseconds versus minutes)
- Monte Carlo sampling for thousands of designs
- Gradient-based or global optimization
- Interactive visualization tools for non-experts.

DETAILED WORKFLOW

The workflow comprises six phases, as demonstrated in ***Table 1***.

1. **Parameterization Determination and Sampling**: Define geometric parameters and bounds based on requirements and constraints. Use Latin Hypercube Sampling (LHS) to generate 200 to 1000 designs efficiently covering the space.
2. **Physics Model**: Set up a detailed 3D physics model of the electromagnetic wave propagation in COMSOL and test some nominal cases.
3. **High-Fidelity Data Generation:** Run batch COMSOL simulations

Generate Any Signal. Anywhere, Anytime.

Get the performance and versatility of an enterprise-grade vector signal generator in a compact form factor.

The VSG200 from Signal Hound is a 20 GHz vector signal generator with 40 MHz of real-time streaming bandwidth, capable of generating virtually any signal type. A low phase noise, agile local oscillator with 200 µs switching enables fast frequency-hopping and spread-spectrum testing. A compact form factor and expanded software functionality make the VSG200 a powerful, flexible tool for advanced RF test applications.

Signal Hound®

SignalHound.com Made in the USA

TABLE 1

OVERVIEW OF THE SURROGATE-ASSISTED ANTENNA DESIGN WORKFLOW

Determine available parameterization variables
Set up parameterized electromagnetic model for some nominal conditions
Compute S-parameter training data using an optimally sampled parametric space
Train a deep neural network on the S-parameter data
Use inference on the neural network to optimize and refine the design
Verify the optimum design by funning the full FEA model

using the Surrogate Model Training study type. Extract S-parameters (and, if needed, far-field patterns and derived metrics such as gain or efficiency).

4. **Surrogate Training**: Preprocess data (normalize, split train/validation). Train the deep neural network with architectures like three to four hidden layers and 32 to 64 neurons. Use mean-squared error loss.
5. **Deployment and Exploration**: Integrate the surrogate into a dedicated app using the COMSOL Application Builder. The user has the option to explore the parameter spaces manually using sliders or optimize the design using only inference on the surrogate model.
6. Validate the chosen design configuration by re-running the full FEA model at the chosen set of conditions.

This reduces full simulation time by 95 percent or more, reserving them for final verification.

CASE STUDY: RFID TAG LOCALIZATION ANTENNA

RFID tag localization systems require tag antennas with precise impedance matching, moderate gain and controlled radiation patterns for accurate positioning in warehouses or retail environments. Operating at ultra-high frequencies (902 to 928 MHz in North America), these antennas must balance read range, multipath rejection and cost-effective fabrication.

A parameterized meandered-line dipole antenna on FR4 substrate with complex chip impedance was studied. Five geometric parameters are considered:

- Meander amplitude, H
- Conductor width, W
- Meander spacing, S
- Feed gap, G
- Length of the first meander leg, H0.

The key objective was to minimize $|S_{11}| < -20$ dB at 915 MHz or alternatively, minimize S_{11} over a specified frequency range.

Other things can be optimized if needed, for example:

- Maximize realized gain > 6 dBi
- Achieve a hemispherical far-field distribution pattern
- Favor designs with larger feature sizes (> 0.5 mm) for manufacturing ease.

RFID tags contain a small chip that is used to activate the tag. Chip impedance is an important variable in tag design. In this example, the chip resistance R_c is 11.5 Ω and the capacitance C_c is 3 pF. Lower chip resistance tends to make matching more difficult. The goal is to design an antenna whose natural impedance is a conjugate match for the chip impedance. The complex chip impedance is shown in ***Equation 1***.

$$Z_c = R_c - \frac{j}{\omega C_c} \quad (1)$$

So, the antenna needs to have an inherent impedance (***Equation 2***).

$$Z_a = R_c + \frac{j}{\omega C_c} \quad (2)$$

The S-parameter, the quantity to minimize close to

MiCable

Wideband High Accuracy Butler Matrices

Excellent Phase Accuracy, Amplitude Unbalance

Low VSWR / Low Insertion Loss / High Isolation

P / N	Structure	Freq. Range (GHz)	VSWR Max. (:1)	Insertion Loss* Max. (dB)	Amplitude Unbal. Max. (dB)	Amplitude Flatness Max. (dB)	Phase Accuracy Max. (Deg.)	Isolation Min. (dB)
SA-07-4B006050	4x4	0.617~0.821	1.4	8.2	±1.1	±0.8	±10	17
		0.832~0.96	1.4	8.2	±1.1	±0.7	±9	17
		1.427~1.71	1.4	8.3	±0.9	±0.7	±9	16
		1.71~2.2	1.5	8.5	±0.9	±0.8	±10	15
		2.496~2.69	1.5	8.7	±0.9	±0.7	±9	14
		3.3~4.2	1.5	8.9	±1.0	±0.7	±12	14
		4.4~5	1.5	9.2	±1.0	±0.8	±12	14
SA-07-8B006050	8x8	0.617~0.821	1.4	12.3	±1.4	±1.2	±12	17
		0.832~0.96	1.4	12.3	±1.4	±1.0	±12	17
		1.427~1.71	1.4	12.7	±1.3	±1.0	±11	16
		1.71~2.2	1.5	12.9	±1.2	±1.2	±11	15
		2.496~2.69	1.5	13.2	±1.2	±1.0	±12	14
		3.3~4.2	1.5	14	±1.3	±1.1	±14	14
		4.4~5	1.5	14.5	±1.3	±1.2	±14	14
SA-07-4B024073	4x4	2.4~2.5	1.4	7.3	±0.5	±0.3	±4	14
		5.18~5.83	1.5	7.7	±0.6	±0.4	±5	13
		5.9~7.25	1.5	7.8	±0.7	±0.5	±6	13
SA-07-8B024073	8x8	2.4~2.5	1.5	11.2	±0.6	±0.4	±8	13
		5.18~5.83	1.5	11.6	±0.8	±0.5	±10	12
		5.9~7.25	1.55	11.8	±0.9	±0.7	±12	12
SA-07-4B240430	4x4	24~43	2.0	12.4	±1.2	±2.0	±15	10

*Theoretical Insertion Loss Included

Note: The connected components are available from MIcable which include the phase matched assemblies & low loss high isolation phase matched switches.

Typical Test Curve**

SA-07-4B006050

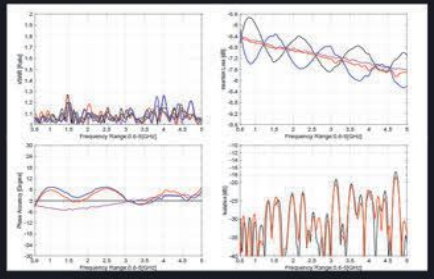

SA-07-4B024073

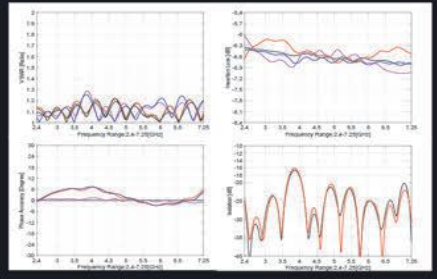

SA-07-4B240430

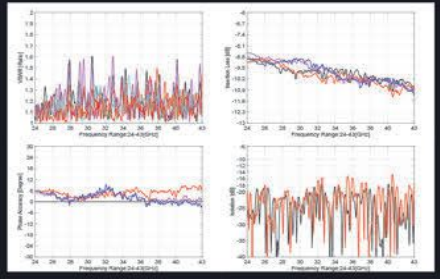

**Corresponding Channels: A1B1、A1B2、A1B3、A1B4

More Information-
Scan the QR Code

MIcable Inc.
www.micable.cn sales@micable.cn +86-591-87382856

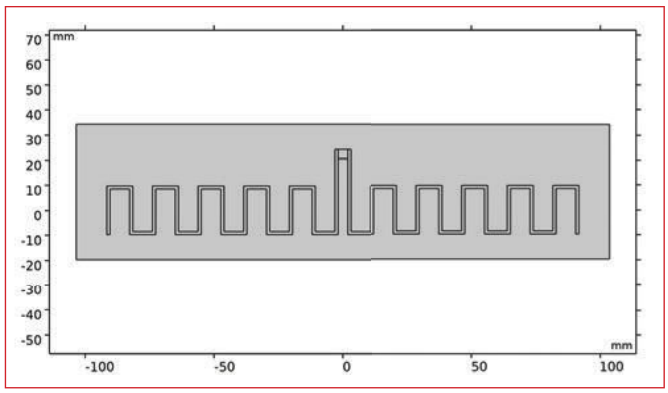

Fig. 1 **Example geometry of a miniaturized single-port meandered-line dipole antenna.**

the target frequency of 915 MHz, is given by ***Equation 3***:

$$S_{11} = \frac{Z_a - \mathrm{conj}(Z_c)}{Z_a + Z_c} \qquad (3)$$

The basic layout of the tag is shown in ***Figure 1***. The geometric features are adjusted and optimized until the antenna meets the performance requirements. The S-parameter plot for these nominal initial values is shown in ***Figure 2***. The initial design does not meet the performance specification or have the correct resonant frequency.

Using LHS, 300 COMSOL frequency sweep simulations are performed (average 3 minutes each on a 32-core workstation, total ~15 hours). The 15-hour simulation time is chosen intentionally, as one can set the model solving at the end of the workday and have the results available for processing the following morning.

RESULTS AND INTERACTIVE EXPLORATION

Once the surrogate model has run, the data can be used to train a deep neural network. When trained, the result is a function that can be evaluated using frequency and the geometric inputs. The function form is thus shown in ***Equation 4***.

$$S_{dnn} = g(H, W, S, G, H0, f_r) \qquad (4)$$

Here, the first five inputs are the geometric parameters, and f_r is the range of frequencies over which to evaluate. Evaluation of this function for different combinations of parameters is practically instant, as a weighted sum (from the weights and biases computed during training) is evaluated under the hood.

The evaluation, result display and convenient method of changing input parameters (using a slider which updates the results and geometry plot in real-time) can be packaged into a simple and intuitive user interface using the COMSOL Application Builder. The app also has a "Verify Results" button in the ribbon. This allows the full FEA solution to be computed once an interesting result has been obtained. This is a crucial step when using this technique; the full model should always be computed for verification purposes.

The interactive dashboard provided by the app allows cross-functional teams to filter designs by constraints (e.g., cost proxies via material volume) and select candidates for prototyping.

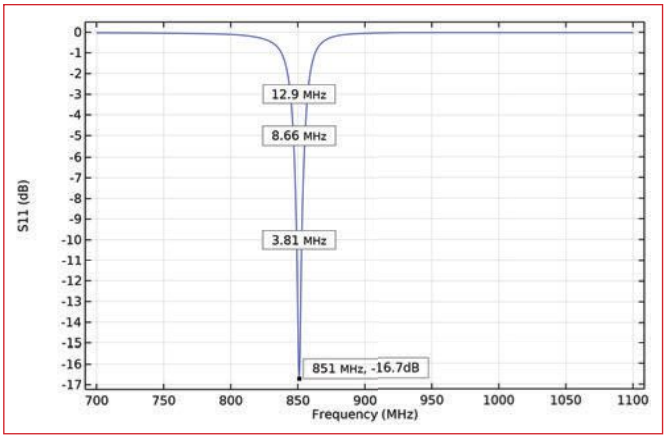

Fig. 2 **S-parameter vs. frequency for an arbitrary initial starting point.**

OPTIMIZATION

Manual tuning of the parameters, while instructive, can be time-consuming, even when just running inference from the surrogate model. Optimization running on inference can compute global minima for a suitable objective function. In this case, the S-parameter is minimized over a user-selected frequency range. The objective function is shown in ***Equation 5***.

$$\mathrm{obj} = \left(\int_{f\min}^{f\max} S_{dnn}\, df \right)^2 \qquad (5)$$

The parameter space of antenna configurations can contain many local minima, but only one true global minimum. COMSOL includes an efficient global optimization (EGO) solver, which can compute a true global minimum. Running this for different objective functions can quickly generate a desirable starting point, which can be manually tweaked given the practical design issues discussed earlier.

The screenshot in ***Figure 3*** shows a result that was first computed using the optimization, then tweaked slightly to get the minimum at exactly 915 MHz. The frequency range in which to optimize is specified in the user interface. If a high bandwidth is required, the frequency limits can be expanded. If the main goal is to have the smallest S-parameter at exactly 915 MHz, the window can be shrunk to a very small value. The user can quickly see the tradeoffs in geometrical footprint and performance given their target specification.

An added benefit to this approach is that derivatives of the objective function can be computed purely from the inference. This allows the sensitivity of the S-parameter with respect to each geometric parameter to be quantified. These values indicate which of the dimensions will affect performance the most if the exact values are not met during manufacturing. These can be explored further using uncertainty quantification, if needed.

The optimized result for a frequency range of 910 to 920 MHz is shown in ***Figure 4***. The antenna meets the target of -20 dB and the resonance is at exactly 915 MHz. Expanding the frequency integration range would result in slightly different solutions, with the antenna obtaining a higher bandwidth, but the fre-

RF-LAMBDA

THE POWER BEYOND EXPECTATIONS

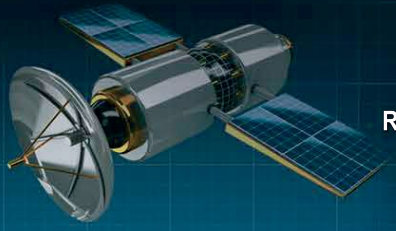

ITAR & ISO9001
Registered Manufacturer
Made in USA

RF T/R MODULES UP TO 70GHz

DREAM? WE REALIZED IT

LOW LOSS **NO MORE CONNECTORS**
GaN,GaAs SiGe **DIE BASED BONDING**
SIZE AND **WEIGHT REDUCTION 90%**

HERMETICALLY SEALED AIRBORNE APPLICATION

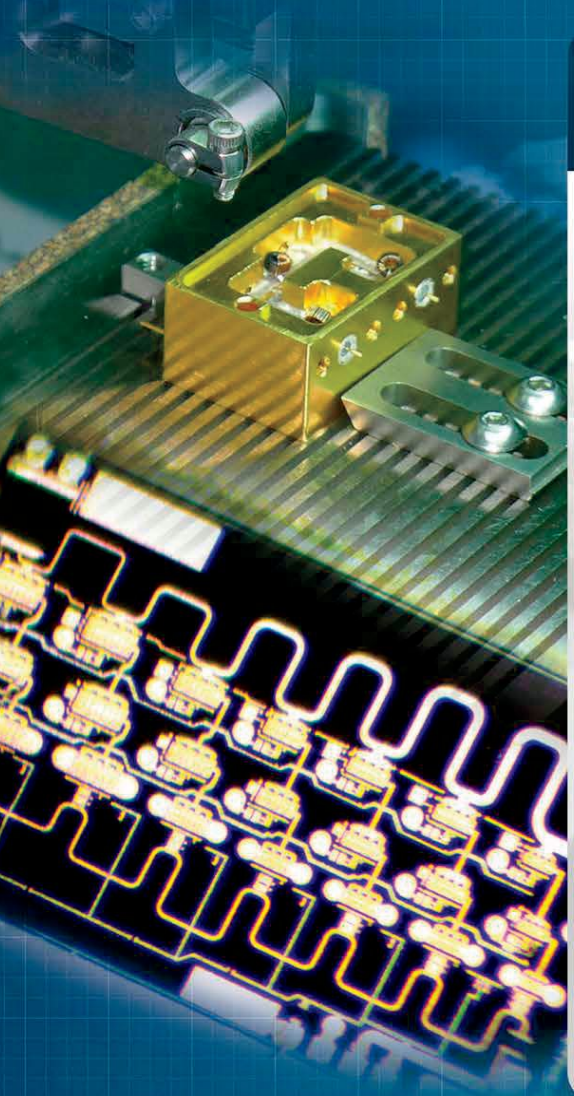

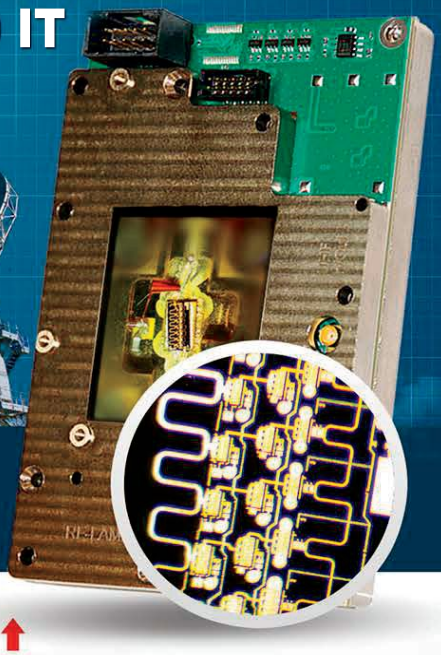

SATCOM TR MODULE
RX 50GHZ TX 22GHZ

TX/RX MODULE
Connectorized
Solution

RF Switch 67GHz
RFSP8TA series

RF Filter Bank

RF RECEIVER

RF TRANSMITTER

DC-67GHz
RF Limiter

0.01- 22G 8W PA
PN: RFLUPA01G22GA

RF Switch 67GHz
RFSP8TA series

0.05-50GHz LNA
PN: RLNA00M50GA

0.1-40GHz
Digital Phase Shifter
Attenuator
PN: RFDAT0040G5A

LO SECTION
Oscillator

RF Mixer

RF Mixer

OUTPUT

INPUT

www.rflambda.com
sales@rflambda.com

1-888-976-8880
1-972-767-5998

San Diego, CA, US
Carrollton, TX, US

Ottawa, ONT, Canada
Frankfurt, Germany

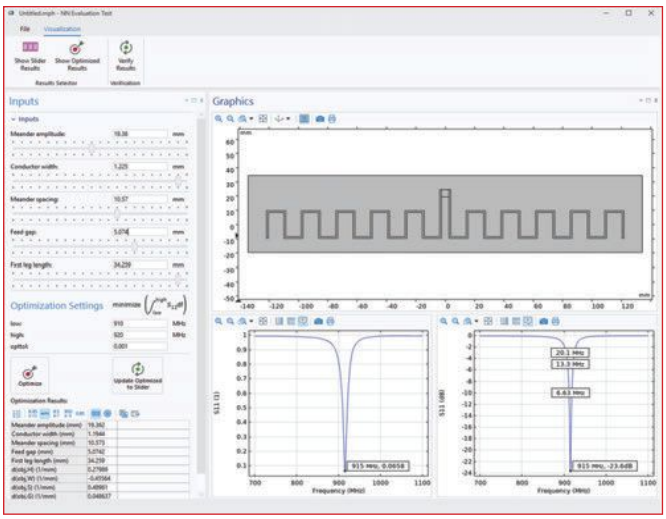

Fig. 3 **Screenshot of the app, which allows rapid tag design iteration.**

quency at which the S-parameter is minimized might be slightly away from 915 MHz.

Note: Running optimization on the full FEA model would require an inordinate number of solutions to be computed, limiting runs to overnight or possibly over weekends. Crucially, if the objective function changes, the optimization needs to be re-run.

DISCUSSION

This workflow shifts antenna design from simulation-constrained iteration to data-driven collaboration. Surrogates democratize access, enabling product managers to quantify tradeoffs early. The simple RFID case demonstrates practical benefits: identifying manufacturable designs without sacrificing core performance.

Limitations include initial data generation cost (mitigated by cloud and batch compute) and surrogate validity only within training bounds.

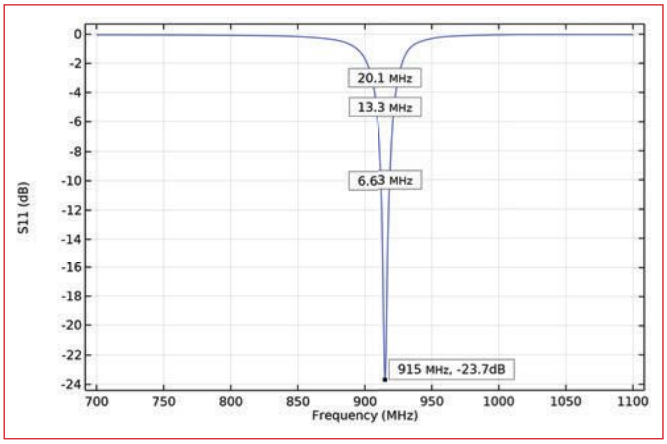

Fig. 4 **Optimized S_{11} plot for the antenna design, showing resonance frequency and bandwidths at -3, -5 and -10 dB.**

CONCLUSION

Neural network surrogate models trained on COMSOL Multiphysics simulation data enhance and speed up antenna design and development. By enabling millisecond evaluations, this approach facilitates interactive exploration, rapid robustness analysis and balanced decision-making across electrical and practical constraints. The RFID tag case study illustrates accelerated early-stage design with fewer full simulations required. As computational tools evolve, such hybrid simulation-ML workflows promise more innovative, reliable and cost-effective antenna solutions. Running global optimization with different objective functions can be used in conjunction with manual adjustments to ensure performance requirements are met, while also meeting manufacturing constraints and costs. This technique is generally applicable to all types of physics using COMSOL Multiphysics, making it a powerful modeling tool for rapid design optimization. ■

DUAL or SINGLE LOOP
SYNTHESIZER & PLO MODULES

Features:

- Proprietary digital Integer and Fractional PLL technology
- Lowest digital noise floor available -237 dBc/Hz figure of merit
- Output frequencies from 100 MHz locked crystal to 30 GHz
- Available with reference clean up dual loop, or single loop for very low noise reference
- Parallel fixed band stepping or SPI interface synthesized up to octave bandwidths
- Reference input range 1 MHz to 1.5 GHz
- Dual RF output or reference sample output available
- +12 dBm standard output power +16 dBm available
- Standard module size 2.25 X 2.25 X 0.5 Inches (LxWxH)
- Standard operating temperature -10 to 60 °C, -40 to +85 °C available

Up to 30 GHz*

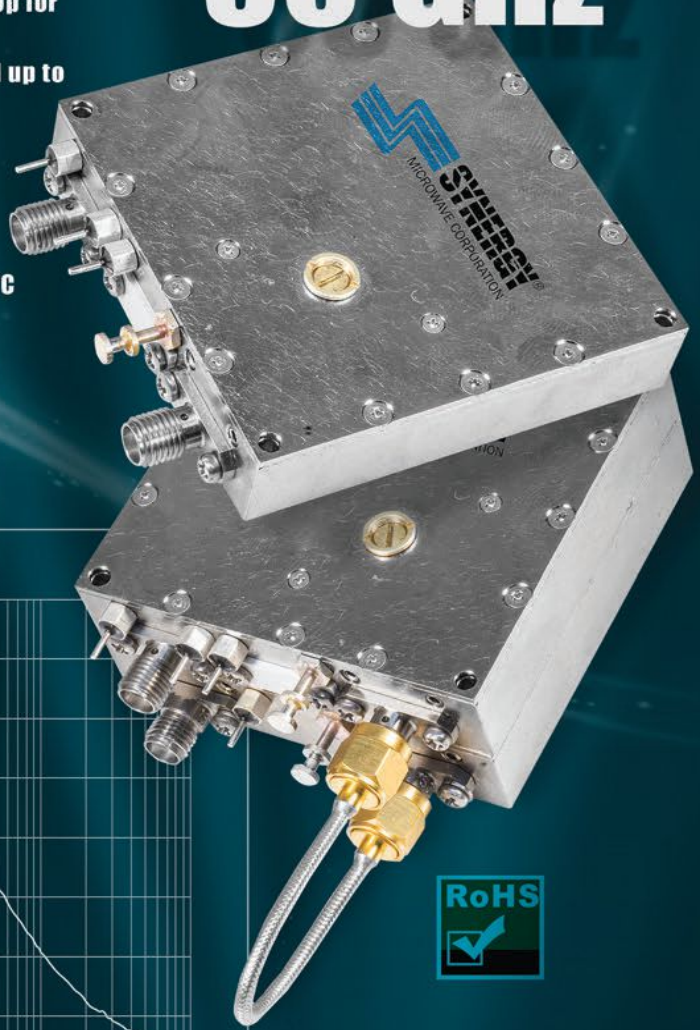

Applications:

- SATCOM, RADAR, MICROWAVE RADIO

* *16 - 30 GHz with added x2 module < 1" in height.*

Talk To Us About Your Custom Requirements.

SYNERGY®
MICROWAVE CORPORATION

Phone: (973) 881-8800 | Fax: (973) 881-8361
E-mail: sales@synergymwave.com
Web: WWW.SYNERGYMWAVE.COM
Mail: 201 McLean Boulevard, Paterson, NJ 07504

47 GHz Dual-Mode Feedhorn with Internal Transition to WR22 Rectangular Waveguide

Jeffrey Pawlan and Sembiam Rengarajan
Institute of Electrical and Electronics Engineers (IEEE) Members

A strong need has been expressed both in the U.S. and in Europe for a high-quality feedhorn optimized for operation around 47 GHz. Previously, this frequency was a military allocation in the U.S., but now the FCC has auctioned off most of this band for commercial use. Amateur radio uses 47.1 GHz for long-distance propagation studies. The military still uses adjacent bands, so a slight modification of this design is applicable to the military as well. This new feedhorn is designed for minimal return loss with a beamwidth to produce a 10 dB edge taper for a reflector antenna with an f/d ratio of 0.6 and a 90-degree subtended angle by the feed. It has nearly no side or back lobes. To accomplish this at a wavelength of 6.38 mm, tight machining tolerances are needed. The antenna is divided into several pieces to make it easier to fabricate accurately and to produce in large quantities.

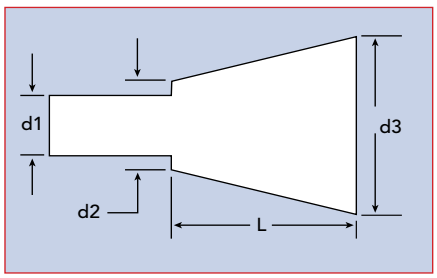

▲ Fig. 1 **Pickett-Potter horn block diagram.**

This feedhorn is a novel augmentation of the dual-mode feedhorn patented by Philip D. Potter at Jet Propulsion Laboratory in 1962.[1] It is important to note that this design includes the removal of the phasing chamber in Potter's design. This was described by Herbert M. Pickett and John C. Hardy in 1984.[2,3] The second augmentation is this author's addition of a simple, easy-to-fabricate and almost lossless internal transition from the native internal circular waveguide to a WR22 rectangular waveguide input. This article presents a design of a third change to the Pickett-Potter horn as well.

The Pickett-Potter horn has a circular waveguide input that contains the TE_{11} mode of the desired signal (see ***Figure 1***). The input is diameter d1, and there is an abrupt step to a larger diameter d2 at the beginning of the flared horn. The dimension d2 is such that some TM_{11} mode is generated in this region. The TM_{11} higher-order mode generated at the step up to d2 is at a level of approximately 15 percent of the dominant mode. Potter found through experimentation that the primary mode should contain approximately 85 percent of the total energy, and the higher-order mode the remaining 15 percent. Other higher-order modes are either cut off or are not excited due to symmetry.

In the Pickett-Potter horn, the length of the flare L and the final open end diameter d3 are chosen so that the dominant

MiniRF

DOCSIS Future-Proofed!

MRFSP9725

5-3000 MHz, 75Ω SMT Splitter

Excellent Performance Without the Need for External Resistor Load or Inductor

Passives with a Passion for Performance

Couplers

Splitters

Transformers

RF Chokes

MiniRF is a proven, preferred leader in passive component supply for Broadband/CATV and Wireless Communications, with 1+ billion components shipped. MiniRF passives enable DOCSIS 4.0 & FDX system requirements, max RF output power, and have excellent repeatability and reliability with 100% RF testing. The USA-based design center supports standard and custom components, while multiple low-cost overseas manufacturing operations with no tariffs deliver competitive pricing.

RFMW®

Contact our team of experts for information, samples and sales: sales@rfmw.com | rfmw.com

mode and the TM_{11} mode arrive at the mouth of the flare d3 with the phase values shown in ***Figure 2***. Since the two modes have different guide wavelengths, the flare length is optimized to achieve this. Once the correct phases for the two modes are achieved, the higher-order mode cancels the dominant mode near the conducting wall of the open end of the conical flare. This results in a significant reduction of side and back lobes. An almost complete cancellation is possible.

This article presents a third change to the Pickett-Potter horn. Instead of using the abrupt step between the circular waveguide d1 and the diameter of the flared taper input d2 to generate the TM_{11} mode, this horn uses the small diameter circular waveguide solely as a complex impedance match between an oval transition and the input to the tapered horn. In this design, the TM_{11} higher-order mode is generated within the flared taper and the open mouth d3 at the end of the taper. This requires extensive optimization.

Many offset-fed satellite dish antennas are available with an f/d of 0.6. Most offset dishes have an f/d of 0.6 or 0.8. Also, driving the Cassegrain secondary subreflector of a circular parabolic dish usually requires an f/d of 0.6 to 0.8. The difference in the edge taper with an f/d ratio of 0.6 or an f/d ratio of 0.8 is within 2 dB at ± 45 degrees, so this feedhorn can be used with either. This article concentrates on an f/d = 0.6 design and results, which corresponds to a -10.5 dB full beamwidth of 90 degrees.

RECTANGULAR TO CIRCULAR WAVEGUIDE TRANSITION BACKGROUND

The original idea upon which this transition is based was J. R. Pyle's work in Southern Australia in 1964.[4] All the other transitions reviewed, including Dan Bathker's,[5] require manufacture by electroforming or very complex non-planar machining with soldering or welding. One interesting paper is by Stuchly and A. Kraszewski.[6] Another similar design is by Eric Holzman, who roughly adopted this in his manufacture of a V-Band antenna.[7] However, he depended on making the rectangular waveguide completely oval, and it was not an easily manufacturable design.

47 GHz Dual-Mode Feedhorn Design

The matched transition from the WR22 rectangular waveguide TE_{10} mode to the circular waveguide TE_{11} mode is initially done as a homogenous structure. The impedance, cutoff frequency fc and guide wavelength lg of the WR22 waveguide are calculated. Then the inside diameter of a circular waveguide is selected to provide an identical impedance, cutoff frequency and guide wavelength. The calculated diameter of the circular waveguide is .263 in. corresponding to a value of ka = 3.295, where k is the wave number, and a is the radius of the circular waveguide. At this frequency, the TE_{11} and TM_{01} modes are above cutoff with $k_c a$ values of 1.841 and 2.405, respectively, with k_c being the cutoff wave number. The TM_{01} mode is not excited by the rectangular waveguide TE_{10} mode because of symmetry. For use at 47.1 GHz, it is unnecessary to use a multi-stepped transition because the bandwidth of one matching section is more than enough for the application.

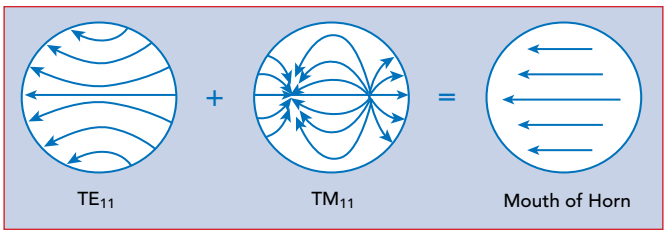

Fig. 2 **Combination of modes at the conical flare opening.**

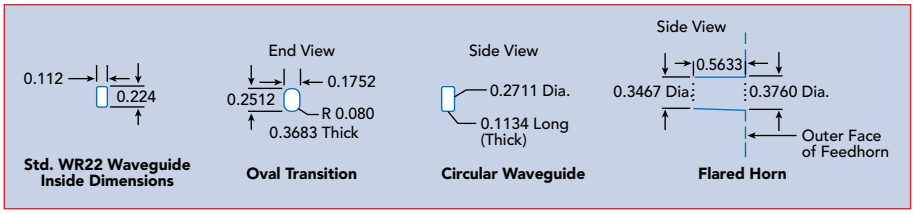

Fig. 3 **Final dimensions of the feedhorn's four sections (in.).**

Now the first serious manufacturing problem is apparent. The quarter-wave matching section designed at this frequency is too thin to manufacture, so an odd multiple of ¼ λ_g is chosen (i.e., 5/4 λ_g), where λ_g is the full guide wavelength. However, the thickness is not an exact multiple of ¼ λ_g because the guide wavelength within the oval matching section changes due to its shape. This requires recalculation and optimization.

The wavelengths of the primary circular TE_{11} mode and the higher TM_{11} mode are clearly not identical either. Given that the two modes have different wavelengths and different power levels, optimization techniques work far better than electromagnetic calculations.

The cylindrical waveguide diameter is slightly changed from .263 to .2711 in. This provides a better match to the rectangular waveguide. The final dimensions (in inches) of the four parts of the feedhorn are shown in ***Figure 3***.

The flared horn with its abrupt step presents a complex impedance to the circular waveguide. Therefore, optimization of several parameters is done iteratively in groups to achieve the desired result of low side and back lobes simultaneously, with a very good match to the WR22 waveguide. Reoptimizing with changes of the inner and outer diameters of the flared horn is done many times to achieve the correct beamwidth while continuing to suppress the side and back lobes.

Physical Structure

The physical structure comprises a mounting plate for the WR22 rectangular waveguide flange, followed by an oval matching section to a circular waveguide that drives a tapered horn with a low flare angle (see ***Figure 4***). The assembled feedhorn is shown in ***Figure 5***.

There is a manufacturing reason why the UG-599/UM square waveguide flange is chosen rather than the more common UG-383/U

LEARNING CENTER

Microwave Journal

Keep these can't-miss online events on your radar in 2026!

Online Panels

August 26
Digital Twins and AI

This panel of experts will discuss the benefits and challenges of developing digital twin models along with how AI is being used to assist in modeling and design of RF and microwave circuits.

Registration coming soon at mwjournal.com

1/2 DAY SUMMITS

March 18	Satellite and Space
April 22	Extreme RF (ex. Space, Quantum Computing, High Power, High Frequency, mMIMO, Harsh Environment, etc.)
May 20	AI in RF
October 21	Advancements in Military Radar & EW
November 11	5G/6G & IoT

For Sponsorship Information Contact your MWJ Sales Rep today!
mwjournal.com/salesoffices

round flange. Round mmWave flanges must include two precision locating pins and four threaded screw holes. More problematic, the UG383/U flange is larger than the square flange and therefore necessitates a larger diameter feedhorn.

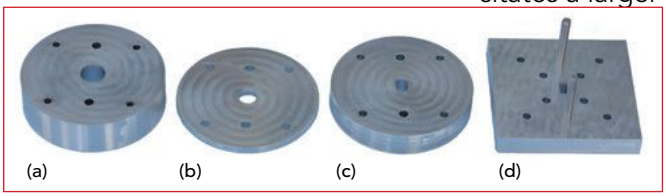

Fig. 4 **Photograph of the prototype's four sections: flared horn (a), circular waveguide (b), oval transition (c) and waveguide mounting plate (d).**

There are many adapters available between the round and rectangular flanges in the WR22 waveguide for the users of this feedhorn. One can also use a WR22 waveguide that has the UG-599/UM rectangular flange already attached.

SIMULATED AND MEASURED PERFORMANCE

Simulated $|S_{11}|$ (see ***Figure 6***) shows a minimum at 47.1 GHz. Simulated far-field performance (see ***Figure 7***) exhibits a gain of 12.3 dB with sidelobes less than -36 dB. The simulated main lobe level at ± 45 degrees is -10.7 dB. The simulated axial ratio is 27.7 dB.

A 70 GHz VectorStar vector network analyzer (VNA) is used to measure the antenna reflection coefficient. A calibration set of three offset shorts in WR22 is made for 47.1 GHz rather than the mid-band of the entire waveguide range. Also, a custom adapter from a WR22 waveguide to a 2.4 mm coaxial connector is made and tuned for 47.1 GHz.

Five samples are measured (see ***Figure 8***). Some ripples in the $|S_{11}|$ traces are expected as explained in an older Anritsu application note on understanding directivity in VNAs.[8] This application note is not the current one on the website, but it may be requested. Although the directional coupler in the Anritsu VectorStar VNA is not a waveguide, it is low loss and has finite directivity. This causes ripple and inaccuracy when measuring devices such as this antenna, which has a high return loss.

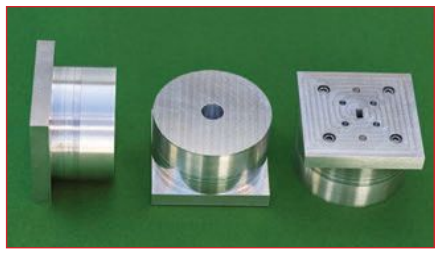

Fig. 5 **Assembled prototype.**

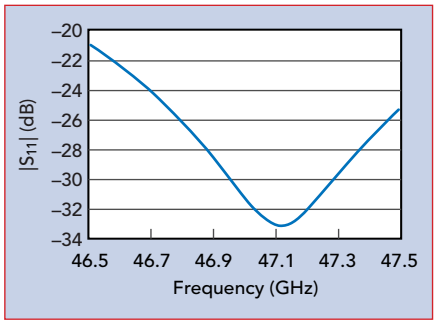

Fig. 6 **47 GHz dual-mode feedhorn simulated $|S_{11}|$.**

Because a suitable antenna test chamber was not available, measurements were made with the antennas placed in the center of a long table in a very large conference room at Anritsu. Due to the lack of absorption material, the observed ripple changes with the antenna pointed toward different parts of the room. It is not possible to avoid some of the ripples caused by reflections from the walls and ceiling, although most of the ripples are predictably caused by the directivity of the VNA's directional coupler.

Measurements of the five antennas are comparable except for a larger ripple in Antennas 4 and 5. It is likely that those antennas were pointed differently from the others while the measurements were taken. Even with the ripple, the reflected levels of -27 and -30 dB are very low.

The calibrated VNA is then used to measure the -10 dB beamwidth of each antenna as well as side and back lobe levels. Field patterns are measured between feedhorn pairs using $|S_{21}|$. The power is consistently 10 dB down at ± 45 degrees compared to the maximum power with the receive antenna pointed at the transmit antenna. This is within 1 dB of the simulation. The receive antenna is then slowly rotated from 0 degrees through 180 degrees, and then continues to 360 degrees. There are no observable sidelobes, which correlates with the simulation. The back lobe level from 170 to 190 degrees is in the noise of the VNA

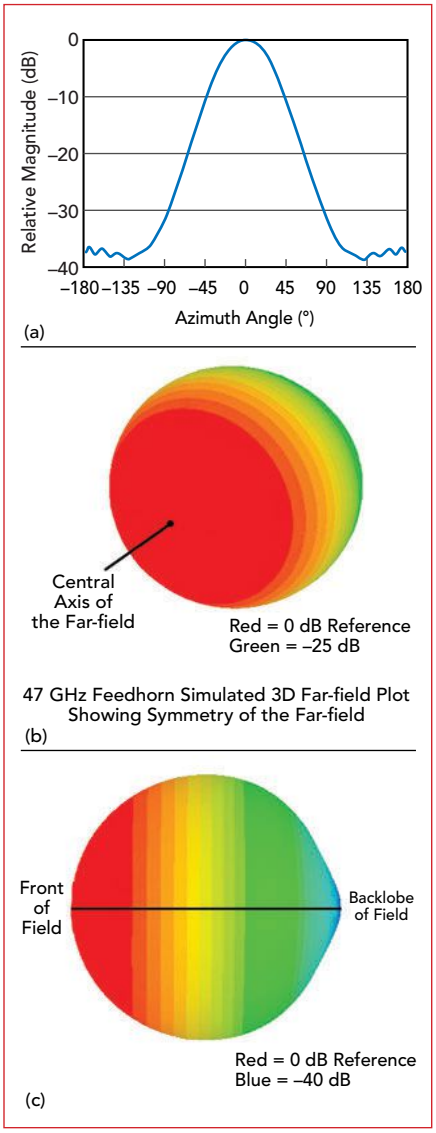

Fig. 7 47 GHz dual-mode feedhorn simulated far-field performance: azimuth pattern (a), 3D pattern showing symmetry (b) and 3D pattern on-axis showing mainlobe-to-backlobe relative magnitude (c).

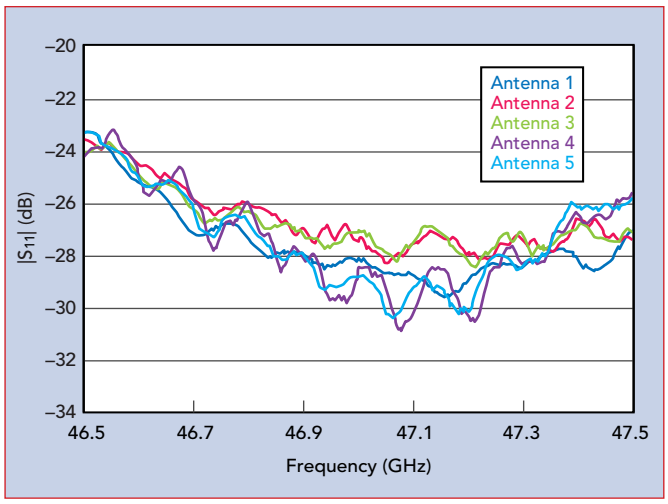

Fig. 8 Measured $|S_{11}|$ of five prototype 47 GHz dual-mode feedhorns.

(between -45 and -50 dB). This corresponds closely with simulation. To measure below -45 dB, a Q-Band test chamber is required as well as a 47 GHz inline coaxial amplifier to compensate for cable loss.

COMPARISON OF PERFORMANCE AND MANUFACTURABILITY WITH OTHER DESIGNS

Compared to all previously published papers of dual-mode feedhorns for mmWave operation, this one has been uniquely designed to comprise four planar parts that are easy to manufacture in large quantities, making it suitable for commercial or military applications. There are no published designs of dual-mode feedhorns in this (Q-Band) frequency range. There are two commercially manufactured antennas available:

- The Q-Band Scalar Feed Horn Antenna by Eravant offers 15 dBi nominal gain with a 35-degree typical half-power beamwidth and -25 dB typical side lobe levels.
- Millimeter Wave Products, Inc. sells a wide-angle scalar feedhorn, also called a choke horn, that has been designed to be used in applications where a wide beam width is required (i.e., low F/D ratios of .5 and .4) in a parabolic horn. The gain is 10 dBi and the beamwidth is 55 degrees. The sidelobes are -25 dBc and the VSWR is 1.5:1.

Only two references for feedhorns in this band could be found, although there are many planar antenna designs. The first is a probe-fed waveguide that was compared to a standard gain rectangular horn antenna.[9] The second is a comparison of three conventional designs: a choke ring feed horn, a quad-ridged feed horn and a corrugated feed horn (modified by tapering the corrugation depth).[10]

Of these, only the conventional choke ring feed horn has performance comparable to the feedhorn described here. Even though the authors named it choke ring, it is a traditional corrugated feed horn with ten narrow, ¼ λ deep, corrugations. The sidelobe

SIX DAYS ■ THREE CONFERENCES ■ ONE EXHIBITION

EUROPE'S PREMIER MICROWAVE, RF, WIRELESS AND RADAR EVENT

EUROPEAN MICROWAVE WEEK
EXCEL, LONDON
4th-9th OCTOBER 2026
www.eumw.eu

EUROPEAN MICROWAVE WEEK 2026

SUBMIT YOUR PAPER ONLINE

EXCEL LONDON, UNITED KINGDOM

4TH – 9TH OCTOBER 2026

To electronically submit a technical paper for one or more of the three conferences, all you have to do is:

1. Visit our website www.eumw.eu
2. Click on `CONFERENCES' to view the individual conference details
3. From the Home page, click on "More info" under the "Authors" heading for author instructions on abstract submission

EuMA EUROPEAN MICROWAVE ASSOCIATION

Media partner: Microwave Journal

Co-organiser: horizon house

Technical co-sponsors: MTT-S IEEE MICROWAVE THEORY & TECHNOLOGY SOCIETY; IEEE AP-S Antennas and Propagation Society; AESS; Electron Devices Society

EuMIC THE EUROPEAN MICROWAVE INTEGRATED CIRCUITS CONFERENCE

EuMC THE EUROPEAN MICROWAVE CONFERENCE

EuRAD THE EUROPEAN RADAR CONFERENCE

Supported by: IEEE; EurAAP; APMC 2026; GAAS; esa THE EUROPEAN SPACE AGENCY

SUBMIT PRELIMINARY PAPERS ONLINE AT WWW.EUMW.EU BY 27TH MARCH 2026

level is -35 dBc. The annular beamwidth (58 degrees) is not suitable for illuminating offset-fed reflectors or Cassegrain-fed parabolic antennas. The $|S_{11}|$ is only -20 dB in the best part of the bandwidth. This type of feedhorn generally takes considerable time and effort to manufacture as well.

CONCLUSION

A new design of a dual-mode feedhorn for the mmWave frequency of 47 GHz (Q-Band) has no measurable side or back lobes, which makes it impervious to picking up ground noise and heat. This greatly lowers the antenna noise temperature and increases G/T. It has an extremely good return loss as well. The feedhorn includes an internal transition from the circular antenna to a standard rectangular waveguide (WR22).

Together, these characteristics make this design more efficient than all previously published antenna and feedhorn designs for this frequency. Its overall performance exceeds that of previously published papers and commercially available products made for this frequency range. ■

ACKNOWLEDGMENTS

The Chief Field Applications Engineer at Anritsu, Arno Pettai, was extremely helpful and provided the use of a 70 GHz VectorStar VNA for measurements in the Anritsu facility.

References

1. P. D. Potter, "A New Horn Antenna with Suppressed Sidelobes and Equal Beamwidths, *Jet Propulsion Laboratory, California Institute of Technology*, 1963.
2. H. M. Pickett, J. C. Hardy and J. Farhoomand, "Characterization of a Dual-Mode Horn for Submillimeter Wavelengths," *IEEE Transactions on Microwave Theory and Techniques*, Vol. 32, No. 8, August 1984, pp. 936–937.
3. C. Yao, C. Ai-xin and S. Dong-lin, "The Optimization Design of the Pickett Potter Horn Antenna for Ka Band," *Asia-Pacific Symposium on Electromagnetic Compatibility and 19th International Zurich Symposium on Electromagnetic Compatibility*, May 2008.
4. J. R. Pyle, "A Circular to Rectangular Waveguide Transition Maintaining a Constant Cutoff Wavelength, Department of Supply, Australian Defence Scientific Service Weapons Research Establishment," Salisbury, South Australia, Technical Note Pad 94, September 1964.
5. D. Bathker, "A Stepped Mode Transducer Using Homogeneous Waveguides," *IEEE Transactions on Microwave Theory and Techniques*, Vol. 15, No. 2, February 1967, pp. 128–130.
6. S. Stuchly and A. Kraszewski, "Wide-Band Rectangular to Circular Waveguide Mode and Impedance Transformer (Correspondence)," *IEEE Transactions on Microwave Theory and Techniques*, Vol. 13, No. 3, May 1965, pp. 370–380.
7. E. L. Holzman, "A Simple Circular-to-Rectangular Waveguide Transition," *IEEE Microwave and Wireless Components Letters*, Vol. 15, No. 1, January 2005, pp. 25–26.
8. "Understanding Directivity in Vector Network Analyzers," *Anritsu*, Doc. No. 11410-00580 rev A.
9. Y. A. B. Ahmad, N. H. Kamaruddin, M. N. A. A. Hamid and K. Badron, "Q and V Band Dual Offset Feed Parabolic Antenna for Satellite Communication in Equatorial Region," *9th International Conference on Computer and Communication Engineering*, Kuala Lumpur, Malaysia, August 2023.
10. S. S. Hesari and L. Knee, "Design and Analysis of Three Q-Band Feed Horns for Radio Astronomy Applications," *IEEE USNC-CNC-URSI North American Radio Science Meeting (Joint with AP-S Symposium)*, July 2020.

2026 Asia-Pacific Microwave Conference

APMC 2026

Nov. 8-11, 2026 / Fukuoka, Japan at Fukuoka Convention Center

Microwave Innovation from Kyushu as Japan' s Historical Gateway

Conference topic

- Active Devices and Circuits
- Field Analysis, Simulation and Characterization
- Microwave, Millimeter-Wave, and THz Systems and Applications
- Passive Components
- Antennas and Propagation
- Emerging Technologies and Applications

Important Dates

- Proposal Deadline (Workshops/Short Courses/Special and Focused Sessions) ---------- Mar. 2, 2026
- Paper Submission Deadline ---------- May 18, 2026
- Notification of Acceptance ---------- Aug. 12, 2026
- Final Manuscript Submission Deadline ---------- Aug. 31, 2026

Fukuoka is one of the largest cities in Japan and is the political and economic center in the Kyushu region. Kyushu has long served as Japan's historical gateway to the world. Fukuoka has many tourist attractions such as the historic area. Fukuoka is also famous for its food. You can enjoy Fukuoka's yatai (food stalls) in Hakata. The Grand Sumo Tournament will be taking place at a nearby venue concurrently with our conference, providing an exciting glimpse into Japan's rich traditions.

"© Fukuoka Prefecture Tourism Association"

Organized and sponsored by

The Institute of Electronics, Information and Communication Engineers (IEICE) of Japan

Technically co-sponsored by

IEEE MTT-S, IEEE AP-S, European Microwave Association(EuMA), Union Radio-Scientifique Internationale (URSI), IEEE MTT-S Japan/Kansai/Nagoya Chapters, IEEE AP-S Tokyo Chapter, IEICE Technical Committee on Microwaves, Electronics Simulation Technology, Integrated Circuit and Devices, Electron Devices, Antennas and Propagation, Electromagnetic Compatibility, Wireless Power Transfer, Microwave Photonics and Terahertz Photonic-Electronics Technologies, Japan Society of Electromagnetic Wave Energy Applications, Japan Institute of Electronics Packaging, IEEJ Technical Committee on Communications, IEEJ Investigating R&D Committee on Advanced Technology for Pioneering Next-Generation Electromagnetic Applications, JSPS R074 Committee on Electromagnetic Wave Processing for Decarbonization of Industries, JSPS R062 Committee on Metamaterials, and Wireless Power Transfer Consortium for Practical Applications

Contact

Prof. Kenjiro Nishikawa
Chair, Steering Committee
secretariat@apmc2026.org

https://www.apmc2026.org/

DC TO 65 GHz

RF & MW Test Solutions

Flexible, Reliable, Affordable & Fast

Software Controlled Building Blocks and RF Interface Units

Custom Test Systems

Test Accessories

Switching, attenuation, distribution, signal source, amplification, sensing, measurement and more

LEARN MORE

Mini-Circuits

Microwave Journal

SPECIAL**FOCUS**

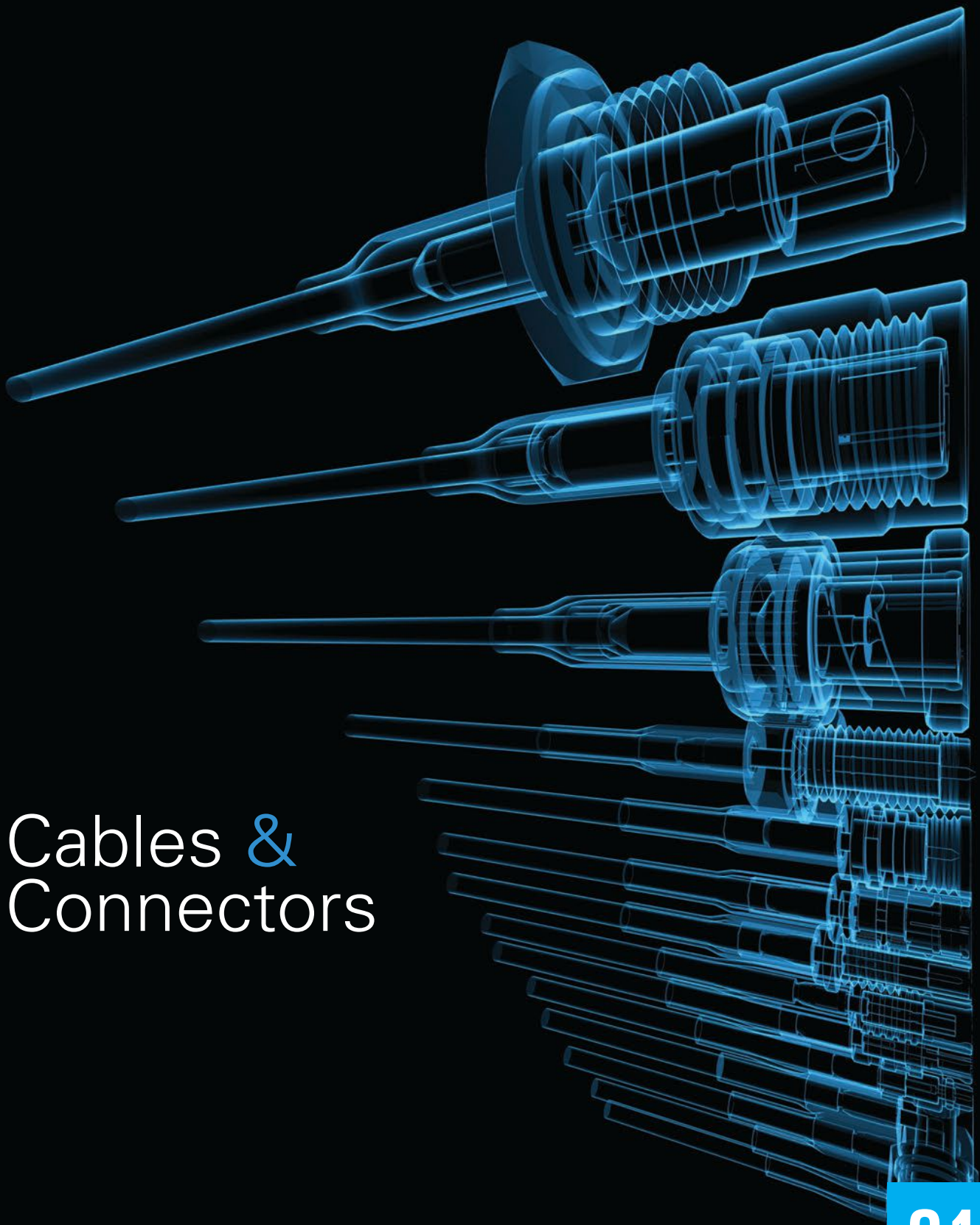

Cables & Connectors

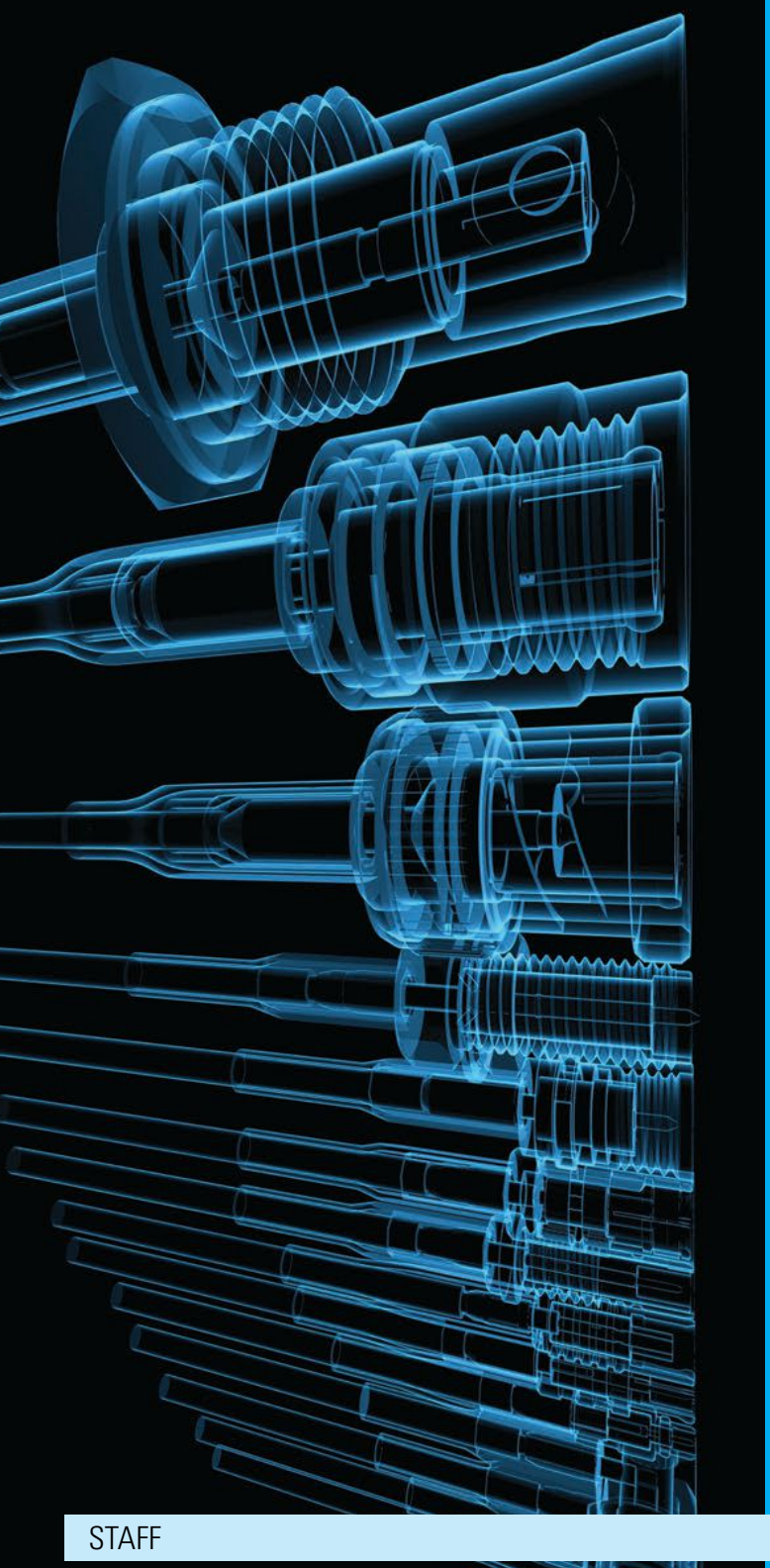

SPECIAL**FOCUS**

Table of Contents

STAFF

Group Director: Carl Sheffres
Associate Publisher: Michael Hallman
Media Director: Patrick Hindle
Brand & Content Director: Jennifer DiMarco
Technical Editor: Del Pierson
Associate Technical Editor: Cliff Drubin
Editorial & Media Specialist: Kelley Roche
Associate Editor: Kaitlyn Joyner
Multimedia Staff Editor: Barbara Walsh
Electronic Marketing Manager: Chris Stanfa
Senior Digital Content Specialist: Lauren Tully
Digital Content Specialist: Vincent Carrabino
Director of Production & Distribution: Edward Kiessling
Art Director: Janice Levenson
Graphic Designer: Ann Pierce

EUROPE
Office Manager: Nina Plesu

CORPORATE STAFF
CEO: William M. Bazzy
President: Ivar Bazzy
Vice President: Jared Bazzy

San-tron

FIELD REPLACEABLE
RF Connectors

BREAK FREE
SUPPLY CHAIN CONSTRAINTS

DESIGNED • MACHINED • ASSEMBLED • TESTED

A New Direction

10 YEARS EXPERIENCE

MADE IN U.S.A

FREE SAMPLES

www.santron.com info@santron.com

978-356-1585

Shielding Effectiveness of SMPM Microwave Cable Assemblies

Joshua Allebach
W. L. Gore & Associates, Inc., Newark, Del.

Modern electronic warfare (EW) systems continue to push toward higher operating frequencies, higher RF power and increased packaging density to meet aggressive size, weight and power constraints. As a result, a typical line-replaceable unit (LRU) may contain dozens of microwave cable assemblies routed near sensitive receivers, high-power devices and digital subsystems. To meet density requirements and ease installation, designers often select push-on interfaces rather than threaded connectors with full-sized coupling nuts, since push-on solutions offer reduced center-to-center spacing.

The density advantage, however, can come with an electromagnetic compatibility (EMC) penalty. In general, push-on connectors offer lower shielding effectiveness than properly torqued threaded connectors due to their design. Push-on connectors have exposed gaps at the mating interface, which increase RF leakage. In addition, push-on connectors are more susceptible to improper installation at the mating interface — partial engagement or angular misalignment — which can further degrade shielding effectiveness, increase VSWR and increase insertion loss.

The threaded SMPM provides a compromise between large threaded connectors and push-on alternatives. The threaded SMPM uses a compact coupling nut that covers the exposed gaps at the SMPM interface, improving EMC. The compact size of the coupling nut supports dense packaging applications while providing a locking mechanism between the mating connectors, reducing installation variability and maintaining performance in use.

EMC CONSIDERATIONS OF COAX CONNECTORS

The increasing number of microwave assemblies within LRUs presents a challenge for system engineers addressing electromagnetic compatibility concerns. As the number of subsystems within a single LRU increases, assemblies are routed closely together and near components operating at high RF power and high frequencies. Electromagnetic interference (EMI) concerns for coax assemblies can be considered reciprocal, as an assembly can be both vulnerable to interference from surrounding components and a potential source of interference.[1]

Noise from external EMI is coupled into a coax assembly through gaps in the outer conductor shield. These gaps can occur within the connectors, cable or the solder termination between the connector and cable. When external noise penetrates a coax assembly, it induces a signal on the inner conductor that propagates along the line with the desired signal. This acts as interference in a system, decreasing the signal-to-noise ratio and interfering with key EW requirements.

Shielding effectiveness describes a transmission line's ability to withstand external EMI and limit radiated RF power. It is a standardized metric that allows the performance of different cable assemblies and connectors to be directly compared.

For RF characterization, shielding effectiveness can be measured using the mode-stirred method detailed in ANSI/EIA-364-66B-2025.[2] A test sample is placed within a shielded metal chamber, where transmitting antennas radiate power into the chamber and induce a signal on the sample. This signal is compared to a measured reference value, and the resulting ratio, given in dB, is the shielding effectiveness, with larger values indicating better shielding.

A useful metric for comparing microwave connectors and assemblies is the requirement defined in MIL-T-81490A (AS),[3] which specifies a minimum shielding effectiveness of 90 dB. EMI on a cable is generally considered insignificant if the shielding effectiveness reaches 90 dB or higher in applications through 18 GHz. Depending on the system design, EMI becomes more challenging to manage above 18 GHz, and the minimum shielding effectiveness requirement can be lowered. Each LRU has unique signal requirements, cable routing and connector spacing constraints that impact the choice of connectors and the allowable shielding effectiveness.

CONNECTOR CONSIDERATIONS FOR EW SYSTEMS

Threaded Connectors and Push-On Alternatives

Since push-on connectors offer higher packaging density than traditional threaded options, system engineers often prioritize them. Threaded connectors are density-limited by their coupling nuts. For example, an SMA connector, typically rated to 26.5 GHz, has a 0.3125 in. hex size coupling nut (i.e., wrench flats) per MIL-STD-348B.[4] For frequencies through 40 GHz, a 2.92 mm connector is a popular alternative but is also limited by the coupling nut. The 2.92 mm connector is specified in IEEE 287.1[5] with a 0.315 in. hex size. The actual center-to-center spacing for threaded connectors is larger than the hex size because the corners of a coupling nut exceed the wrench flat width. These values vary between manufacturers, so the hex size is used in this discussion as a common reference.

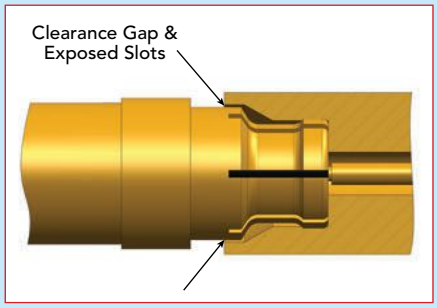

Fig. 1 **SMPM socket connector mated to a smooth bore pin connector.**

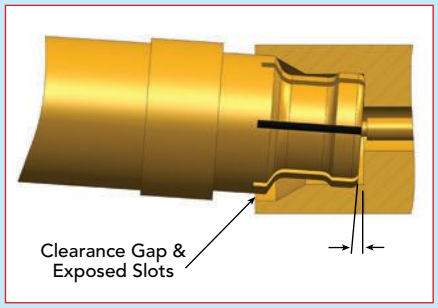

Fig. 2 **Example of an SMPM socket improperly installed.**

The SMPM interface demonstrates low VSWR through 40 GHz while enabling tighter connector spacing compared to 2.92 mm and SMA connectors. While the overall diameter of an SMPM socket is not defined by MIL-STD-348B, the microwave connector industry has converged on a typical value of 0.125 in. for standard cable connectors. This results in a 60 percent increase in interconnect density compared to the hex size of a 2.92 mm connector's coupling nut.

The SMPM socket interface is designed with a slotted outer conductor that flexes inward when engaging the mating pin connector. The connector's flexed fingers apply a radial outward force against the outer conductor of the pin, making an electrical connection. This radial force provides limited retention between the connectors and partially mitigates the need for a coupling nut, simplifying assembly installation. ***Figure 1*** shows an SMPM socket connector mated with a smooth bore pin connector. The socket version is one of W. L. Gore & Associates, Inc.'s standard SMPM connectors and the pin model is drawn to the nominal MIL-STD-348B dimensions. A smooth bore pin connector features a continuous outer conductor diameter, which minimizes the required insertion force.

SMPM Considerations

While the SMPM interface enables higher interconnect density, it introduces two primary design constraints that system engineers must account for, shielding effectiveness and interface engagement.

Firstly, an SMPM has poorer EMI performance than a threaded connector due to the exposed slots in the socket connector. By design, a clearance exists around the outer conductor bodies to allow proper mating without mechanical interference. However, this gap exposes the slots in the socket outer conductor and produces leakage. Figure 1 shows the clearance gap around the mated SMPM connectors.

The second design constraint for push-on connectors is improper mating. When SMPM connectors are misaligned or tilted during installation, shielding effectiveness is further reduced. Tilting the connectors increases the clearance gap and further exposes the socket slots. ***Figure 2*** shows an improperly installed SMPM socket mated with a smooth bore pin connector.

Interface engagement also impacts connector retention during operation. For the SMPM, the socket's flexed fingers provide a radial outward force onto the outer conductor of the pin connector, resulting in limited mechanical retention between the mating connectors. To increase retention force, a full detent SMPM pin connector can be used in place of a smooth bore. As implied by its name, a full detent connector has a detent feature within the pin outer conductor that acts as a small mechanical "speed bump." The detent requires the socket connector to flex inward further than a smooth bore, increasing the retention force and securing the connectors during use. However, the increased mating force also makes installation more challenging.

During system integration, care must be taken to ensure that the socket connector is fully engaged for

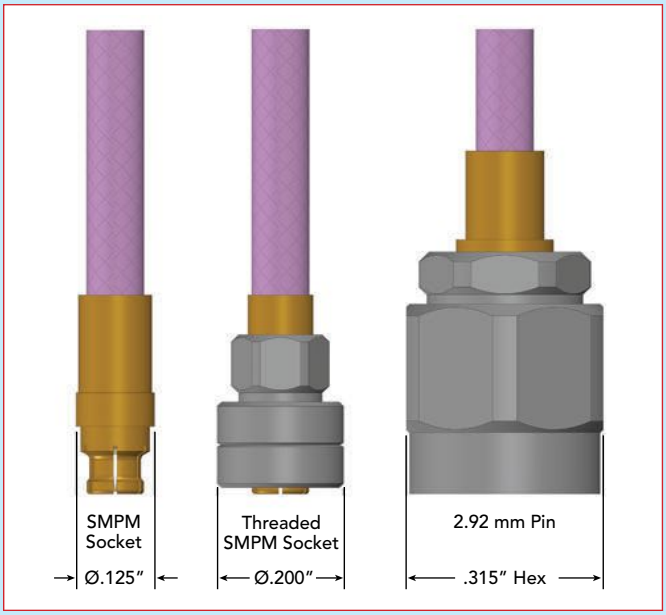

Fig. 3 Comparison of a standard SMPM socket connector, threaded SMPM socket and 2.92 mm pin connector.

proper performance. This requirement becomes more challenging as packaging density increases and access is limited. An installer must connect each assembly by hand and ensure proper mating of the connectors without the support of a torque wrench. Improperly installed connectors can result in a discontinuity at the mating interface, resulting in a high impedance that degrades VSWR performance. Misaligned connectors, such as those shown in Figure 2, are also at risk of becoming entirely uninstalled in field use.

Threaded SMPM

The threaded SMPM is an alternative option that reduces the SMPM design constraints with a modest reduction in packaging density. This design is derived from the standard SMPM interface and incorporates a compact coupling nut on the socket connector with external threads on the pin connector. During installation, the socket is mated by hand. The nut is then slid overtop the socket, threaded onto the pin and torqued using a calibrated wrench. The coupling nut provides a standardized engagement force, pulling the socket forward and ensuring the connectors are fully mated.

In addition to mechanical retention, the coupling nut provides an additional ground path between the mating connectors, fully covering the exposed socket slots and improving shielding effectiveness. The consistent engagement force of the threaded SMPM gives system engineers greater confidence that the connectors are fully mated, optimizing VSWR performance and reducing the risk of disengagement in use.

Figure 3 shows three connectors manufactured by W. L. Gore & Associates, Inc. The standard SMPM socket connector, threaded SMPM socket and 2.92 mm pin connector are shown together with the same scale. The threaded SMPM offers a practical compromise because of the coupling nut's compact size. The version manufactured by W. L. Gore & Associates, Inc. has a diameter of 0.200 in., giving a 36 percent increase in density compared to the hex of a 2.92 mm connector's coupling nut.

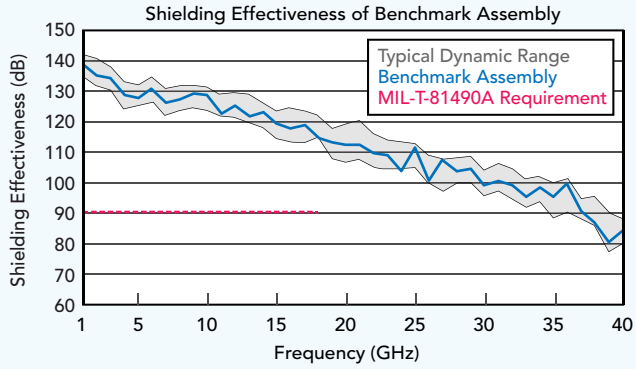

Fig. 4 Shielding effectiveness of a benchmark assembly.

SHIELDING EFFECTIVENESS OF EW CONNECTORS

Measuring Shielding Effectiveness

The mode-stirred method (ANSI/EIA-364-66B-2025) is used when evaluating the shielding effectiveness of microwave assemblies at RF frequencies. It provides an end-to-end measurement of an assembly's shielding performance, evaluating the cable, connectors and quality of the connector termination simultaneously. The shielding effectiveness is measured in 1 GHz steps from 1 to 40 GHz.

The dynamic range is the noise floor of the mode-stirred equipment and is a characterization of the equipment's capabilities. To ensure measurement accuracy, the dynamic range must be at least 10 dB greater than the target value of the sample.[2] For microwave assemblies, the MIL-T-81490A requirement is 90 dB. Most mode-stirred chambers have capabilities much greater than that requirement through 18 GHz, with typical dynamic range values near 140 dB at 1 GHz and 110 dB at 18 GHz.

The equipment's dynamic range is measured after calibration and plotted together with test results to indicate sample quality. If the shielding effectiveness of a sample measures near the dynamic range, it indicates excellent performance.

Shielding Effectiveness of Threaded Connectors

For flexible cables, an outer conductor composed of helically wrapped metal foil gives the best shielding effectiveness. W. L. Gore & Associates, Inc. manufactures microwave cable with a helically wrapped silver-plated copper foil. Wrap designs offer mechanical and electrical contact between the layers, eliminating gaps while maintaining flexibility for installation and routing.[6] Pairing this cable with threaded connectors and good solder termination results in excellent shielding effectiveness for the assembly — on par with the typical dynamic range of a mode-stirred chamber.

Figure 4 shows a representative benchmark ex-

Stability™ Cables deliver the Measurement Stability you need!

Stability Wafer™ Maury Microwave

Light-weight and stable to improve your on-wafer measurements.

Stability VNA™ Maury Microwave

Stable, repeatable, flexible and durable for the most precise VNA measurements.

Stability plus™ Maury Microwave

Armored and stable to minimize uncertainties in your critical mw &RF measurements.

Stability flex™ Maury Microwave

Extremely flexible and easy to use your test benches.

Stability TV-A.C™ Maury Microwave

Low Profile and optimized for high density applications.

Guaranteed performance for your critical thermal vacuum chamber measurements.

Learn More at maurymw.com

maury

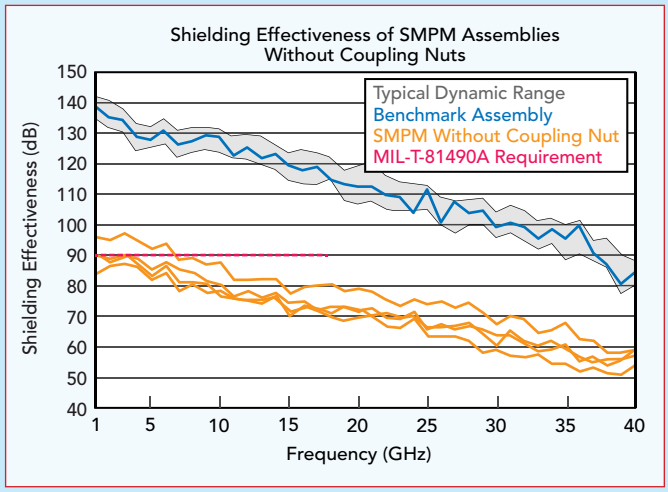

Fig. 5 Shielding effectiveness of SMPM assemblies without a coupling nut.

ample of W. L. Gore & Associates, Inc.'s flexible cable terminated with threaded connectors. The gray region in the plot shows the typical dynamic range of the test equipment, calculated from multiple runs over several days. The blue trace shows the shielding effectiveness of the benchmark assembly. The benchmark overlaps the dynamic range through 40 GHz and far exceeds the MIL-T-81490A requirement of 90 dB through 18 GHz, shown by the red dashed line.

Shielding Effectiveness of SMPMs With and Without Coupling Nuts

Threaded SMPM cable assemblies were built using the same type of flexible cable as the benchmark example. These samples were used to evaluate the shielding effectiveness of the SMPM connector with and without a coupling nut. On one end, the assemblies were terminated with a threaded connector and attached to the test equipment. The second end used a threaded SMPM socket connector, which was the connector under evaluation.

The shielding effectiveness of an SMPM interface without a coupling nut was evaluated by mating the socket connector to a pin adapter and leaving the interface exposed. An effort was made to verify the socket connector was fully engaged and not tilted off-axis. The coupling nut was left retracted, away from the mating interface. Representative results of the SMPM without a coupling nut are shown in ***Figure 5*** as orange traces. The typical dynamic range, benchmark assembly and MIL-T-81490A specification are also included for comparison.

The shielding effectiveness of an SMPM connector without a coupling nut is significantly reduced compared to the benchmark across all frequencies. The results fall below the 90 dB requirement by 7 GHz and approach 60 dB by 35 GHz. Depending on the LRU application needs and frequency of operation, this level of performance may require additional consideration by a system designer. Assemblies may need to be spaced further apart, or RF power levels reduced to mitigate

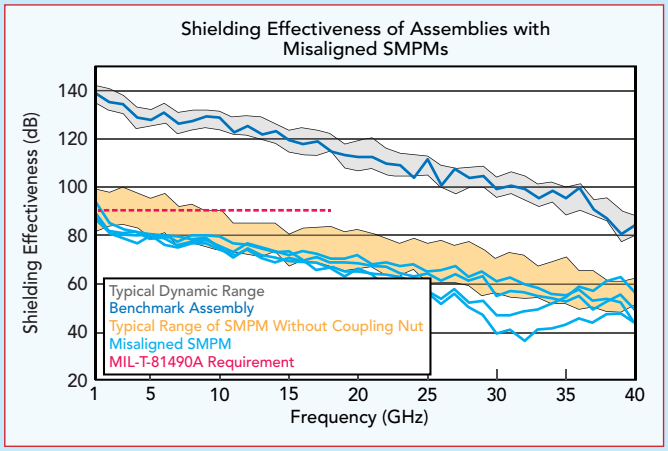

Fig. 6 Shielding effectiveness of assemblies with misaligned SMPM connectors.

EMI concerns.

Another experiment evaluated the performance of improperly mated SMPM connectors. The samples were intentionally tilted within the pin adapter. Again, the coupling nut was left retracted and away from the SMPM interface. This attempted to recreate the situation shown in Figure 2, where the socket connector is incorrectly installed, and there is a gap at the interface between the two connectors.

The shielding effectiveness results of the misaligned samples are plotted in ***Figure 6*** as light blue traces. The typical range of an SMPM connector without a coupling nut, calculated from the previous results, is also plotted as an orange shaded region. The benchmark example, typical dynamic range and MIL-T-81490A specification are also shown for comparison.

The improperly mated SMPMs have reduced shielding effectiveness compared to the properly installed SMPM connectors without a coupling nut. The results of the misaligned samples fall below the 90 dB specification immediately, near 1 to 2 GHz. There is a sharp downward trend, and the traces diverge from the properly mated examples. Around 32 GHz, the performance is at its worst, with values as low as 40 dB. The results are also inconsistent between samples because each connector is uniquely misaligned. This increases the challenge for the system designer, as shielding is not only degraded by misaligned samples but also yields variable, unpredictable results. These examples highlight the importance of ensuring proper installation when using push-on connectors.

Another round of testing measured the shielding effectiveness of the threaded SMPM connector. In this test, the SMPM socket was installed onto a threaded SMPM pin adapter. The coupling nut was engaged and torqued using a calibrated wrench, ensuring the connectors were fully mated.

With the coupling nut engaged, the shielding effectiveness of the threaded SMPM assemblies is excellent. ***Figure 7*** shows representative samples plotted as dark orange traces. Also included are the previous results and MIL-T-81490A specification. The typical

Optimize Your RF Testing with Solderless PCB Connectors

Teledyne Storm Microwave's new solderless PCB connectors redefine speed and efficiency in high-frequency test environments. Built for rapid setup changes, these interfaces—SMA, 2.92mm, 2.4mm, 1.85mm, 1.35mm, and 1mm—deliver rock-solid performance up to 110 GHz.

Forget soldering. Forget PCB wear. These connectors let you reconfigure and retest again and again, thanks to a rugged mechanical design that maintains secure mating and exceptional electrical integrity. Optimize your workflow. Protect your boards. Advance your RF designs with confidence.

110 GHz Performance

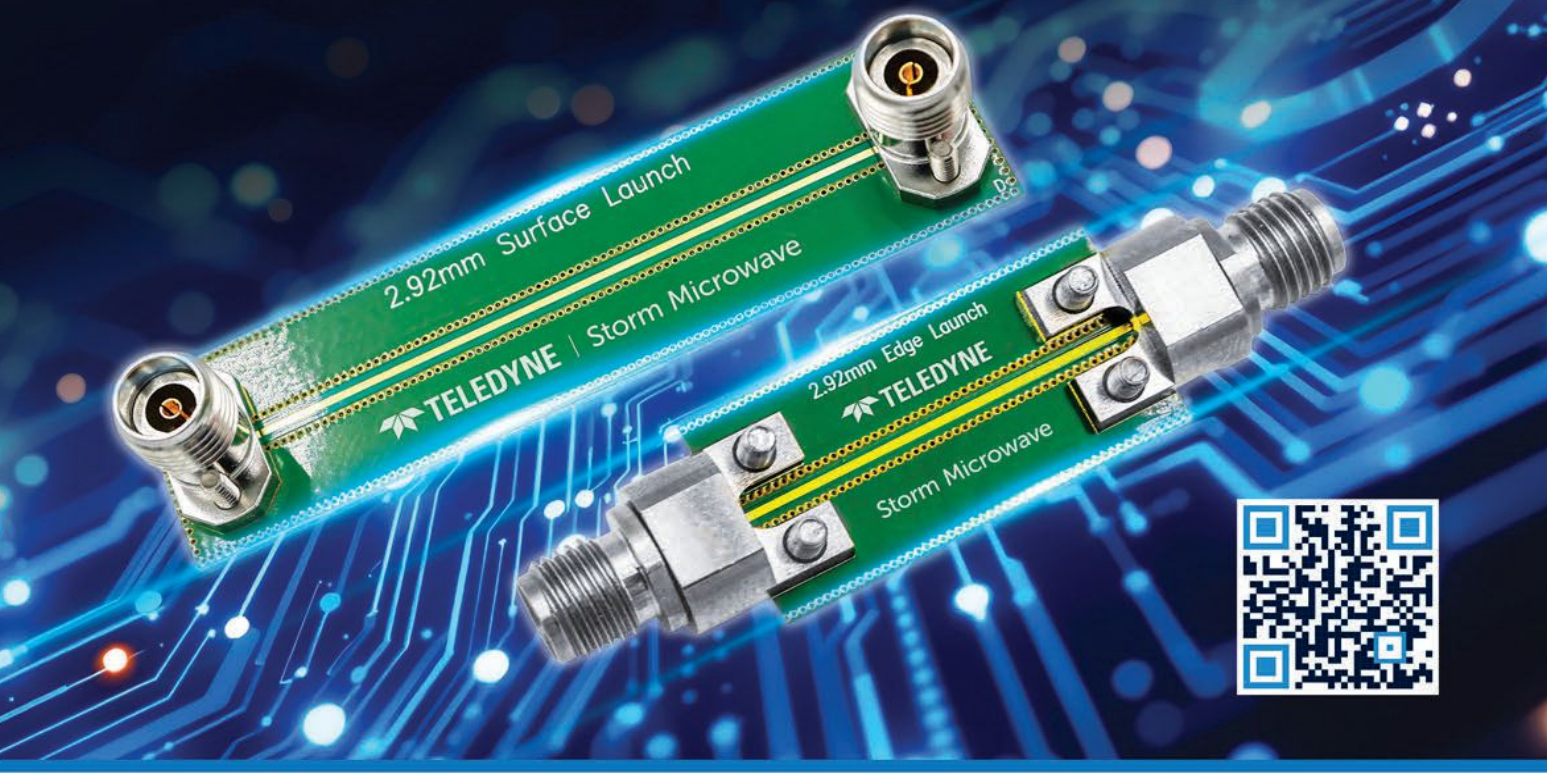

Teledyne Storm Microwave | Aerospace and Defense Electronics
TeledyneStorm.com

TELEDYNE

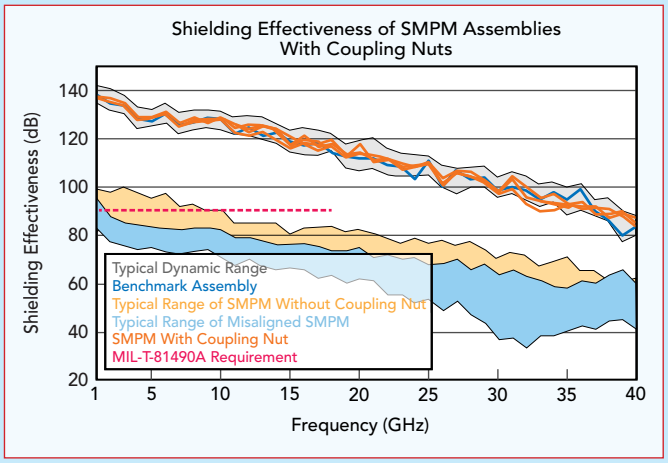

Fig. 7 Shielding effectiveness of SMPM assemblies with a coupling nut.

range of a misaligned SMPM connector, calculated from previous results, is shown plotted as a light blue shaded region.

The shielding effectiveness of the threaded connectors overlaps the dynamic range at most frequencies and greatly outperforms a standard SMPM without a coupling nut. The performance is on par with the benchmark assembly, offering excellent performance through 40 GHz. The threaded SMPM samples far exceed the MIL-T-81490A requirement with headroom through 18 GHz. This level of shielding indicates the connectors have minimal EMI impact on LRU system performance.

CONCLUSION

Upgraded and new EW systems require higher RF power at higher frequencies within the same LRU footprint or smaller. This combination naturally leads to EMI concerns for microwave assemblies, as they are tightly routed together near subsystem electronics within the LRU.

When choosing microwave connectors, engineers should compare the advantages and limitations of each option. Traditional threaded connectors offer excellent shielding effectiveness but are space-limited by their relatively bulky coupling nuts. Push-on connectors, such as the SMPM, offer the highest density advantage and allow for tight packaging within LRUs. However, they require careful installation to ensure proper mating, and their shielding effectiveness is reduced compared to threaded connectors. The threaded SMPM provides a third alternative, offering excellent shielding effectiveness. The connector's compact coupling nut delivers significant space savings while providing a locking mechanism between the mating connectors, reducing installation variability and maintaining performance in use. Regardless of the application, proper selection of microwave cable and connectors help maximize system performance. ■

References

1. P. Pino, "Reducing EMI/RFI in Microwave Cable Assemblies for A&D Systems," *Microwave Journal*, November 14, 2019, Web: https://www.microwavejournal.com/articles/33098-reducing-emirfi-in-microwave-cable-assemblies-for-ad-systems.
2. "ANSI/EIA-364-66B-2025: EMI Shielding Effectiveness Test Procedure for Electrical Connectors," *Electronic Components Industry Association*, Revisions B, June 17, 2025, Web: https://store.accuristech.com/standards/eciaeia-364-66b?product_id=2949540&srsltid=AfmBOoqWYNMnTjhVBFyQnW53qjkgaPSuKrw5WTaWQtnEDaCz9ZEtditl.
3. "MIL-T-81490A (AS): Transmission Lines, Transverse Electromagnetic Mode," *Department of Defense*, Revision A, April 22, 1991, Web: https://quicksearch.dla.mil/qsSearch.aspx.
4. "MIL-STD-348B: Radio Frequency Connector Interfaces," *Department of Defense*, Revision B with Change 4, August 12, 2024, Web: https://quicksearch.dla.mil/qsSearch.aspx.
5. "IEEE 287.1: IEEE Standard for Precision Coaxial Connectors at RF, Microwave, and Millimeter-Wave Frequencies-Part 1," *IEEE*, Revisions 2021, September 16, 2022, Web: https://ieeexplore.ieee.org/document/9889249/versions.
6. P. Pino, "Shielding Effectiveness of Microwave Cable Assemblies," *Microwave Journal*, March 12, 2018, Web: https://www.microwavejournal.com/articles/29809-shielding-effectiveness-of-microwave-cable-assemblies.

MegaPhase

Our Customers Connect With Us™

High-Performance RF Space Cables

Engineered for Extreme Environments

Designed for *mission-critical performance*

MegaPhase Phase3™ Space Cables are engineered for RF and microwave applications where performance stability is non-negotiable. Designed to withstand the extreme conditions of space, these cables maintain phase and signal integrity through wide temperature excursions, vacuum exposure, and mechanical stress.

Built with space-qualified materials and rugged construction, Phase3 cables support mission-critical systems requiring repeatable performance, low loss, and long-term reliability – on the ground, in orbit, and beyond.

- Ultra low loss
- High power-handling capability
- Low outgassing (TML ≤ 1%, CVCM ≤ 0.1%)
- Multipaction-free in vacuum
- Meets ESCC 3408 space qualification
- Vented connector options available
- Operating range: -65°C to +200°C

Learn more about our Space Qualified Products

megaphase.com

How to Select the Best RF Cabling for Harsh Environments

Tibor Urbanek
Cinch Connectivity Solutions, Lombard, Ill.

CHOOSING BETWEEN COAX, TWINAX AND TRIAX CABLES

RF signals move through a cable via an alternating current on the conductor. This sets up the surrounding electric and magnetic fields. The signal's energy is sent down the line on these fields. RF energy's behavior differs fundamentally from conventional low frequency and DC electricity because it lives primarily in these fields. Naturally, that means the RF cables that guide it must be engineered to address this distinction. ***Figure 1*** shows a coaxial cable cross-section with the electric (E) and magnetic (B) field distribution. The red arrows illustrate the electric field extending from the center conductor to the inner face of the shield, while blue loops demonstrate how the magnetic field encircles the conductor.

There are three common cable types used for RF signal transmission, including:

- Coaxial (Coax) cable: A single center conductor surrounded by a dielectric, braided shield and outer jacket.
- Triaxial (Triax) cable: A coax core with an additional intermediate shield and insulation layer that creates a second return path to isolate sensitive signals, or bias lines, from ground noise.
- Twinaxial (Twinax) cable: Two balanced conductors twisted together inside a common shield.

COAX CABLES FOR RF SIGNAL TRANSMISSION

Coax cables are the most common configuration for RF signals. In these cables, the central conductor of the cable is a wire of either stranded or solid construction, depending on the mechanical requirements and expected frequencies. This is surrounded by an electrically conductive shield and the two are separated by an insulating layer, known as the dielectric. In short, the anatomy of coaxial cables is made of a center conductor, dielectric, outer shield and protective jacket, as shown in ***Figure 2***.

The dielectric does not protect the center conductor from harm or adjacent cables; it shapes the cable's electrical behavior. It is vital in controlling the relationship between the inner conductor and the shield. It ensures a precise separation of conductor and shield to control the impedance of the cable, which is also affected by the material from which the dielectric is formed.

CHALLENGES THAT COAX CABLES OVERCOME

Transmission Integrity

Coaxial cables provide a controlled impedance path so fast edges and higher frequency signals can be carried with reduced reflections and waveform distortion when properly terminated. Impedance is how much the cable resists the flow of the alternating current. The dielectric's physical spacing

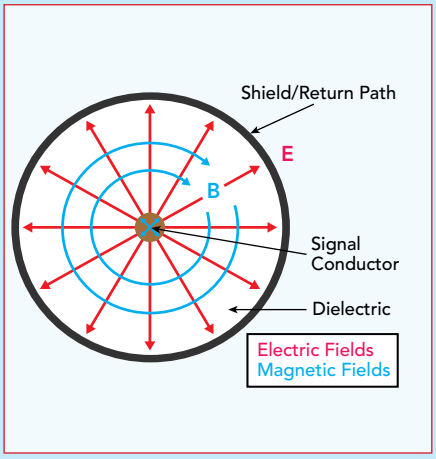

▲ Fig. 1 **Coaxial cable cross-section showing the electric and magnetic fields.**

Low Loss. High Isolation. Delivered Fast.

Backed by over 50 years of switching technology expertise.

Frequency Bands	Designs covering DC to 18, 26.5, 43, 33, 53 and 67 GHz		
Switch Types	SPDT	TRANSFER	SPMT (up to 12 positions)
Available Actuator	Failsafe, Latching	Failsafe, Latching	Normally Open, Failsafe, Latching
Actuator Voltage (Vdc)	12, 15, 24, 28 volts (DC) standard		
50Ω Termination Option	Internal or External	N/A	Internal or External
RF Cycle Life	1, 2 and 5 million cycles		
RF Power handling	SMA: 40-500W | Type-N: 100-2,000W | K: 10-180W | 2.4mm: 3-100W		
DC Control Connection	Solder Terminal, D-Sub, 16pin Dip Socket, USB		
Options	Indicators, Self Cut-Off (SCO), TTL, TTL Decoders, +COM, Auto Reset, Suppression Diodes, LoPIM, Ruggedized, “Optimized RF”, High-Power		
RF Connectors	SMA, 2.92mm (K), 2.4mm, Type-N, TNC, SC, 7/16 & 4.3-10 DIN		

Our high-performance RF coaxial switches are engineered to meet the stringent requirements of RF and microwave test applications up to 67 GHz.
Trusted by engineers worldwide, they offer exceptional signal integrity, repeatability, and reliability - backed by responsive, expert-level support.

e360microwave

e360microwave, Inc. | 753 Ames Ave., Milpitas, California 95035 | www.e360microwave.com
sales@e360microwave.com | +1-408-650-8360

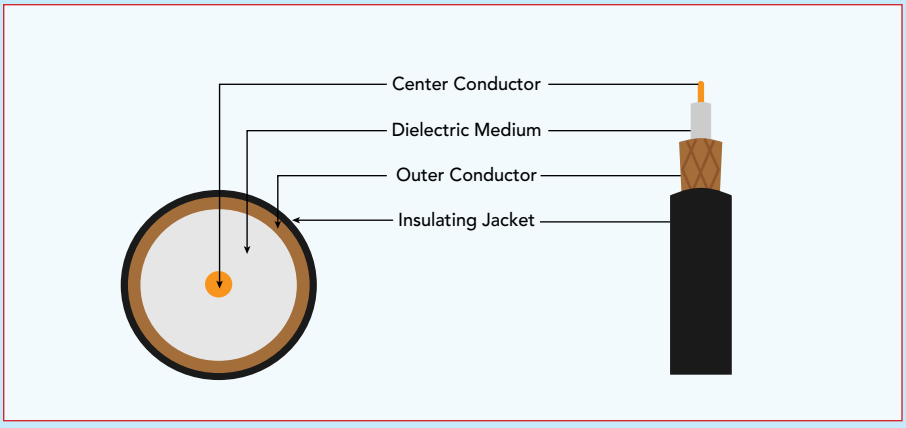

Fig. 2 **Anatomy of a coaxial cable.**

and material properties determine the cable's impedance. Coax creates the optimum physical separation between the conductor and the shield, and its permittivity governs the ease with which an electrical field can form inside it.

Some materials used in dielectric construction include:

- Solid PE – economical, rugged, ~66 percent velocity
- Foamed PE – lighter, lower ε_r, reduced loss
- PTFE (Teflon®) – microwave-stable, wide-temperature
- Expanded PTFE – porous, phase-stable, ultra-low loss
- FEP – extrudable fluoropolymer, low-smoke
- Air-spaced (ribbed) – mostly air, minimal attenuation.

Noise Pickup

The outer conductor in a coax cable acts as an electrostatic barrier to help reduce capacitive coupling of unwanted fields into the signal conductor, which is especially important for low-level signals routed near other wiring and equipment. How much energy is stored within the cable (capacitance) and the magnetic field caused by changes in current (inductance), both affect signal velocity. There is no perfect impedance for a coax cable; it depends on the requirements of the application.

Interference Management

Our world is awash with radiation. Some is a byproduct of the radio transmissions the modern world relies on. Other radiation can come from faulty electrical devices or even just the background radiation of the natural world. Any of these radiation sources can upset high speed links. With appropriate bonding/grounding, coaxial cables reduce the impact of radiated and magnetic field environments, and with a carefully selected grounding strategy, they can avoid ground-loop and common-mode return noise.

APPLICATIONS WHERE COAX CABLES SHINE

The controlled impedance of coax cables supports predictable transmission line behavior. This means that signal quality is maintained as frequency content increases, and proper termination minimizes reflections. The surrounding shield reduces electric field coupling from adjacent wiring and can limit susceptibility to radiated interference, especially important in dense systems where cables often share space with power wiring, motors, transmitters and other noise sources.

For example, in broadcast and cable TV systems where there are many RF carriers packed together, controlling ingress and egress is essential. Coax cables offer excellent shielding in these dense RF environments. Coax geometry is also stable and well-understood, so designers can count on consistent characteristic impedance, a predictability that helps maintain signal integrity across long lengths and through components like splitters.

Coaxial cables have been used in certain telecom trunks or baseband/broadband distribution where the signal spans a wide frequency range. Coax supports high information rates because it behaves like a controlled impedance transmission line with good shielding. That combination is useful when the signal contains fast edges or spans broad frequency content. It also has a reduced susceptibility to radiated electrical noise and a cleaner return path.

Coax keeps a stable 50 Ω or 75 Ω impedance from kilohertz IF stages up to microwave front-ends, a consistency that makes it the default single-ended choice for broadband RF.

ADDING ADDITIONAL SECURITY WITH TRIAX

There are applications where the level of protection provided by coaxial cables is not sufficient. Adding a second shield boosts immunity and cuts leakage. It also provides an independent ground reference, eliminating the multiple return paths that create ground-loop currents.

The design of a triax cable features an additional conductive layer around the core and inner shield, separated by a conventional insulating layer, as shown in ***Figure 3***. While the more intricate construction of triaxial cable increases its cost, triax cables are important solutions for superior signal integrity.

TRIAX CABLES REDUCE LEAKAGE CURRENT EFFECTS

In a coaxial cable, the signal conductor sits at some voltage while the outer shield is at ground. The plastic dielectric is never a perfect insulator (see ***Figure 4***). Its finite resistance acts like a parasitic resistor across the measurement, and that voltage can lead to a small current flow "leakage" from the center conductor to the shield. Moisture, dirt, added length and heat can drop that resistance, and the resulting leakage can bury the true signal and delay settling.

Triax introduces a driven guard shield held at the same potential as the signal. A driven guard in a triax cable holds the inner shield at the same potential as coaxial, cancel-

Custom and Standard RF Cable Assemblies for Embedded Systems

SV can design and manufacture high-performance VITA 67 discrete and harness cable assemblies in both custom and standard lengths.

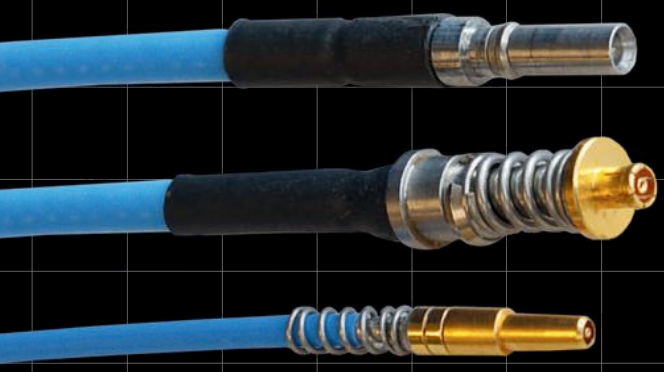

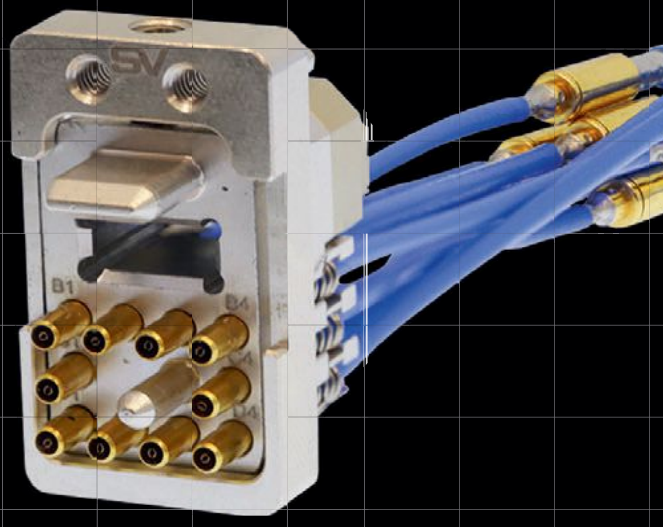

Available Cable Options

- *Ø.047" coax: compact for dense routing and tight bends*
- *Ø.085" coax: versatile and rugged for wider bandwidth needs*
- *Ø.087-LL" coax: low insertion loss cable for precision signal integrity*

Discrete and Harness Cable Assemblies Supported Across Following Standards:

- *VITA 67.1/67.2/67.3 & 66.5*
- *VITA 46/65/90/100 (for backplane, payload card, and optical integration)*
- *SOSA-aligned and OpenVPX embedded platforms*

Applications

- *OpenVPX / VNX+/ VITA-based embedded systems*
- *FACE / CMOSS / VICTORY / MORA / HOST Initiatives and Standards*
- *EW / SIGINT / A-PNT / COMMS / Radar payloads*
- *Digital receiver front-ends*
- *Ruggedized ground, airborne, space, and naval platforms*

Amphenol SV MICROWAVE

www.svmicrowave.com

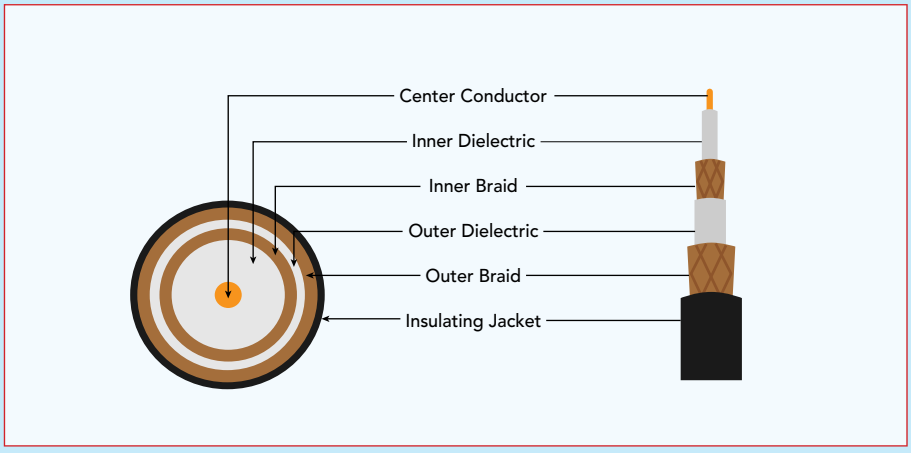

Fig. 3 **Anatomy of a triaxial cable.**

ling the voltage across the leakage path and cutting the current to zero, eliminating leakage. Any tiny residual current flows between the guard and the grounded outer shield, not through the measurement node.

TRIAX ADVANCED SHIELDING BENEFITS

Triax cables are ideal for use in driven-shield and guarded instrumentation applications because the shield is intentionally driven to reduce leakage and noise coupling. They also pair well with high frequency transducer data systems where improved noise performance helps maintain data accuracy. And because of their capability to support high information rates, and to serve as a low impedance line for pulse transmission in certain configurations, they can deliver high-current pulses as a low impedance transmission line for laser lamps or exploding bridge wire ordnance systems. Shipboard digital data-bus standards also call out triax implementations specifically.

Shielding and Ground-Loop Immunity

A driven guard shield wraps the signal core in triax cables. The guard is held at the same potential as the center conductor. With the field collapsed, leakage current vanishes and ground-loop paths never form. The outer shield still ties to chassis ground, providing a second 360-degree Faraday cage that protects against stray electromagnetic fields and static discharge that can inject microvolt errors or full-blown image artifacts into sensitive links. The result is lab-grade noise rejection for pico-amp instrumentation, HD broadcast camera feeds and low-level medical sensors.

HIGH SPEED DATA APPLICATIONS USE TWINAX CABLE

Instead of a single conductor, twinax cables use two parallel wires held in a precise relationship to each other. Surrounding the pair is a dielectric and a single, common shield. In twinax, the dielectric's role is not to maintain the relationship between conductor and shield; it governs the impedance between the two conductors.

Twinax cable is a twisted, balanced pair surrounded by a shielding braid, as shown in ***Figure 5***. The twist helps cancel low frequency magnetic field pickup, while the braid improves isolation from capacitive coupling and helps manage ground-loop-related interference. This can affect bandwidth, so twinax is most useful at lower frequencies as transmission losses rise with frequency.

Prime Twinax Use Cases

Twinaxial cables have improved low frequency magnetic-noise immunity due to the twist of the balanced pair, a defined impedance for predictable interconnect design and shielding coverage that reduces capacitive pickup, cross-talk and susceptibility to ground-loop noise. They are designed for military aircraft data-bus distribution. Twinax is used in guidance/control, navigation and communications systems. Twinax also thrives in video and broadcast distribution applications where shielded twisted-pair constructions are used at scale, as well as low frequency digital and video distribution systems where balanced signaling and shielding offer practical noise hardening. That geometry of twinax cables cancels common-mode noise, making it ideal for 10 to 100 Gb Ethernet DACs, NVLink GPU links and MIL-STD-1553 buses.

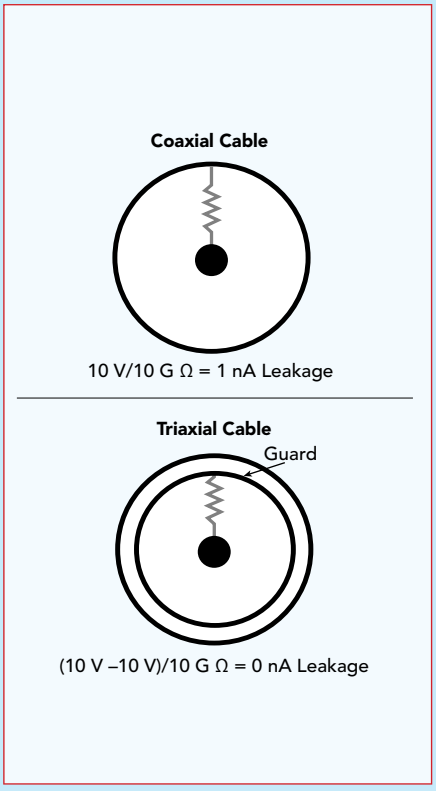

Fig. 4 **The guarding advantage of triax over coax.**

ADDITIONAL CONSIDERATIONS FOR CABLE SELECTION

Every meter of copper and dielectric adds loss. The farther users need to go without active repeaters, the lower the cable's attenuation must be. A solid conductor coax can carry the distance load, spanning tens of meters before attenuation or dispersion forces regeneration. Triax pays for its guard with a little extra loss. Twinax trades long reach for blistering differential bandwidth, so it shines inside a rack

LOVE AT FIRST SPEC

Not Flowers

When Compatibility Really Matters, Choose the Perfect Cable

LEARN MORE

Key Features

- 400+ models in stock (custom lengths & configurations available)
- Cable construction options from jumpers to VNA cables & more
- Wide range of connector types, genders, orientations and mounts
- Rugged construction for high reliability & long life

Mini-Circuits

or on a bench.

Large data centers, aircraft and telecom huts can hold thousands of links. Every added gram or dollar multiplies fast. Coax is a proven commodity technology with the lowest cost-per-meter and the widest connector ecosystem. Twinax uses less copper and dielectric than equal-performance coax, keeping short-haul cloud links lightweight and inexpensive. Triax is wider and pricier than the alternatives. Engineers reserve it for mission-critical, low-level signals where noise failures are costlier than the cable.

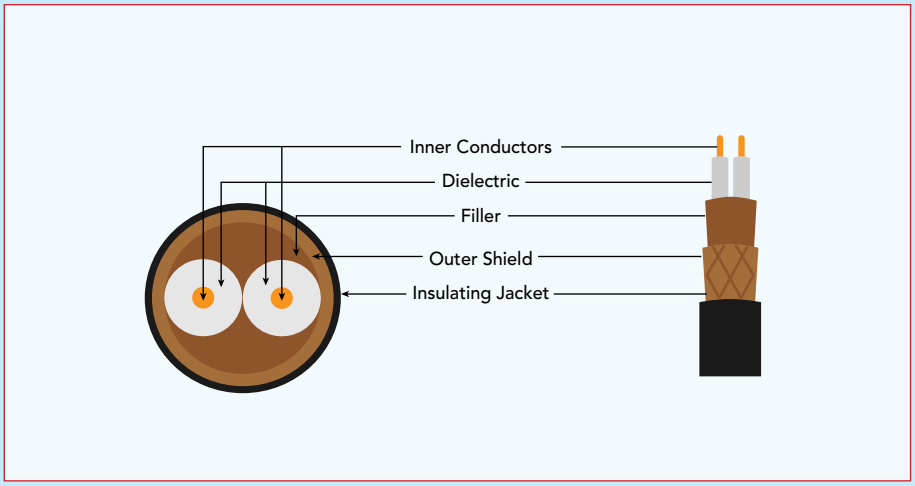

▲ Fig. 5 **The internal components of a twinax cable.**

THE BEST CABLE FOR DIFFERENT APPLICATIONS

Coaxial, triaxial and twinaxial cables each deliver advantages in signal integrity, resistance to interference and cost. By understanding the differences between them, engineers can choose the option that provides optimal performance across applications from TV broadcasting to data centers. The composition of components is also a consideration, with increasing emphasis on flame-retardant and low-toxicity materials for public safety, as well as specialized materials for aircraft environments where exposure to fuels and cleaning solvents must be tolerated. The options for any application exist, and choosing the right cable will deliver reliable, high speed data transmission in today's increasingly demanding environments. ■

Frontlynk®
Bridging Gaps

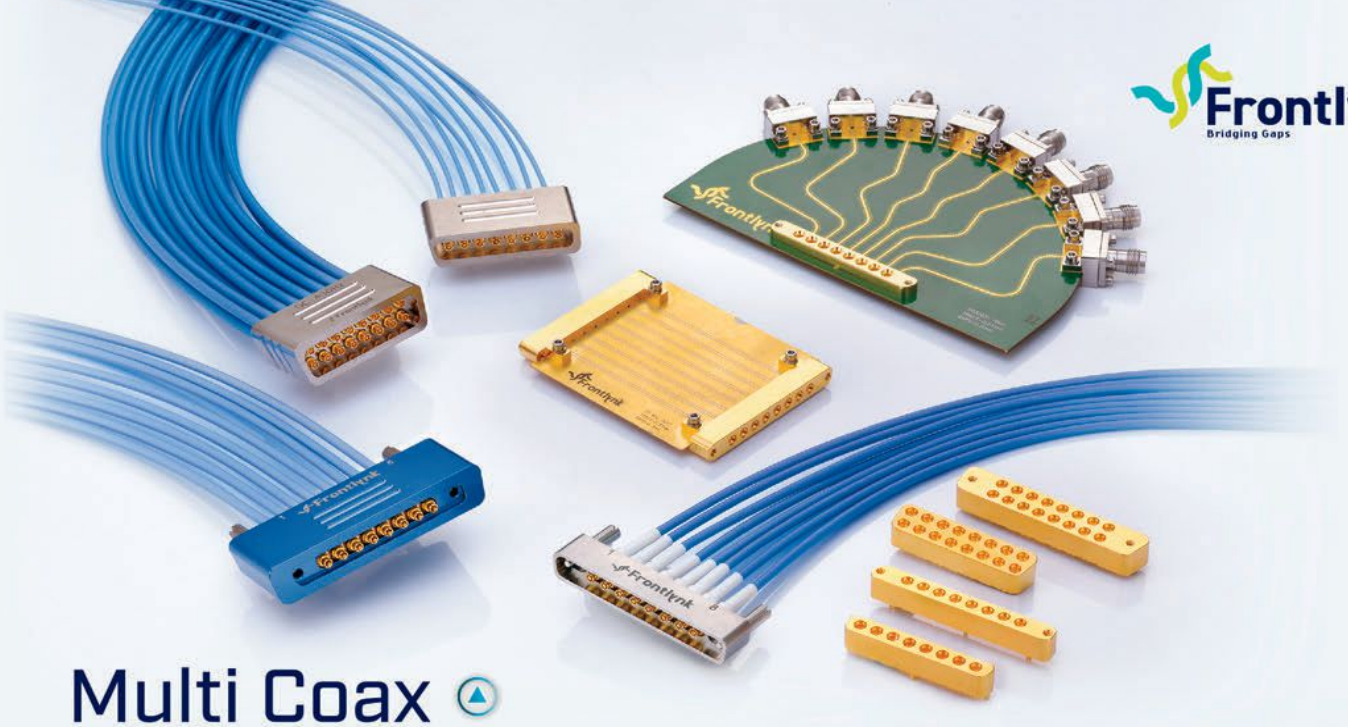

Multi Coax

Probe Multi Coax up to 67GHz

Keysight 250GHz VNA installed already!

RF.Microwave Coaxial Connector & Cable Assembly

1.0mm Series

Connectors, Adaptors, and Cable Assemblies up to 110GHz

0.8mm Connector
DC to 145GHz

- **1.0mm Connector** DC to 110GHz, VSWR≤1.2
- **1.35mm Connector** DC to 90GHz, VSWR≤1.2
- **1.85mm Connector** DC to 67GHz, VSWR≤1.2
- **2.4mm Connector** DC to 50GHz, VSWR≤1.2
- **2.92mm Connector** DC to 40GHz, VSWR≤1.15
- **3.5mm Connector** DC to 34GHz, VSWR≤1.15

1.35mm Series up to 90GHz

Test Cables up to 110GHz

Frontlynk Technologies Inc. www.frontlynk.com

Tel: +886-6-356-2626 Fax: +886-6-356-6268 E-mail: info@frontlynk.com

Cables and Connectors for DC to 250 GHz Test Systems

Junkosha USA Inc.
Irvine, Calif.

The rapid expansion of AI accelerators and high performance data center interconnects is driving increased research and development activity in the mmWave and sub-terahertz (sub-THz) frequency ranges. These emerging applications impose stringent requirements on bandwidth, latency and signal integrity that extend well beyond the capabilities of traditional RF measurement infrastructures. While advances in vector network analyzers (VNAs) and frequency-extension technologies (see ***Figure 1***) have enabled measurements beyond 110 GHz, overall measurement accuracy is increasingly limited by interconnect performance rather than instrument capability. At mmWave and sub-THz frequencies, phase instability, insertion loss, mechanical repeatability and connector robustness of coaxial cable assemblies become dominant contributors to measurement uncertainty. This article examines the role of cables and connectors as critical measurement enablers in DC to 250 GHz test systems and discusses the physical mechanisms that drive interconnect-induced measurement errors, with emphasis on phase stability, mechanical sensitivity and repeatable high frequency device characterization.

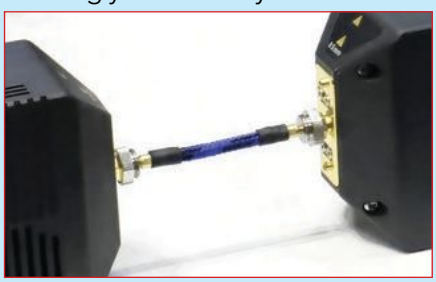

▲ Fig. 1 **MWX0A5 cable connected to Keysight extenders.**

INTRODUCTION

The continued expansion of AI-driven computing and data-intensive applications has significantly increased demand for higher bandwidth interconnect technologies. Data centers, central to the modern digital ecosystem, are undergoing rapid architectural evolution to accommodate escalating traffic volumes and increasing latency-sensitive workloads. Although optical links remain the dominant solution for long-reach data transport, growing limitations in electrical interconnect scalability, power consumption and signal integrity are motivating increased exploration of mmWave and sub-THz solutions for short-reach and intra-system connectivity.

These trends place new demands on RF and microwave test and measurement systems. Accurate characterization of devices, modules and subsystems operating above 110 GHz requires not only advanced instrumentation, but also highly stable and repeatable interconnects. In this frequency regime, cables and connectors can no longer be treated as secondary accessories; instead, they become integral components of the measurement system that directly influence achievable accuracy, repeatability and confidence in measured results.

MMWAVE AND SUB-THZ SYSTEM DRIVERS

Emerging AI and machine learning compute architectures continue to drive increasing bandwidth re-

INTERCONNECT SOLUTIONS

SHAPING THE FUTURE OF RF

From board-to-board connectors to high-frequency cable assemblies and switches, Radiall delivers precision-engineered solutions across the RF spectrum. Backed by deep expertise in developing custom high-performance RF solutions, Radiall partners with engineers to power next-generation systems with confidence.

quirements, reinforcing the need for next-generation interconnect solutions. Operation in the mmWave (30 to 300 GHz) and sub-THz frequency ranges offers a potential path toward higher data rates through short-range wireless or quasi-wireless links. These approaches are supported by ongoing advances in RF integrated circuits, advanced packaging and heterogeneous integration technologies.

Fully digital mmWave transceivers incorporating high speed data converters and beamforming capabilities are expected to play an important role in future 6G and beyond wireless systems. At sub-THz frequencies, however, losses and parasitic effects scale rapidly with frequency, making co-optimization of circuits, packages and interconnects essential. Measurement fidelity in this frequency range is therefore critical for validating both device-level performance and overall system architectures.

MEASUREMENT CHALLENGES ABOVE 110 GHZ

While frequency-extension techniques have expanded the usable range of modern VNAs well beyond 110 GHz, practical measurement accuracy at these frequencies is increasingly dominated by interconnect limitations. Key contributors include elevated insertion loss, phase instability, connector wear and limited mechanical robustness of test cables and interfaces. These effects increase sensitivity to handling, temperature variation and calibration repeatability.

As operating frequency increases, electromagnetic wavelengths shrink to the millimeter and sub-millimeter scale. Under these conditions, even small mechanical or material variations within the measurement setup can produce measurable electrical effects. As a result, maintaining stable and repeatable interconnecting performance becomes one of the primary challenges in mmWave and sub-THz test environments.

PHASE STABILITY AND MECHANICAL SENSITIVITY

Coaxial cable assemblies remain widely used in mmWave and sub-THz test systems due to their shielding effectiveness, controlled impedance and compatibility with precision connector interfaces. However, it is well known that the amplitude and phase response of a coaxial transmission line can vary as a function of mechanical bending, routing and environmental conditions.

These variations arise primarily from small changes in the effective dielectric constant caused by mechanical deformation or temperature fluctuations, which, in turn, alter signal propagation delay. At sub-THz frequencies, even very small phase perturbations can translate into significant amplitude ripple and degraded measurement repeatability. Consequently, cable phase stability under flexure and thermal stress becomes a critical parameter in high frequency measurement environments, particularly for applications requiring frequent reconnection or cable movement.

IMPLICATIONS FOR DC TO 250 GHZ TEST SYSTEMS

In advanced mmWave and sub-THz measurement systems extending to 250 GHz, cables and connectors must be treated as precision components rather than passive accessories. Highly phase-stable, low loss coaxial cable assemblies with mechanically robust, repeatable connector interfaces are essential for minimizing measurement uncertainty and ensuring consistent results.

From a system-level perspective, interconnect performance directly affects calibration validity, long-term measurement stability and confidence in extracted device parameters. As operating frequencies continue to increase, the selection, qualification and handling of coaxial cable assemblies will play an increasingly important role in enabling accurate device characterization and reliable system validation.

▲ Fig. 2 **MWX0A5 cable.**

INTRODUCING JUNKOSHA MWX0A5 0.5 MM CABLE & ACCESSORIES

Junkosha is supporting the industry as it moves toward higher frequencies, including the development and introduction of 0.5 mm cables, as shown in ***Figure 2***. Junkosha offers assemblies with 0.5 mm male and female connectors. They also offer adapters for 0.5 mm female to 1.0 mm male or female, allowing engineers to integrate the new equipment into existing systems. To maintain repeatability and increase durability with such small center pins, Junkosha is leveraging its expertise to develop a proprietary safety-lock mechanism that guides engagement prior to pin insertion, significantly reducing the risk of bent or damaged contacts. This becomes critical as connector durability directly impacts system connectivity, repeatability and long-term measurements.

The return loss and insertion loss performance of the Junkosha® Microwave/mmWave Coaxial Cable Assembly MWX0A5 are shown for reference only in ***Figures 3*** and ***4***, respectively.

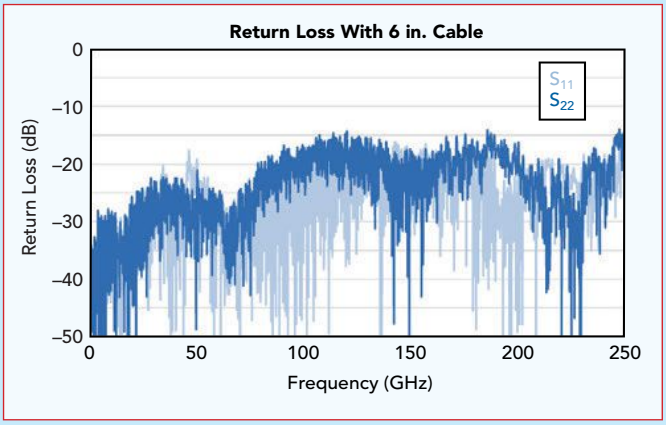

▲ Fig. 3 **Return loss of Junkosha MWX0A5 cable up to 250 GHz.**

NEW

CBN SERIES

Phase Stable Flex Cables

For Precision Measurement Applications

Mini-Circuits' new CBN-series of phase-stable flexible cables is ideal for a wide range of precision applications from DC to 26.5 GHz, including test labs, high-speed data systems and precision measurements. CBN-series models provide exceptional phase and amplitude stability (±6˚, ±0.08 dB) in bend radii as small as 50 mm. 90 dB shielding effectiveness and 74% velocity of propagation ensure outstanding transmission efficiency for outstanding measurement integrity and consistency. These high-performance cables are available from stock in lengths from 1 to 5 ft., with custom lengths available on request.

Key Features

- DC to 26.5 GHz
- Ultra-flexible, 50 mm min. bend radius
- Superior phase & amplitude stability
- (±6.0˚, ±0.8 dB max. @ 26.6 GHz)
- Low loss & high velocity of propagation
- 1 to 15 ft. lengths in stock

LEARN MORE

Mini-Circuits®

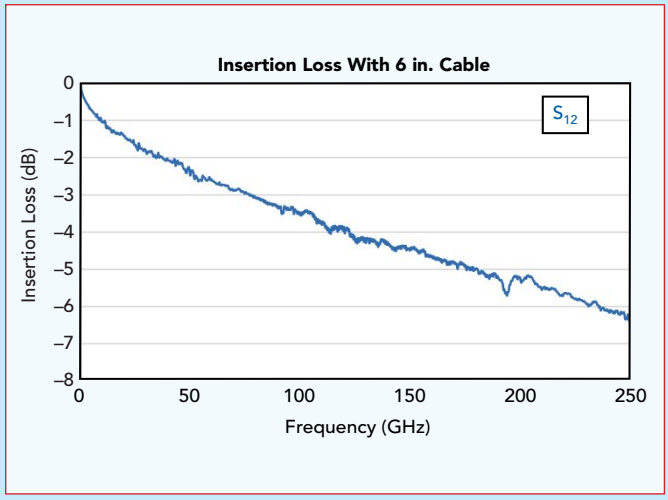

Fig. 4 Insertion loss of Junkosha MWX0A5 cable up to 250 GHz.

Equally important is system integration. The availability of 0.5 mm to 1.0 mm adapters simplifies test setups by allowing compatibility with existing devices while maintaining sub-THz performance. Supplying both the cable and adapter as a unified solution, Junkosha reduces interface variability and supply-chain mismatches that often degrade measurement accuracy.

CONCLUSION

As mmWave and sub-THz technologies mature in response to AI-driven and data-centric applications, the limitations of traditional measurement approaches become increasingly evident. Above 110 GHz, interconnect performance often emerges as a dominant factor in overall measurement accuracy, frequently surpassing instrument capability as the primary source of uncertainty. This article highlights the critical role of cables and connectors in DC to 250 GHz test systems and underscores the importance of phase stability, mechanical robustness and repeatability. Continued progress in high frequency measurement will depend not only on advances in instrumentation, but also on ongoing innovation in precision interconnect technologies.

References

1. T. S. Rappaport et al., "Wireless communications and applications above 100 GHz: Opportunities and challenges," *IEEE Access*, Vol. 7, 2019, pp. 78729–78757.
2. P. Hillger et al., "Towards mobile terahertz communication systems," *IEEE Journal of Selected Topics in Quantum Electronics*, Vol. 26, No. 1, Jan. 2020.
3. G. F. Engen and C. A. Hoer, "Thru-reflect-line: An improved technique for calibrating the dual six-port automatic network analyzer," *IEEE Transactions on Microwave Theory and Techniques*, Vol. 27, No. 12, Dec. 1979.
4. D. F. Williams, *Calibration and Measurement of Millimeter-Wave Devices*, NIST Technical Note 1520, 2006.
5. J. Verspecht and D. F. Williams, "Calibration of millimeter-wave vector network analyzers," *IEEE Microwave Magazine*, Vol. 17, No. 1, Jan. 2016.

High Density Without Compromise!

- **Test & Measurement**
- **Broadcast**
- **Medical**

Learn More

High Density Enhances Efficiency with Improved Performance

Step into the next generation of RF performance and high density with the new PX and PRX connector families. Designed as a superior alternative to traditional coax connectors or as an upgrade for existing multi-pin solutions, these advanced connectors offer exceptional performance and scalability, available in configurations ranging from 13 to 53 pins.

Impedance	Frequency	Housing Contact #	Contact Size	Cable Types
50 Ohm	100 MHz to 67 GHz	13, 26, 28, 53	16	RG-178, 316, 405, M17/151(.047")
75 Ohm	100 MHz to 18 GHz	13, 23, 48	12	RG-179, SS75086

The PHOENIX Company of Chicago

Leading Blindmate Microwave Contact Technology

New Connectors for 224G with Path to 448G

Samtec, Inc.
New Albany, Ind.

RF and microwave technologies have proven their utility in the realm of "digital" test, with test fixtures and evaluation platforms requiring frequencies out to 90 GHz and beyond. Evaluating silicon is highly dependent on the signal quality that loops between the printed circuit board (PCB), test fixture and test equipment. This becomes even more important for 224 Gbps signals, and as the industry looks towards testing 448 Gbps signals, it has become very challenging, with designers asking for an interconnect that handles up to 130 GHz.

While frequencies continue to trend upwards, most of today's leading-edge needs are in the realm of 224 Gbps. One way for designers to set up tests for 224 Gbps signaling is to use single-channel test connectors, which create an immediate and significant real estate issue on PCBs. Alternatively, they could use a ganged, two-piece interconnect (a board connector and cable harness), which can be costly. Additionally, this is not a flexible use case because they require PCB connectors to be hard-mounted on every PCB.

COST, SIZE AND PERFORMANCE

Designed to address these real estate, cost and flexible use case issues, the Samtec BE71A Bulls Eye® Phase & Amplitude Test Assembly combines the Bulls Eye assembly's space-saving compression-mount design with Samtec Nitrowave™ phase-stable high performance cables. The test assembly, as shown in ***Figure 1***, is a solderless design that compression mounts to the board for high speed digital test, SerDes characterization and automated test equipment. It is also well suited for high-density multi-port panel and I/O connections, including quantum computing racks or high-density cable-to-board connections. Optimized for use out to 71 GHz in support of 224 Gbps PAM4 SerDes testing, the BE71A test assembly is configured in a double-row, supporting microstrip/coplanar waveguide or stripline PCB transmission with 50 Ω impedance.

Featuring a standard 1.85 mm connection to instrumentation, the BE71A test assembly also eliminates the need to upgrade to more costly 1.00 mm test equipment that is commonly required for 224 Gbps PAM4 testing.

IMPORTANCE OF PHASE MATCHING

As frequencies increase in today's use cases, concerns about phase matching between the cable assemblies emerge. Precise signal timing is vital when assessing performance or detecting faults in test and measurement. The BE71A offers 0.5 ps phase matching. This matters for signal integrity, transmission reliability and error reduction. While this level of

▲ Fig. 1 **Samtec's BE71A Bulls Eye Phase & Amplitude Test Assembly.**

Fig. 2 **Samtec's BE71A loss performance.**

phase matching in cable assemblies is important, maintaining that phase match while test fixtures and cables are tweaked and moved is even better. The Nitrowave cables in the BE71A were specifically designed to maintain phase match in these types of circumstances. In fact, because it is equipped with Nitrowave LL071 cabling, the BE71A is Samtec's best phase match (0.5 ps) and lowest insertion loss Bulls Eye assembly, as shown in ***Figure 2***. Performance shown in Figure 2 is recorded during 90-degree cable movement.

ENABLING TECHNOLOGY

Samtec first released the Bulls Eye test point system in 2011 for 20 GHz connections. Since then, the product family has rapidly expanded to include 40, 50, 70, 71, 90 and soon 130 GHz (for 448 Gbps testing). ***Figure 3*** shows the Bulls Eye product family across different frequencies.

The BE71A test system is an expansion that takes advantage of Samtec's proprietary Nitrowave cable technology launched in 2025.[1,2] Nitrowave cable was developed to address repeatability and loss margins at mmWave frequencies for improved electrical performance with lower insertion loss and excellent phase matching to 0.5 picoseconds.

BENEFITS TO TEST

Historically, the one-piece, solderless design of the Bulls Eye test assemblies improves cost and ease of use within a lab setting. Customers who are already working with BE71A test assemblies are using them as part of a test fixture setup, and, in some cases, as part of the actual test equipment. For example, the high-density, space-saving Bulls Eye BE71A test assembly can be integrated directly into the front panel of test equipment used for 224 Gbps analysis, such as a bit error rate tester. Outside the box, the BE71A test assembly enables smaller evaluation boards and shorter trace lengths in test and measurement applications. The assembly compression-mounts[3] directly to the board for placement adjacent to the SerDes under characterization, reducing trace length and associated loss.

CONFIGURATIONS AVAILABLE NOW

BE71A test assemblies can be configured with 3, 4, 6, 8, 10, 12, 14 or 16 positions per row. The operating temperature is specified at -65°C to +125°C.

References

1. "Samtec Releases Nitrowave™ Phase and Amplitude Stable Microwave Cable Assemblies to 110 GHz," *Microwave Journal,* June 3, 2025, Web: https://www.microwavejournal.com/articles/44209-samtec-releases-nitrowave-phase-and-amplitude-stable-microwave-cable-assemblies-to-110-ghz.
2. "Fabs and Labs: Samtec," *Microwave Journal,* Vol. 66, No. 9, September 2023, p.98.
3. J. Alexander, D. Birch and D. Beraun, "Evolution of Interconnects in Benchtop RF Test," *Microwave Journal,* March 2025 Special Focus.

Samtec, Inc.
New Albany, Ind.
www.samtec.com

Assembly	130 GHz	90 GHz	71 GHz	70 GHz	50 GHz	40 GHz
Block Bottom View			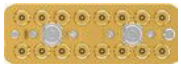		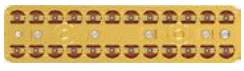	
SerDes Characterization	448 Gbps	448/224 Gbps PAM4	224 Gbps PAM4	112 Gbps PAM4	56 Gbps PAM4	
Phase Matching	0.5 (Half) ps	1, 2 or 5 ps	0.5 (Half), 1, 2 or 5 ps	2 or 5 ps	2 or 5 ps	
End 2 Connector	1.00 mm	1.00 mm; 1.35 mm	1.85 mm	1.85 mm	2.40 mm	2.92 mm
Cable Type	High Performance Nitrowave™	0.047	High Performance Nitrowave™	0.086	MWC-2350CU-01	
PCB Transition	Microstrip/CPW or Stripline					
Bulls Eye® Connector Design	Spring-Loaded Contact; 360° Grounding				Pogo-Pin for Signal & Ground	
Number of Rows/ Positions	**1x**: 2, 4, 8, 12 **2x**: 4, 8, 12, 16		**2x**: 4, 8	**1x**: 2, 4, 8, 12 **2x**: 3, 4, 6, 8, 10, 12, 14, 16	**2x**: 3, 4, 6, 8, 10, 12, 14, 16	
Impedance	50 Ω					
Samtec Series	BE130	BE90A	BE71A	BE70A	BE40A	

Fig. 3 **Bulls Eye product family.**

Tackle Tough Testing Conditions with High Performance Cables

RF engineers face significant challenges when designing systems for radar, missile defense, 5G communications and medical imaging. Demanding test environments require cables with exceptional stability, repeatability and resilience. Variations in phase or insertion loss due to flexure or temperature shifts can compromise measurements and system performance, which makes cable selection a critical design consideration.

P1dB's PinPoint™ high performance test cables are engineered to meet the toughest challenges in the industry. These assemblies deliver phase stability under flexure and temperature variation, ensuring measurement integrity in lab and production settings. With low insertion loss and VSWR across the full frequency band, the PinPoint™ cables series maintains signal integrity even under demanding test conditions.

Durability is built into every assembly. Designed to operate reliably up to 125°C and featuring a robust armor-protected construction, PinPoint™ cables withstand >50,000 flex cycles without degradation. All connector series are rated for 5000 mating cycles, minimizing downtime and replacement costs in high-use environments.

Standard lengths of 24, 36, 48 and 60 in. are available, as well as custom lengths. These cables are compatible with a range of RF interfaces such as SMA, 2.4 mm and 2.92 mm and support applications from vector network analysis to field diagnostics. From MIL-Aero test stands to 5G component validation benches, PinPoint™ cables provide a high performance, cost-effective solution without compromising quality.

VENDORVIEW

RFMW
San Jose, Calif.
www.rfmw.com

High Frequency Connector for Harsh Environments

Smiths Interconnect draws on decades of space heritage to offer SMPM Mini-Lock connectors. They incorporate patented technology to provide reliability and RF performance in harsh shock and vibration environments. More than 50 lbs. of pull strength is assured with an audible click when installed. The connectors operate up to 110 GHz at 50 Ω and deliver a VSWR of 1.25:1 at 26.5 GHz, 1.35:1 at 50 GHz and 1.65:1 at 110 GHz. In addition, the connectors are compact, rugged and blind-mateable for easy integration for use in aerospace, space, defense, telecommunications, industrial equipment and test and measurement applications.

The Mini-Lock Connector features a robust locking mechanism ensuring signal integrity and stable transmission of data between applications. The connector is qualified to vibration per MIL-STD-202, Method 204 and shock per MIL-STD-202, Method 213, Condition I. They have an operating temperature range of -65°C to 165°C and are suitable for harsh mechanical stress environments such as radars, LEO, MEO and GEO satellites, space flight, military, UAV and UGV applications.

The Mini-Lock can be selected for use with Smiths Interconnect high frequency cable assemblies, including the Semi-Rigid and SpaceNXT™ QT Series cables.

Smiths Interconnect is a provider of high-reliability connectivity products and solutions. They have research and development, sales and manufacturing facilities in 12 countries and offer global design, development, manufacturing and testing capabilities.

Smiths Interconnect
Stuart, Fla.
www.smithsinterconnect.com/products/connectors/high-frequency-connectors/mini-lock-connectors/

Flexi RF

Precision RF Components

Same-Day Global Shipping From USA

100,000+
Parts In Stock

10,000+
RF Engineers Rely On

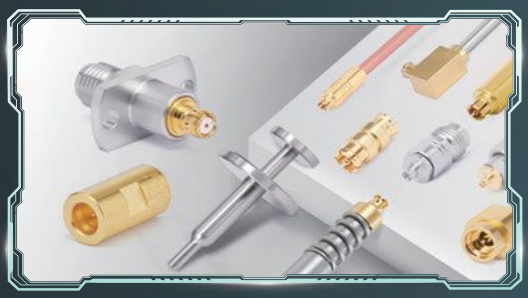

170 GHz
Frequency Up To

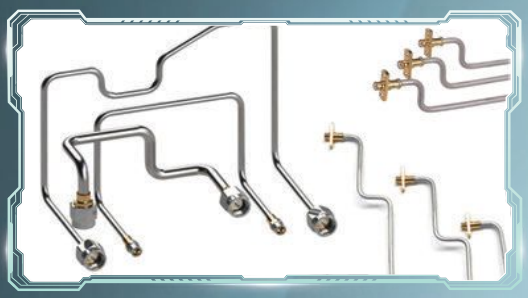

www.FlexiRF.com

Flexi RF,Inc
20045 Stevens Creek Blvd., Suite 2B, Cupertino, CA 95014 (650) 880-9199 Sales@FlexiRF.com

Scan to Shop Now

HYBRID INTERCONNECT SOLUTION

Anoison has successfully deployed a custom-engineered hybrid interconnect solution for a global hyperscale technology leader. By leveraging the rugged MIL-DTL-38999 Series III architecture, its team solved a critical R&D challenge: integrating high speed data and precision control signals into a single, zero-crosstalk interface. The result? Reduced cable clutter. Superior signal integrity and vibration-proof reliability for next-gen hardware testing. At Anoison, they don't just provide cables — they provide the high-fidelity connectivity that powers the future of cloud and AI innovation.

Anoison
www.anoison.com

G3PO MULTI-CHANNEL PCB CONNECTORS

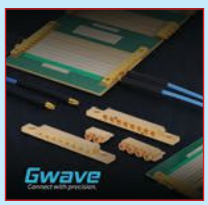

Gwave Technology introduces new 2×, 4× and 8× multi-channel board-to-board G3PO connectors, specifically engineered for semiconductor and high speed PCB testing. Supporting frequencies up to 110 GHz, these connectors deliver industry-leading VSWR and signal integrity. To ensure seamless integration, matching G3PO cable assemblies are available, providing a complete, high-precision interconnect solution for next-generation hardware.

Gwave Technology Inc.
www.gwavetech.com

HIGH RF POWER CABLES AND ASSEMBLIES

IW has been supplying coaxial cable since the 1970s. Based on its proprietary technology of laminating Teflon™, IW manufactures cables from 0.034 to 0.750 in. diameter. There are four primary flexible cable types that provide solutions for high RF power transmission; average ratings: 7506, 10 kW/1 GHz, 4806, 3 kW/1 GHz, 2801, 1.9 kW/1 GHz and RF250 (flexible RG401), 1 kW/1 GHz. IW supplies cable assemblies with C, SC, LC, 7/16, connectors, plus 1 5/8 and 3 1/8 EIA flanges.

Insulated Wire
www.insulatedwire.com

STABILITYPLUS™ PHASE-STABLE CABLE ASSEMBLIES

Setting the standard for high performance ruggedized cable assemblies, the Maury Microwave StabilityPlus™ Series is your interconnect choice for reliable and repeatable measurements, providing amplitude and phase stability with flexure, superior flexibility, ease-of-use, durability and a compact form factor. Color-coded connectors significantly reduce the potential for connection errors, offering clear indications of compatibility and intermatability. Discover how StabilityPlus can enhance your test setup today.

Maury Microwave
www.maurymw.com

SPACE-QUALIFIED CABLES

MegaPhase Phase3™ space-qualified cables deliver phase-stable, low loss RF performance for demanding space applications up to 67 GHz. Engineered to withstand extreme temperatures, vacuum and radiation, these cables feature low outgassing materials, vented connectors and multipaction-free operation. Phase3 cables meet ESCC 3408 space qualification requirements and combine rugged mechanical design with exceptional electrical stability, making them ideal for satellite, payload and spaceflight RF interconnects.

MegaPhase
www.megaphase.com

HIGH-POWER DUAL-DIRECTIONAL COUPLER

VENDORVIEW

Micable 1 to 8 GHz 30/40 dB high-power dual-directional couplers has DC pass capability. They have excellent main line/coupling VSWR (1.4:1 max.), low insertion loss (0.4 dB max.), excellent coupling (30/40±0.8 dB max.) and flatness (±1.1 dB max.), high directivity (14 dB min.) and 600 W CW power handling capability. They can be widely used in 5G, testing, instrumentation, power amplifier, transmitter and other fields.

MIcable Inc.
www.micable.cn

HIGH PERFORMANCE VITA 67.3 RF SOLUTIONS

SV Microwave's VITA RF solutions are built for OpenVPX and SOSA-aligned systems, delivering rugged, high frequency performance for modular embedded platforms. Designed for direct PCB launches, VITA 67.3 solutions support SMPM, SMPS and NanoRF for next-gen modularity. From legacy SMPM integration to NanoRF and hybrid optical-RF deployments, SV Microwave delivers unmatched density, reliability and scalability. Available now at PEI-Genesis for fast shipping.

PEI-Genesis
www.peigenesis.com

"SOLDERLESS" SMA MALE CONNECTOR

1201-273-GG is a "Solderless" SMA male connector for 086 semi-rigid cable. The unique compression clamp design requires no soldering to terminate both the cable inner and outer conductors. Designed to be used for quantum computing and medical applications, the connector uses all non-magnetic materials and plating to

MiCable

「90GHz」
HIGH SPEED MULTI-COAX CABLE ASSEMBLIES

NEW

Channel 8 [Single-row] | 16 [Dual-row]

- Spring-load Design for Both Center & Outer Contact
- Solder-free Installation
- Individual Repair & Replacement for Single Channel

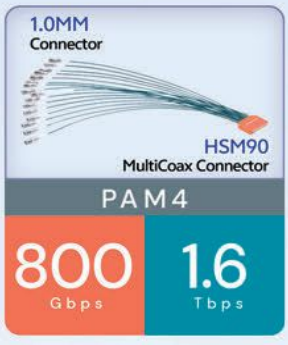

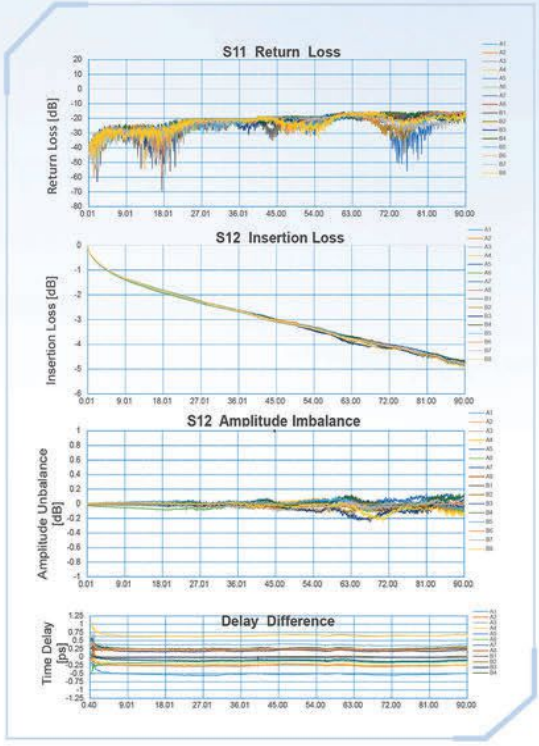

Frequency
DC~90GHz

VSWR
<1.35:1@56GHz
<1.50:1@90GHz

Cable Attenuation
<9.65dB/m@56GHz
<13dB/m@90GHz

Skew Match
<±1ps

Pitch
3mm

Amplitude Consistency
<±0.2dB@90GHz

Application

- Signal Integrity Measurement
- Differential Signal Measurement
- Semiconductor Design &Testing
- Automated Test & Measurement

More Information-
Scan the QR Code

MIcable Inc.
www.micable.cn sales@micable.cn +86-591-87382856

deliver excellent performance from DC to 26.5 GHz while being transparent to other magnetic fields.
San-Tron
www.santron.com

0.8 MM, 145 GHZ HIGH PERFORMANCE VERTICAL LAUNCH CONNECTOR

SMI's newest product is its innovative 0.8 mm, 145 GHz high performance vertical launch connector for micro-strip, CPW and GCPW boards. This cutting-edge design ensures exceptional signal integrity while delivering the industry's lowest VSWR, RF leakage and insertion loss. To learn about its connectors and take advantage of its complimentary board launch, please email connectors@southwestmicrowave.com.
Southwest Microwave
www.southwestmicrowave.com

INTEGRATED RF FILTERS

SV has designed a new line of high frequency, lowpass filters with a small form factor. With DC to 12 or 18 GHz passbands, they are available as standard connectorized offerings for the SMA and SMPM series. These filters remove interference from nearby signals while maintaining low insertion loss in the passband. Additionally, the SMPM filter does not compromise on connector density and maintains the same outer diameter as a typical SMPM bullet.
SV Microwave
www.svmicrowave.com

SOLDERLESS PCB CONNECTORS

Teledyne Storm Microwave's ultra-high frequency solderless connectors are designed for cutting-edge test applications. These new interfaces include SMA, 2.92 mm, 2.4 mm, 1.85 mm, 1.35 mm and 1 mm sizes, supporting frequencies up to 110 GHz. Unlike traditional soldered solutions, these solderless connectors allow repeated engagement without damaging the PCB, making them ideal for lab environments requiring frequent reconfiguration or testing. Their robust mechanical design ensures secure mating while maintaining superior electrical performance, offering a future-proof solution for evolving RF requirements.
Teledyne Storm Microwave
www.teledyne.com

Compact Dome Antennas Bridge Classic Cellular and IoT Applications

The Antenna Company
Eindhoven, The Netherlands

The compact dome is an established antenna style that is both functional and, when well-designed, aesthetically pleasing. Sometimes called saltshaker or shot glass antennas because of the similarity in shape to those common household items, the label "compact dome" better contrasts the relative physical size of this style with other common external antenna formats, such as puck- and blade-style antennas.

Compact dome antennas may be offered with multiple mounting and termination options. Most typical are panel mount offerings with an N-connector termination (see ***Figure 1***) that also serves as the fastener to hold the antenna fast to the panel. Cabled terminations, commonly with SMA-type connectors, may also be used for panel mount installations (see ***Figure 2***). Both connector and cabled terminations can also lend themselves to remote bracket mount installations (see ***Figure 3***).

Mobile application mounts, such as automotive roof mounts, may be implemented by either of these termination types or

Fig. 1 **Panel mount, N-connector antenna (AC85002-NJB).**

Fig. 2 **Panel mount antenna cabled with SMA connector (AC87001-100B).**

Fig. 3 Antenna on a remote mount bracket.

by using an NMO connector termination (see *Figure 4*). These are commonly used in mobile applications because they offer a simple screw-on antenna replacement from outside of the vehicle.

Having a design structure that offers the same base antenna solution across all termination options allows users to make mounting changes during design and supports manufacturing economies of scale, supporting cost effectiveness.

The compact dome antenna format is enduring in the market because it provides a balance of size, physical robustness and RF performance under the cover of an unobtrusive visual.

Fig. 4 NMO mount antenna (AC85002-NMB).

The compact dome profile is lower and employs a stronger mount than most whip-style antennas, reducing the risk of snapping off throughout its lifetime. Additionally, some compact dome products are designed for increased impact resistance, for example, testing to the IEC 62262 IK10 impact standard. Supporting such standards also tends to improve wind resistance ratings, which are important for mobile applications and installations that may be affected by extreme weather conditions.

Other prominent characteristics of superior compact dome antennas include ingress protection (IP rating) and ultraviolet (UV) light resistance. These characteristics imply readiness for outdoor usage in most environments. Ingress protection is typically reported as an IP code specified in IEC 60529. IP65 and IP67 are common specifications, the former specifying dust-tightness with protection from water jets and the latter specifying dust-tightness with protection against immersion up to one meter of depth. UV protection is essential for antenna longevity outdoors. It is implemented with a UV-resistant dome plastic such as ASA and/or with the addition of a UV stabilizer additive to the dome material.

Less prevalent, but also important characteristics for robust usage are salt spray resistance, typically tested to MIL-STD 810F and/or ASTM B117, and dome (in)flammability rating under the UL 94 standard.

Typical compact dome height is tall enough to eclipse puck antenna RF performance while providing performance that rivals taller/bulkier whip solutions. Antenna efficiency and voltage standing wave ratio (VSWR) are the most commonly considered antenna performance parameters, but antenna peak and average gain, omnidirectionality and polarization may also be considered for some applications. Best-in-class performance characteristics vary by technology — wideband cellular, cellular IoT (e.g., Cat-M1), Wi-Fi®, Bluetooth®, low-power wide-area networking (e.g., LoRaWAN®) or others, but in all cases, VSWR should be as close to 1:1 as possible and efficiency as high as possible in the frequency bands of operation.

The termination options of compact domes are suited for many end-user applications. Mobile applications are an historical forte for compact dome antennas. Public safety applications, such as the use of emergency vehicles

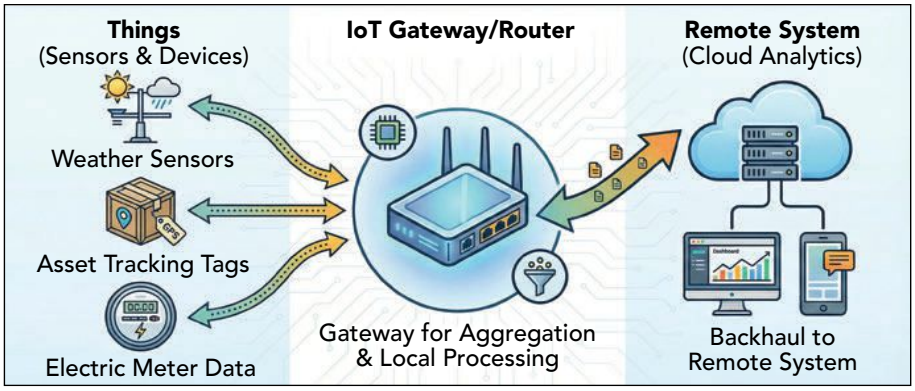

Fig. 5 **Classic IoT application architecture.**

and equipment, represent a large consumer segment for compact dome antennas. This, along with mobile IoT applications like off-highway vehicle usage on heavy equipment for mining and smart agriculture (e.g., wirelessly connected harvest equipment), comprises significant markets for all compact dome termination types.

Many other IoT applications are served well by compact dome antennas. The classic IoT architecture wirelessly connects "things" — weather sensors, asset tracking tags, electric meter data, etc. — and aggregates them at a gateway or router for local processing or backhaul to a remote system (see *Figure 5*). The size and performance of compact dome antennas serve the router/gateway elements of the application, and "thing" reporting may be accomplished by an antenna appropriate to an endpoint, which could also be a compact dome antenna. Some gateways may even use compact dome antennas to serve multiple applications, for example, managing the Wi-Fi-based sensor network with one compact dome antenna and then providing data backhaul via the cellular network using another compact dome antenna.

Compact domes work well as single antennas on such devices, but they also lend themselves to use in pairs for MIMO applications that can provide spatial and polarization diversity, as shown in *Figures 6* and *7*, respectively, for improved communication with IoT sensors in an area-efficient configuration.

External antenna formats have many well-known styles, including whips, blades, pucks and parabolics. Each has its place, but when it comes to combining performance, ruggedness and aesthetics, the compact dome antenna is a versatile and suitable option.

The Antenna Company
Eindhoven, The Netherlands
www.antennacompany.com

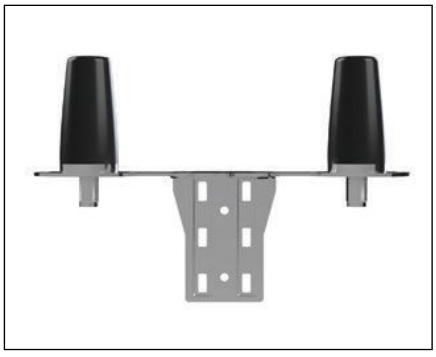

Fig. 6 **Spatial diversity MIMO configuration.**

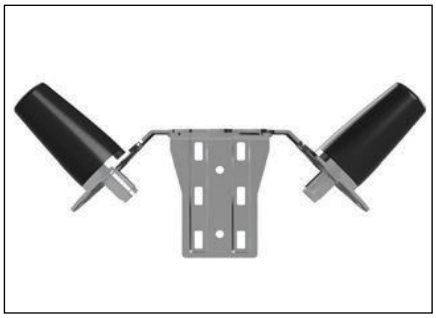

Fig. 7 **Polarization diversity MIMO configuration.**

Entry-level Oscilloscopes with up to Eight Channels

Rohde & Schwarz
Munich, Germany

Rohde & Schwarz has expanded its next-generation MXO oscilloscope portfolio with the compact four- and eight-channel MXO 3, bringing big capabilities in a small package. The MXO 3 delivers advanced MXO technology from Rohde & Schwarz, originally pioneered in the MXO 4 and MXO 5/5C series instruments, in a compact form factor and allows engineers to see more of their DUT's signal.

FAST INSIGHT

All MXO 3 models come standard with up to 99 percent real-time capture, enabling users to instantly observe more signal detail and rare signal events. Like other MXO models, these oscilloscopes leverage the cutting-edge MXO-EP ASIC technology developed by Rohde & Schwarz to achieve speed and performance across multiple dimensions. With an acquisition rate of 4.5 million waveforms per second, the MXO 3 allows users to instantly detect additional signal details and capture infrequent events.

The oscilloscopes also feature a 600,000 trigger events per second with zone triggering, offering a flexible solution for isolating events in the time domain, including complex signals in the math and frequency domains. Furthermore, the MXO 3 delivers 50,000 fast Fourier transforms (FFTs) per second and enables faster, more comprehensive analysis for applications such as EMI and harmonic testing. ***Figure 1*** shows an example of the MXO 3 creating its spectrum display by processing FFTs in hardware, revealing details in the frequency domain, including dynamic signal changes. With 600,000 math operations per second, the MXO 3 allows users to accurately analyze signals such as power, which require the precise multiplication of voltage and current.

PRECISION

All MXO 3 models are engineered with advanced technology to ensure accurate measurement isolation and results that users can trust. With 12-bit vertical resolution implemented in hardware at all sample rates, users can observe small signal changes even of larger signals. This represents 16x more resolution compared to traditional 8-bit oscilloscopes. To further enhance precision, the MXO 3 features an HD mode that reveals signal details typically buried in noise (see ***Figure 2***). This mode provides both noise reduction and up to 18 bits of vertical resolution. Unlike other oscilloscopes, the HD mode operates at full sample rate and is implemented in hardware, ensuring precision without sacrificing speed.

The MXO 3 also offers a wide offset range, allowing users to leverage the most sensitive vertical scale setup for capturing more of their signal while minimizing measurement system noise. With a ±3 V offset at 1 mV/div on both 50

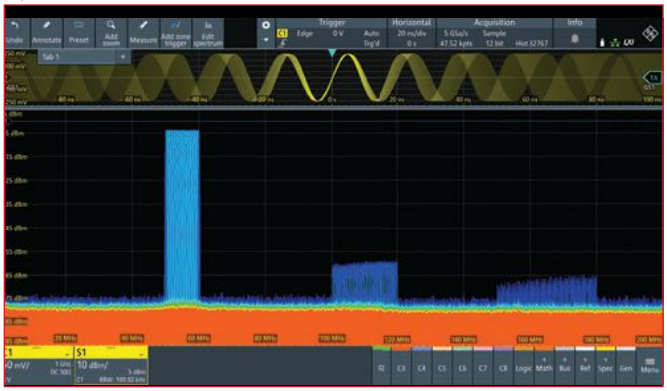

Fig. 1 **An MXO 3 spectrum display.**

Ω and 1 MΩ input paths, the MXO 3 delivers high performance for its class.

COMPACT FORM FACTOR

Both the four- and eight-channel MXO 3 oscilloscopes are designed with a compact, portable form factor, making them easy to fit anywhere, including on crowded benches. Their small footprint allows more space for the creative chaos of engineering workspaces. With a weight of about 4 kg, users can easily move the MXO 3 to a new measurement location as needed. The instrument requires only 5U of rack height, ensuring efficient use of space.

Oscilloscopes are highly visual tools, as users spend significant time interacting with their instruments' displays. The MXO 3 series incorporates an 11.6 in. full-HD capacitive touchscreen paired with an intuitive user interface for enhanced user experience. Additionally, the instrument's compact size, industry-leading low audible noise and Video Electronics Standards Association (VESA) mounting make it an excellent choice for engineering environments.

MODEL CONFIGURATIONS

The MXO 3 series oscilloscopes are available in both four- and eight-channel models, with bandwidth options including 100 MHz, 200 MHz, 350 MHz, 500 MHz and 1 GHz. For users with more demanding requirements, a variety of upgrade options are available. These include 16 integrated digital channels with a mixed signal oscilloscope (MSO) option, a 50 MHz arbitrary waveform generator, protocol decoding and triggering options for numerous industry standard buses and a frequency response analyzer to expand the instrument's capabilities.

ADDRESSED APPLICATIONS

The MXO 3 is a versatile bench instrument, combining multiple traditional devices, such as oscilloscopes, generators and power supplies. It handles general-purpose measurements, analyzing time and frequency domain signals and their correlation — crucial for embedded system testing, control loop analysis (including Bode plots) and logic/protocol debugging.

Its capabilities extend to power electronics with support for high voltage, current and optically isolated probes, alongside HD mode noise suppression and eight-channel models. For power conversion, the MXO 3's eight channels and 18-bit HD mode provide critical visibility into complex systems like motor drives and inverters, enabling precise measurements for efficiency and optimization.

Furthermore, it simplifies power sequencing analysis with simultaneous multi-channel observation and deep memory of up to 500 Mpts, enabling longer recording durations and precise analysis of small signal events. It features 3 V offsets and high sensitivity (1 mV/div), making it ideal for measuring power ripple and noise. Additionally, its fast spectrum analysis capability makes it an excellent tool for quickly identifying EMI issues and noise sources.

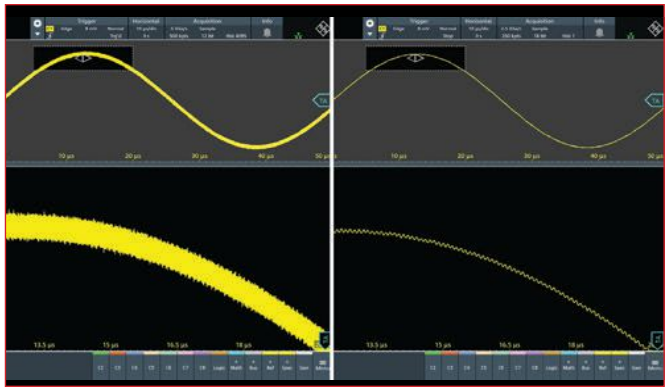

Fig. 2 HD mode reveals signal detail that would normally be buried in noise.

VENDORVIEW

Rohde & Schwarz
Munich, Germany
www.rohde-schwarz.com

Next-Level DDS Signal Generation

Spectrum Instrumentation
Grosshansdorf, Germany

Until recently, signal generators using direct digital synthesis (DDS) technology generally fell into two groups: simple, low-cost devices suited for producing single-channel periodic signals around 10 MHz, and more expensive benchtop units capable of generating one or two signals into the GHz range.

A new offering from Spectrum Instrumentation changes this landscape. The company has added DDS capability to its entire arbitrary waveform generator (AWG) product line, which includes more than 70 different product variants. This upgrade enables multitone DDS signal generation, with multi-channel operation, reaching frequencies up to 3.9 GHz.

In DDS mode, the AWGs can generate up to 64 individual sine waves (tones) per channel. Simple commands allow each tone's frequency, amplitude and phase to be adjusted within just a few nanoseconds. With the ability to apply frequency and amplitude slopes, along with command sequencing, it becomes easy to create waveform trains, frequency sweeps or finely tunable reference signals. These fast, straightforward waveforms enable reliable testing across a broad range of industries, including communications, medical science, lasers, quantum research, radar, LiDAR, ultrasound, sonar, automotive, aerospace, ATE, semiconductor testing, fiber optics and materials science.

Designed for automated, computer-controlled test environments, the products are offered in three popular form factors:

- PCIe cards, which plug directly into PC systems
- PXIe modules, which plug into a PXIe chassis
- LXI stand-alone instruments, which connect to any PC or network using a standard Ethernet cable.

This lineup allows users to choose the performance level they require.

At the top of the range is the 63xx series (22 models), offering 1 to 16 fully synchronized channels, output rates from 3.2 to 10 GSPS, 16-bit resolution and bandwidths up to 3.9 GHz. These units are ideal for applications in telecommunications (including 5G and radar), aerospace, quantum research and advanced test and measurement.

The 66xx series (23 models) serves the mid-range segment, with 1 to 32 channels, output rates of 625 MSPS or 1.25 GSPS, 16-bit resolution and up to 400 MHz bandwidth.

Fig. 1 Radar with Barker code.

The 65xx series (32 models) is designed for general-purpose use and offers the most compact form factor. Individual cards provide one to eight channels, while complete systems support up to 128 channels. This series delivers output rates from 40 to 125 MSPS, with 16-bit resolution and up to 60 MHz bandwidth. These characteristics make them well-suited for simulating networks or automating the testing of filters and amplifiers. They are also effective when used with medical and industrial sensors, where agile frequency sources help locate resonant frequencies or compensate for system drift.

With both AWG mode (replaying waveforms from stored data) and the DDS mode (generating command-based sine waves) in one device, Spectrum Instrumentation products are versatile signal sources. The entire product family, along with the company's extensive digitizer lineup, uses a unified software toolkit. This simplifies upgrades, model changes and system integration. All products include software support for Windows and Linux, programming examples for popular languages such as Python, MATLAB, C++ and LabVIEW and a high-level Python API. They also come with lifetime technical support directly from Spectrum's engineers, as well as free software and firmware updates.

EXAMPLE 1: RADAR WITH BARKER CODE

This example uses the ultrafast AWGs of the 63xx series in DDS mode, with up to 64 sine waves on one output channel.

DDS Waveform: This is a 1 GHz carrier and 20 µs radar pulse with a phase-modulated Barker code to improve the radar resolution, as shown in ***Figure 1***. This uses a combination of both the DDS amplitude and DDS phase modulation capabilities.

Usage: Radar simulation and electronic warfare simulation, where multiple independent radar sources are required.

EXAMPLE 2: FOCUSING AN ANTENNA WAVEFRONT

Here, the AWGs of the fast 66xx series are used in DDS mode, with up to 20 sine waves on one output channel.

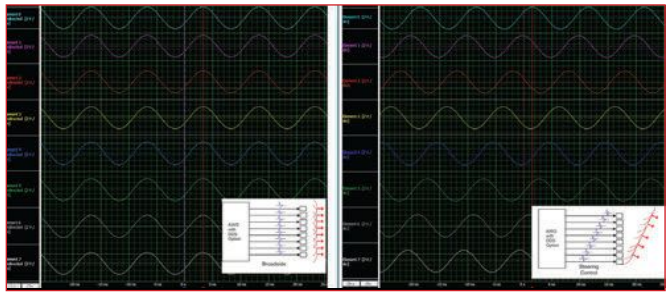

Fig. 2 Focusing an antenna wavefront.

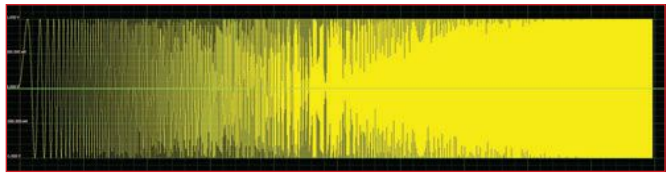

Fig. 3 Vibration test.

DDS Waveform: Multiple sine outputs are used for driving a phased array system by controlling the amplitude and phase of every individual DDS sine wave to steer or focus the wavefront of an array of antennas or transducers (see ***Figure 2***).

Usage: Developing and testing antenna and transducer arrays, e.g., for radar or ultrasound in medical science.

EXAMPLE 3: VIBRATION TEST

For this example, the medium-speed AWGs of the 65xx series are used in DDS mode, with up to 16 sine waves on one output.

DDS Waveform: One slowly changing swept sine is generated over the range of 20 Hz to 20 kHz. Up to 16 sweeps with different frequency ranges are possible in parallel.

Usage: These sweeps are used in vibration testing for automotive and aerospace applications. An example of data from a vibration test is shown in ***Figure 3***. A device (for example, a car) is mounted on a vibration shaker, which applies a frequency sweep to identify mechanical resonances and fatigue. In automotive testing, multitone sweeps are now standard because they significantly reduce test time. By using 10 simultaneous swept sines, each covering one-tenth of the total frequency range, the test can be completed in one-tenth of the time.

Spectrum Instrumentation's AWGs with DDS capabilities enable multitone DDS signal generation with multichannel operation. General DDS explanations, programming examples, details about the DDS products and product videos can be found here:

https://spectrum-instrumentation.com/support/knowledgebase/hardware_features/DDS_mode.php

VENDORVIEW

Spectrum Instrumentation
Grosshansdorf, Germany
www.spectrum-instrumentation.com

10 MHz to 110 GHz Ultra-Wideband Distributed Amplifier

Eravant's SBB-0111141708-1F1F-E1 is an ultra-wideband (UWB) distributed amplifier designed for operation from 10 MHz to 110 GHz. The amplifier delivers a typical gain of 17 dB up to 70 GHz, 16 dB up to 90 GHz and 10 dB up to 110 GHz. The UWB performance enables advancements for applications in 6G communications, AI research and development, high speed test and measurement, data centers and more.

The mechanical package features two standard 1.0 mm coaxial connectors as the input and output RF ports. The housing is designed to be compatible with Eravant's proprietary Uni-Guide™ waveguide connectors, which can convert the amplifier's coaxial RF ports to standard WR-15, WR-12 or WR-10 waveguides. This offers flexibility in system implementation and custom solutions tailored to specific needs. Different port configurations are available under different model numbers.

SBB-0111141708-1F1F-E1 offers the one-stop solution to various test systems, eliminating the need to swap components for measurement across different frequency bands. The amplifier can be connected to broadband VNAs such as the Rohde & Schwarz R&S®ZNA67EXT, Keysight N5251A and Anritsu VectorStar ME7838EX to reduce errors introduced by the constant connect/disconnect motions.

As part of its mission to make mmWave technology accessible, Eravant designs high performance components and systems that reduce the barriers of cost, complexity and capability, empowering engineers to innovate faster at higher frequencies.

VENDORVIEW

Eravant (Formerly Sage Millimeter Inc.)
Torrance, Calif.
www.eravant.com

MAKING WAVES

FR2 Signal Generation Signal Chain using Apollo MxFE™

This demonstration highlights a complete wideband spectrum analyzer signal chain that supports the emerging 6G FR3 band with instrument grade error vector magnitude (EVM) performance of < -50 dB.

Analog Devices
www.analog.com

New Machine Learning Toolkit

Keysight's new Machine Learning Toolkit features an ML optimizer, auto-extraction flows and utilities within Device Modeling MBP 2026, introducing a framework that combines advanced neural network architectures with ML-based optimization.

Keysight Technologies, Inc.
www.keysight.com

A New Digital Home for ETS-Lindgren

ETS-Lindgren introduced their newly redesigned website. Simplified navigation, enhanced tools and selectors and expanded technical resources make it easier to explore ETS-Lindgren capabilities and identify the right solutions.

ETS-Lindgren
www.ets-lindgren.com

Product Highlight: ZVA-24443HP+ Ka-Band Amplifier

In this product highlight video, Mini-Circuits Product Line Engineering Manager Dan Ford shares an overview of the ZVA-24443HP+ Ka-Band Amplifier, supporting applications from 24 to 43.5 GHz with high gain, low noise figure and +29 dBm output power at saturation.

Mini-Circuits
www.minicircuits.com

Rohde & Schwarz Opens Larger Office in Japan

Rohde & Schwarz has opened a new larger office in Osaki, Japan, with increased capabilities to deliver an innovation advantage for the Japanese automotive community. The new location, which replaces the original one in Shinjuku, has significantly enhanced facilities for service, repair, calibration and engineering support of test equipment as well as increased space for hosting customer events.

Rohde & Schwarz
www.rohde-schwarz.com

Product Navigator Directs You to the Right Component

Würth Elektronik introduces a new online tool that significantly simplifies the search for the right components. The Product Navigator helps users select electronic and electromechanical components through practical example applications and typical topologies.

Würth Elektronik
www.we-online.com

NEW PRODUCTS

DEVICES

6501 Series Up/Down-Converters

The 6501 Series converters deliver two fully independent RF up/down channels in a single 6U VPX slot, reducing size, weight and power without compromising performance. Designed for mission-critical environments, it supports fast switching, wide frequency coverage, low phase noise and high dynamic range — making it ideal for EW, SIGINT, satcom and radar applications.

FEI-Elcom Tech, Inc.
www.fei-elcomtech.com

Compact Digital Optical-Electrical Converter

Highland Technology presents the K420, a compact digital optical-electrical converter supporting data transport up to 2 GHz (4 Gbps). Featuring a single or bi-directional E-O/O-E link, differential I/O and dual input and output SMA connectors. Inputs accept PECL, ECL, CML or LVDS; AC-coupled outputs are CML/LVDS compatible. Serial header enabling SFP diagnostics. Extending up to 400 m over OM4 fiber, the K420 eliminates ground loops and EMI susceptibility inherent in copper links, making it ideal for long-distance systems and high-noise environments.

Highland Technology
www.highland-technology.com

Transition Time Converter

HL9457 transition time converters (also known as lowpass absorptive rise time filters) provide superior return loss and flat group delay. This model comes in options with bandwidth above 28 GHz (12.5 ps). For filters at different speeds, please see its relegated models in the HL945x Series. Designed using HYPERLABS' proprietary absorptive filtering, these filters offer a similar frequency response as fourth-order Bessel-Thompson filters. These filters are suitable for OEM use in high speed telecom and digital networks and to limit the RF bandwidth to known values.

Hyperlabs
www.hyperlabs.com

50 Ω RF Switches

VENDORVIEW

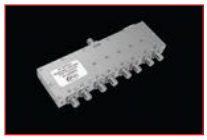

JFW has a line of 50 Ω solid-state RF switches that operate from 20 MHz to 8.4 GHz. These models are ideal for automated RF testing. Their solid-state design has no mechanical wear, resulting in accurate, repeatable RF testing. The switches are controlled with TTL control lines. The switches can hot switch up to +26 dBm.

JFW Industries, Inc.
www.jfwindustries.com

New**Products**

Two-Way MLDD Power Divider

VENDORVIEW

KRYTAR, Inc. announces a new two-way power divider offering high performance over the broadband frequency range of 7.125 to 15.35 GHz (C- through Ku-Bands) in a compact package. The new power divider offers the ultimate solution for designs and test and measurement applications including emerging mmWave and 6G markets. KRYTAR's technological advances provide excellent operating performance of this new two-way unit.

KRYTAR, Inc.
www.krytar.com

S-Band Filter

Built for crowded RF environments where performance matters. This cavity-based S-Band filter supports satellite and wireless systems operating from 2200 to 2300 MHz, delivers excellent selectivity, low insertion loss and high out-of-band rejection through precision-machined resonant cavities. Rated for 2 W CW power handling, its rugged construction ensures stable electrical performance across temperature variations and harsh operating conditions, with compact form factor options for space-constrained designs. Get the edge in your RF designs.

Renaissance AEM
www.aeminc.com/RF

Ka-Band Up-converter

RFE is introducing a satcom broadband Ka-Band up-converter module to address commercial and military bands. Features include integrated LO synthesizers, which can be tuned to convert L-Band to anywhere in the RF band and include jitter reduction for the 10 MHz REF. The product consumes just 12 W from a single 28 VDC. Housed in a compact 3 × 8 × 1 in. package, the design is fully hermetic for deployment in rugged airborne or ground environments.

RFE
www.rfe-mw.com

Dual 1000 W Directional Coupler

Sigatek introduces a dual high-power 50 dB directional coupler with an operating frequency of 2 to 32 MHz. Forward and reverse coupling is 50 dB and flatness is less than 1 dB with a low insertion loss of 0.25 dB maximum. Directivity is 20 dB minimum in each direction and VSWR is 1.10:1 in/out. Power handling is 2500 W CW. In/out connectors are N female and coupling ports are SMA female. Dimensions are 4 × 3 × 1.5 in.

Sigatek LLC
www.sigatek.com

0.45 to 8 GHz 10 dB Dual Directional Coupler

VENDORVIEW

URF's 10 dB dual directional coupler captures forward and reverse signals simultaneously, providing ultra-low 2.4 dB insertion loss and 17 dB minimum directivity. Engineered for radar, satcom and 5G, URF's rugged design handles 3000 W peak and 20 W CW without performance drift. Monitor high-power L-, S- and C-Band signals with absolute precision via 1.10:1 typical VSWR, ensuring high fidelity sampling in the most demanding environments.

URF Inc.
www.urfinc.com

CABLES & CONNECTORS

MCX Assemblies

Amphenol RF announced the expansion of their cable assembly portfolio with MCX straight and right-angle plug configurations that feature rugged IP67 bulkhead SMA, TNC, RP-TNC and N-Type straight jacks. These assemblies are designed on flexible RG-316 cable, which provides excellent electrical performance up to 6 GHz and high heat resistance, durability and low signal loss in high frequency RF applications. These between-series assemblies allow a cable to be connected from outside of a panel where a threaded interface is located.

Amphenol RF
www.amphenolrf.com

Vertical Launch 0.8 mm Connectors

The Vertical Launch 0.8 mm connectors from Withwave operate from DC to 145 GHz. They consist of three precisely designed notches that ensure accurate alignment with the PCB copper. These notches, in combination with specific reference marks on the PCB surface, help position the connector accurately and ensure stable electrical performance. These connectors have a VSWR of less than 1.80:1. The Vertical Launch 0.8 mm connectors have M1.4 screws for bolting and support easy and solderless installation.

Withwave
www.with-wave.com

AMPLIFIERS

1 to 22 GHz, 15 W, GaN Power Amplifier

The ADPA1112 delivers powerful wideband performance, offering 42 dBm saturated output power across 8 to 16 GHz with 14 dB gain and 25 percent power-added efficiency. Designed for seamless integration, it features 50 Ω matched, AC-coupled RF input and output ports, simplifying wideband front-end design. Operating from a 28 V supply with a 600 mA quiescent drain current set via a gate control pin, the ADPA1112 enables high-power performance without added complexity.

Analog Devices
www.analog.com

AMP20184, 0.8 to 2.5 GHz, 500 W

VENDORVIEW

Exodus AMP20184 is a solid-state high-power amplifier, with 500 W minimum and 57 dB gain, designed for EMI/RFI, lab, CW/pulse and all communications applications. The Class A/AB linear design with high-power advanced technology devices supports instantaneous ultra-wide bandwidth. Featuring built-in protection circuits with extensive monitoring, local LCD and flexible remote interfaces. Unprecedented reliability and ruggedness in a compact 5U rack-mountable chassis.

Exodus Advanced Communications
www.exoduscomm.com

GaN-on-SiC HEMTs

Richardson RFPD, Inc., an Arrow Electronics company, now offers full design support and availability for two new high performance GaN RF power transistors from Guerrilla RF: the GRF0020 and GRF0030. These GaN-on-SiC HEMTs deliver exceptional efficiency and bandwidth for demanding RF applications. Both devices operate on 50 V supply rails and support 28 V operation for flexibility. They are housed in industry-standard 3 × 3 mm QFN-16 surface-mount packages and are also available as bare die: GRF0020D and GRF0030D.

Richardson RFPD
www.richardsonrfpd.com

SOURCES

Phase-Locked Dielectric Resonator Oscillator

VENDORVIEW

Planar Monolithics (PMI) Model PLO-48D4G-EXT is an externally referenced phase-locked dielectric resonator oscillator covering the frequency of 48.4 GHz with a load VSWR: 1.5:1, an output power of 10 dBm minimum, a spurious of 60 dBc, a phase noise of 102 dBc/Hz at 100 kHz, harmonics of 20 dBc and a 100 MHz (sine wave) external reference. Housing size is 2.25 × 2.25 × 0.62 in. with 2.4 mm female (RF OUT) and SMA female (REF IN) connectors.

Planar Monolithics
www.pmi-rf.com

ANTENNAS

Wideband Antenna Matrix MATF

Wisycom launched its new wideband antenna matrix, MATF, which supports RF and fiber for demanding multi-zone wireless infrastructures. The MATF debuted at the 2026 NAMM Show and ISE 2026 (Stand 7P800), where attendees could experience firsthand how the brand has reimagined centralized RF distribution management for today's most challenging installation, theatre production, live event, outside broadcast and TV station environments.

Wisycom
www.wisycom.com

TEST & MEASUREMENT

44 GHz FPL Spectrum Analyzer

VENDORVIEW

The new R&S FPL1044 from Rohde & Schwarz offers a frequency range of 10 Hz to 44 GHz. It is the first and only spectrum analyzer in this price range on the market to reach the 44 GHz milestone, drastically lowering the entry barrier for high frequency testing. Setting itself apart within the FPL family, the FPL1044 is the only model to offer a DC coupling option, expanding the measurable frequency range starting from as low as 10 Hz.

Rohde & Schwarz
www.rohde-schwarz.com

20 GHz Vector Signal Generator with Advanced Software

Signal Hound released the VSG200, a 20 GHz vector signal generator (VSG) offering 40 MHz of real-time streaming bandwidth. The VSG200 expands their popular VSG series and unlocks access to higher frequency ranges and updated features. In addition, Signal Hound made a major update to their VSG software. It now includes a brand-new UI redesign, the addition of live plotting, support for SigMF file types, the ability to export waveforms and more. This is all available at no cost to users.

Signal Hound
www.signalhound.com

FOR MORE NEW PRODUCTS, VISIT
WWW.MWJOURNAL.COM/BUYERSGUIDE
FEATURING VENDORVIEW STOREFRONTS

Reviewed by:
Katerina Galitskaya

Bookend

Over-the-Air Measurement for Wireless Communication Systems

Yihong Qi and James L. Drewniak

Over-the-air (OTA) measurement has become an essential aspect of wireless system evaluation, providing a realistic method for assessing RF performance. "Over-The-Air Measurement for Wireless Communication Systems" is a thorough and well-structured guide that covers both theoretical and practical aspects of OTA testing. The book starts with an introduction to the importance of OTA, explaining its necessity for modern wireless systems, including 5G, IoT and intelligent connected vehicles. It provides a clear progression from fundamental OTA measurement principles to advanced techniques, which makes it valuable for both newcomers and experienced engineers. The authors do an excellent job of explaining key performance metrics such as total radiated power and total isotropic sensitivity, which are critical for evaluating wireless communication systems.

One of the strongest aspects of this book is the detailed coverage of standardized OTA measurement methodologies, including those from 3GPP and CTIA. The discussions on SISO and MIMO OTA testing are particularly valuable, as they provide insight into the challenges and evolving requirements of modern wireless technologies. The inclusion of topics like massive MIMO and intelligent connected vehicle OTA measurements makes this book relevant to current and future wireless applications. The book also addresses practical engineering considerations, including OTA setup design, calibration techniques and measurement accuracy. The chapter on calibration antennas is valuable since it highlights their role in reducing measurement uncertainty and ensuring consistency in test results.

Overall, this book is a valuable resource for RF engineers, wireless system designers and certification professionals. Its combination of theoretical depth and practical guidance makes it an excellent reference for anyone working with OTA measurements. Whether you are developing wireless communication products or working in standards development, this book provides the knowledge needed to navigate the complexities of OTA testing effectively.

ISBN: 9781630819958
Pages: 350
Copyright: 2024
To order this book, contact:
Artech House
us.artechouse.com

EUROPE'S PREMIER MICROWAVE, RF, WIRELESS AND RADAR EVENT

EUROPEAN MICROWAVE WEEK EXCEL, LONDON 4th-9th OCTOBER 2026 www.eumw.eu

EUROPEAN MICROWAVE WEEK 2026

THE EUROPEAN MICROWAVE EXHIBITION

EXCEL LONDON, UK

6TH – 8TH OCTOBER 2026

- 10,000 sqm of gross exhibition space
- Around 5,000 attendees
- 1,700 - 2,000 Conference delegates
- In excess of 300 international exhibitors (including Asia and US as well as Europe)

INTERESTED IN EXHIBITING?

Please contact one of our International Sales Team:

Richard Vaughan,
International Sales Manager
rvaughan@horizonhouse.co.uk

Gaston Traboulsi, France
gtraboulsi@horizonhouse.com

Mike Hallman, USA
mhallman@horizonhouse.com

Victoria and Norbert Hufmann,
Germany, Austria & Switzerland
victoria@hufmann.info
norbert@hufmann.info

Katsuhiro Ishii, Japan
amskatsu@dream.com

Jaeho Chinn, Korea
inter11@jesmedia.com

CALL +44(0) 20 7596 8742 OR VISIT WWW.EUMW.EU

Advertising**Index**

SPECIAL FOCUS:
Cables & Connectors

ADVERTISERS ARE HIGHLIGHTED IN BLUE

Sales Representatives

Eastern and Central Time Zones
Carl Sheffres
Group Director
(New England, New York, Eastern Canada)
Tel: (781) 619-1949
csheffres@mwjournal.com

Michael Hallman
Associate Publisher
(NJ, Mid-Atlantic, Southeast, Midwest, TX)
Tel: (301) 371-8830
Cell: (781) 363-0338
mhallman@mwjournal.com

Pacific and Mountain Time Zones
Scott Blackburn
Western Reg. Sales Mgr.
(CA, AZ, OR, WA, ID, NV, UT, NM, CO, WY, MT, ND, SD, NE & Western Canada)
Cell: (303) 819-3958
sblackburn@mwjournal.com

International Sales
Michael O'Kane
Tel: +44 (0) 1875 825 700
Cell: +44 (0) 7961 038 245
mokane@horizonhouse.com

Germany, Austria, and Switzerland (German-speaking)
Victoria and Norbert Hufmann
Tel: +49 911 9397 6442
victoria@hufmann.info
norbert@hufmann.info

Korea
Jaeho Chinn
JES MEDIA, INC.
Tel: +82 2 481-3411
inter11@jesmedia.com

China
Shanghai
Linda Li
ACT International
Tel: +86 136 7154 0807
lindal@actintl.com.hk

Shenzhen
Linda Li
ACT International
Tel: +86 136 7154 0807
lindal@actintl.com.hk

Beijing
Cecily Bian
ACT International
Tel: +86 135 5262 1310
cecilyb@actintl.com.hk

Hong Kong
Floyd Chun
ACT International
Tel: +86 137 2429 8335
floydc@actintl.com.hk

Taiwan, Singapore
Simon Lee
ACT International
Tel: +852 2838 6298
simonlee@actintl.com.hk

Japan
Katsuhiro Ishii
Ace Media Service Inc.
Tel: +81 3 5691 3335
amskatsu@dream.com

Submitting ad material?
Visit: www.adshuttle.com/mwj
(866) 774-5784
outside the U.S. call
+1-414-566-6940

Ed Kiessling
(781) 619-1963
ekiessling@mwjournal.com

Corporate Headquarters: 685 Canton Street, Norwood, MA 02062 • Tel: (781) 769-9750

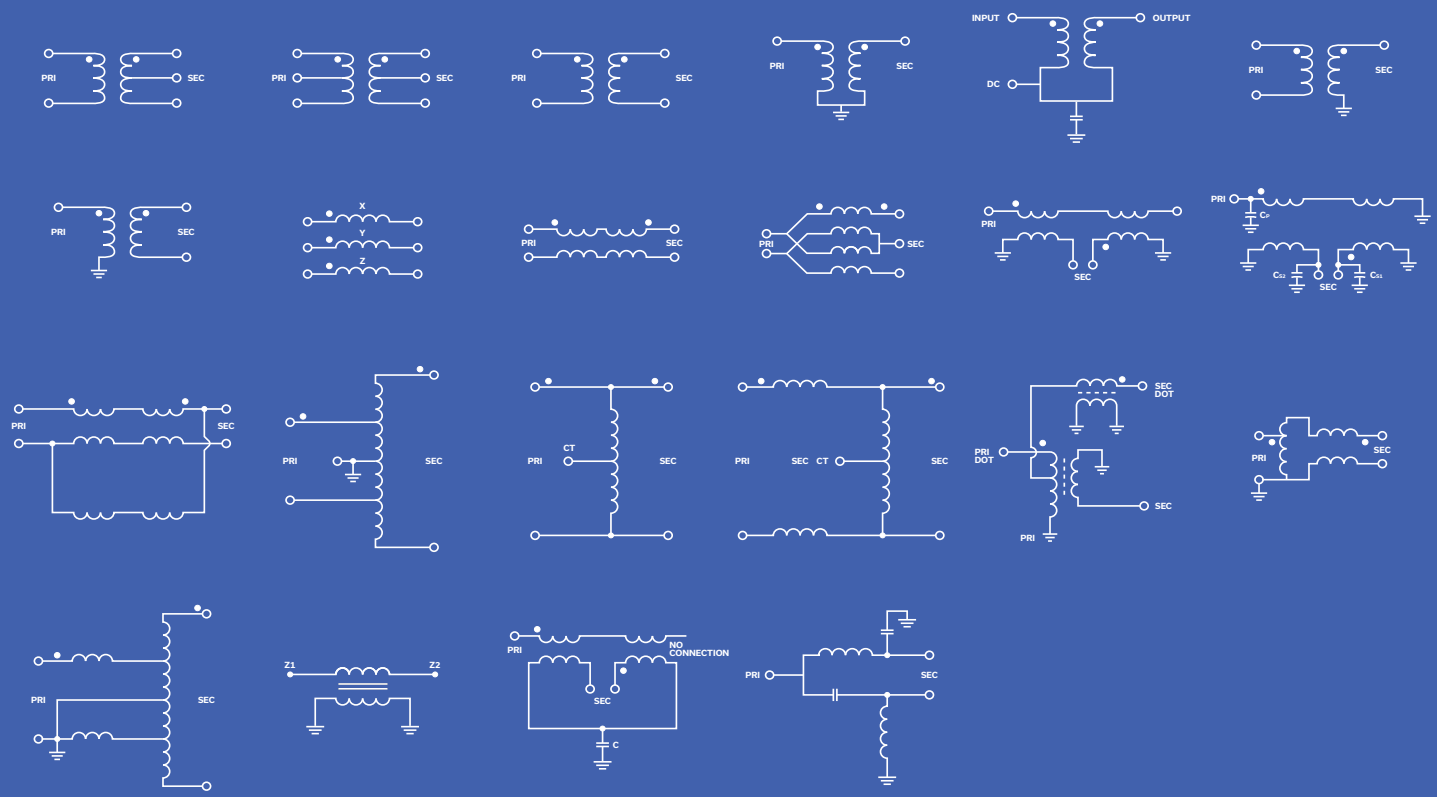

DC TO 24 GHz

Transformers from A to Z...

Configurations for Every Requirement

LEARN MORE

- 350+ models in stock plus custom designs
- 22 configurations
- MMIC, µCeramIQ™ and core & wire construction
- Impedance ratios from 0.11 to 36
- SMT, connector, plug-in & die form factors

Mini-Circuits®

SV Microwave: RF Engineering for Harsh Environments

SV Microwave, a manufacturer of RF and microwave coaxial connectors, cables and passive components, has grown significantly since its start in 1968. The company was founded under a different name, Solitron Devices, and spun off into SV Microwave in 1993. Following this transition and growth period, SV established headquarters in West Palm Beach, Fla., in 2001. Four years later, they were purchased by Amphenol Corporation under their military and aerospace group. In 2018, SV expanded its Florida operation with a new R&D facility, and in 2019, expanded to a facility in Mesa, Ariz., to support its growing number of West Coast customers.

More recently, SV has invested significant funding and effort into expanding these facilities in order to fulfill customer needs. SV Microwave's Mesa location was transformed in 2025 from two separate buildings totaling 20,000 sq. ft. of production space to one continuous building with a 30,000 sq. ft. footprint. In addition to providing more production space, the unification has promoted and improved collaboration across departments and product lines, better supporting customer needs. SV's Florida location saw two major updates as well, including an office space expansion and restructuring to gain 4000 ft. of additional manufacturing space. Most recently, SV added 4600 sq. ft. of space dedicated to CNC and Swiss lathe machines. SV will continue to support customer needs through its careful design, detailed manufacturing and customer support.

Within these facilities, SV Microwave designs, manufactures and tests products for military, IoT, 5G, satellite, high speed, aerospace, commercial, EW and telecom applications. SV supports these industries with cable harnesses, semi-rigid cables, SOSA-aligned products, armored assemblies, LTI connectors, glass-sealed connectors, embedded phase tuners, PCB mounting hardware and more. SV's J-STD certified cable harness technicians have been supplying customers with reliable products for over 15 years. They manufacture a variety of cable harness types, including pure-play and complex, multi-signal bundles and can service build-to-print or design-to-spec approaches. Additionally, they offer fully and partially armored cables for harsh environments. SV has the full range of capabilities to design, build and test these cables and harnesses in-house, including automated wire cutting and stripping, over-braiding, over-molding, potting, in-process RF testing, automated RF testing, real-time X-ray, shock and vibration. In addition to these in-house capabilities, SV has access to Amphenol's more extensive test equipment to fill any gaps quickly and precisely.

In addition to their cable assemblies, SV produces connectors for harsh environments, both for on-wire and PCB-mounted applications. As temperature requirements become more complex due to higher powers and frequencies, many engineers are turning to glass dielectrics to replace PTFE dielectrics. SV supports this with glass-dielectric SMP, SMPM and SMPS connectors that operate up to 500°C without reflowing, warping or breaking. They further support PCB connector durability with customizable mounting hardware that protects connectors from axial and radial forces created by frequent motion and vibration.

Ultimately, SV Microwave is a dedicated partner to RF users in harsh environments, and continues to support them through product development, manufacturing and supportive facility expansion.

svmicrowave.com

SPECTRAN® V6

BEYOND REALTIME

Setting **the Mobile Benchmark**

The **ULTIMATE** Real-Time Spectrum Analyzer Tablet

8 | 18 | 55 | 140 GHz 2x 490 MHz RTBW

HIGH-END SPECTRUM ANALYZER:

- 9 kHz up to 140 GHz
- Optional Tx (Generator)
- 2x 490 MHz Bandwidth
- 3 THz/s Sweep Speed
- 16-Bit ADC
- -170dBm/Hz | 4dB NF
- IQ Recording & Playpack
- 8h Continuous Runtime
- Temp. Range -40° to +60°
- GPS & Time Server
- Opt. Handle & Stand
- Incl. RTSA-Software

RUGGED PREMIUM PC POWER:

- 15.6" 1500nit FullHD Touchscreen
- AMD 8-Core 8845HS CPU
- 64 GB LPDDR5 RAM
- Up to 64 TB Highspeed SSD
- 2x M.2 2280 & 3x M.2 2242
- Many I/Os incl. USB4, SD & HDMI
- SIM slot, opt. WiFi, Bluetooth, 5G
- SFP+ 10G Ethernet, SATA, RS232
- Rugged Aluminum Casing
- Hot-Swap Batteries
- Front & Rear Cameras, Smart Pen
- Windows or Linux

MADE IN GERMANY

www.aaroniausa.com
ubuy@aaroniausa.com
+1 (214) 935-9800

www.aaronia.com
mail@aaronia.de
+49 6556 900 310

AARONIA AG
WWW.AARONIA.COM

WERLATONE 60TH ANNIVERSARY

UNLEASH THE POWER

SUPERIOR EMC/EMI TESTING SOLUTIONS

WIDE BANDWIDTH | HIGH POWER | SUPERIOR PERFORMANCE

0.01 TO 220 MHZ | 0.01 TO 1000 MHZ | 80 TO 1000 MHZ | 600 TO 8000 MHZ | 6 TO 18 GHZ

QUADRATURE HYBRIDS

HIGH-POWER COMBINERS

DIRECTIONAL COUPLERS

DIGITAL POWER METERS

WERLATONE'S EMC/EMI TESTING SOLUTIONS ARE EMBEDDED IN EMC AMPLIFIERS, TEST CHAMBERS, AND TEST LABS WORLDWIDE.

WE OFFER A VARIETY OF POWER LEVELS RANGING FROM 10 W CW TO 20 KW CW.

WERLATONE'S HIGH-POWER, MISMATCH-TOLERANT® SOLUTIONS ARE DESIGNED TO OPERATE IN EXTREME LOAD MISMATCH CONDITIONS.

BRING US YOUR CHALLENGE | WWW.WERLATONE.COM

WERLATONE 60TH ANNIVERSARY

LEARN MORE

eXclusive Digital Content

REVIEW BOARD MWJ APPROVED

User-Friendly CAD Tool for Cascaded Wilkinson Power Dividers Based on Analytical Methods

Kok Yeow You and Man Seng Sim
Universiti Teknologi Malaysia, Johor, Malaysia

Yeng Seng Lee
Keysight Technologies, Pulau Pinang, Malaysia

The Wilkinson power divider/combiner is extensively used in RF and microwave devices due to its excellent isolation between output ports compared to other types of power dividers/combiners.[1] Design specifications for single-section Wilkinson power dividers/combiners are well established, and numerous web-based open-source CAD tools are available for their design. However, achieving wideband operation requires a multi-section or cascaded power divider/combiner.

User-friendly CAD tools for designing multi-section Wilkinson power dividers/combiners are scarce in online repositories and commercial software markets. Most available CAD tools are numerically based and require precise initial definitions of the characteristic impedance of transmission lines and the isolation resistors in the microstrip circuit. This complexity poses challenges for junior designers who may lack a strong theoretical understanding of cascaded Wilkinson power dividers/combiners. Additionally, these tools often demand significant computational resources, increasing the design cost.

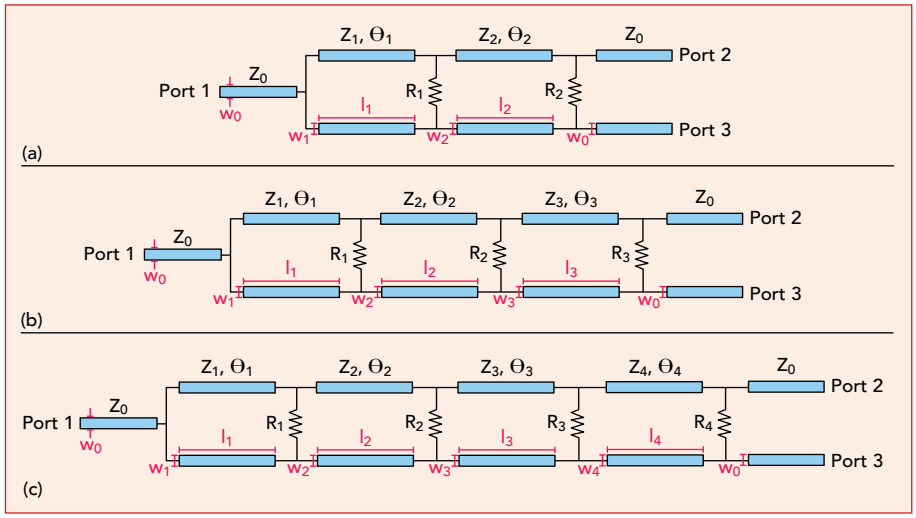

Fig. 1 Schematics of second- (a), third- (b) and fourth- (c) order Wilkinson power dividers.

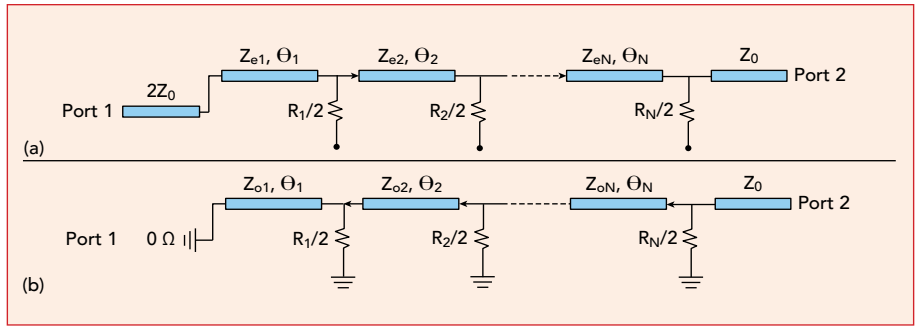

Fig. 2 Multi-section Wilkinson power divider equivalent circuit under even- (a) and odd- (b) mode excitation.

This article introduces a user-friendly, analytically based CAD tool for designing cascaded Wilkinson power dividers/combiners. The tool's reliability and accuracy are validated by comparing the computed S-parameter results of the cascaded Wilkinson power divider with those obtained from various commercial simulators. In the development of the CAD tool, the focus is on second-, third- and fourth-order Wilkinson power dividers, as illustrated in ***Figure 1***.

TABLE 1

EMPIRICAL DESIGN FORMULATIONS FOR SECOND-, THIRD- AND FOURTH-ORDER CASCADED POWER DIVIDERS

N	Design Formulations
2	$\tilde{Z}_{e1} = -4.81666210722 \times 10^{-2}\left(\frac{f_U}{f_L}\right) + 1.73095261376$, $r^2 = 0.99992$ $\tilde{Z}_{e2} = 3.98832689742 \times 10^{-2}\left(\frac{f_U}{f_L}\right) + 1.13946915787$, $r^2 = 0.99984$ $\tilde{R}_1 = \begin{Bmatrix} 1.53970177591 \times 10^{-2}\left(\frac{f_U}{f_L}\right)^4 - 0.122355292186\left(\frac{f_U}{f_L}\right)^3 + 0.382955367587\left(\frac{f_U}{f_L}\right)^2 \\ -0.330822018541\left(\frac{f_U}{f_L}\right) + 1.84037317491 \end{Bmatrix}$, $r^2 = 0.99996$ $\tilde{R}_2 = \begin{Bmatrix} -8.31100849461 \times 10^{-3}\left(\frac{f_U}{f_L}\right)^4 + 0.116161639937\left(\frac{f_U}{f_L}\right)^3 - 0.469681551748\left(\frac{f_U}{f_L}\right)^2 \\ -0.198212647484\left(\frac{f_U}{f_L}\right) + 6.30135802182 \end{Bmatrix}$, $r^2 = 0.99997$ Only valid for $1.2 \le f_U/f_L \le 4$. The f_U and f_L are the upper and lower operating frequency in unit Hertz, respectively.
3	$\tilde{Z}_{e1} = -4.96074283995 \times 10^{-2}\left(\frac{f_U}{f_L}\right) + 1.88699735552$, $r^2 = 0.99980$ $\tilde{Z}_{e2} = 2.22723813161 \times 10^{-4}\left(\frac{f_U}{f_L}\right) + 1.41309690474$, $r^2 = 0.89900$ $\tilde{Z}_{e3} = 3.49962390119 \times 10^{-2}\left(\frac{f_U}{f_L}\right) + 1.04034014963$, $r^2 = 0.99967$ $\tilde{R}_1 = \begin{Bmatrix} 1.0738682428 \times 10^{-3}\left(\frac{f_U}{f_L}\right)^4 - 1.97457097685 \times 10^{-2}\left(\frac{f_U}{f_L}\right)^3 + 0.144011988844\left(\frac{f_U}{f_L}\right)^2 \\ -0.235909310737\left(\frac{f_U}{f_L}\right) + 1.98396406723 \end{Bmatrix}$, $r^2 = 0.99999$ $\tilde{R}_2 = \begin{Bmatrix} 1.77067206192 \times 10^{-3}\left(\frac{f_U}{f_L}\right)^5 - 2.5303380437 \times 10^{-2}\left(\frac{f_U}{f_L}\right)^4 + 0.131035783269\left(\frac{f_U}{f_L}\right)^3 \\ -0.24263804778\left(\frac{f_U}{f_L}\right)^2 + 0.280949532668\left(\frac{f_U}{f_L}\right) + 3.53237359151 \end{Bmatrix}$, $r^2 = 0.99988$ $\tilde{R}_3 = \begin{Bmatrix} -2.03201609337 \times 10^{-3}\left(\frac{f_U}{f_L}\right)^5 + 0.426873511274\left(\frac{f_U}{f_L}\right)^4 - 3.52020424523\left(\frac{f_U}{f_L}\right)^3 \\ +14.4891308493\left(\frac{f_U}{f_L}\right)^2 - 31.359051888\left(\frac{f_U}{f_L}\right) + 36.7178456366 \end{Bmatrix}$, $r^2 = 0.99984$ Only valid for $2 \le f_U/f_L \le 6$.

TABLE 1 CONTINUED

EMPIRICAL DESIGN FORMULATIONS FOR SECOND-, THIRD- AND FOURTH-ORDER CASCADED POWER DIVIDERS

4	$\tilde{Z}_{e1} = -3.94442444493 \times 10^{-2}\left(\frac{f_U}{f_L}\right) + 1.96417446343$, $r^2 = 0.99944$ $\tilde{Z}_{e2} = 5.30935567102 \times 10^{-4}\left(\frac{f_U}{f_L}\right)^2 - 2.16642298624 \times 10^{-2}\left(\frac{f_U}{f_L}\right) + 1.63874691691$, $r^2 = 0.99839$ $\tilde{Z}_{e3} = 1.51170785847 \times 10^{-2}\left(\frac{f_U}{f_L}\right) + 1.23140938439$, $r^2 = 0.99434$ $\tilde{Z}_{e4} = 2.45640827865 \times 10^{-2}\left(\frac{f_U}{f_L}\right) + 1.02201377466$, $r^2 = 0.99885$
	$\tilde{R}_1 = \left\{\begin{matrix} 2.09440950108 \times 10^{-4}\left(\frac{f_U}{f_L}\right)^6 - 7.54540450451 \times 10^{-3}\left(\frac{f_U}{f_L}\right)^5 + 0.108435634927\left(\frac{f_U}{f_L}\right)^4 \\ -0.784722541991\left(\frac{f_U}{f_L}\right)^3 + 2.9432869079\left(\frac{f_U}{f_L}\right)^2 - 5.09875892154\left(\frac{f_U}{f_L}\right) \\ +4.66811582386 \end{matrix}\right\}$ $, r^2 = 0.99946$
	$\tilde{R}_2 = \left\{\begin{matrix} -3.27992793113 \times 10^{-4}\left(\frac{f_U}{f_L}\right)^3 + 6.7702456282 \times 10^{-2}\left(\frac{f_U}{f_L}\right)^2 - 0.274091937245\left(\frac{f_U}{f_L}\right) \\ +3.28009725174 \end{matrix}\right\}$ $, r^2 = 0.99995$
	$\tilde{R}_3 = \left\{\begin{matrix} 9.46961079738 \times 10^{-4}\left(\frac{f_U}{f_L}\right)^4 - 1.700876107 \times 10^{-2}\left(\frac{f_U}{f_L}\right)^3 + 0.15922471878\left(\frac{f_U}{f_L}\right)^2 \\ -0.504343985417\left(\frac{f_U}{f_L}\right) + 6.18282587405 \end{matrix}\right\}$ $, r^2 = 0.99992$
	$\tilde{R}_4 = \left\{\begin{matrix} -8.14537217 \times 10^{-4}\left(\frac{f_U}{f_L}\right)^5 + 3.506784422 \times 10^{-2}\left(\frac{f_U}{f_L}\right)^4 - 0.5855752228\left(\frac{f_U}{f_L}\right)^3 \\ +4.851880192\left(\frac{f_U}{f_L}\right)^2 - 20.87547073\left(\frac{f_U}{f_L}\right) + 44.85863364 \end{matrix}\right\}$ $, r^2 = 0.99993$
	Only valid for $2 \le f_U/f_L \le 9$.

DETERMINATION OF TRANSMISSION LINE IMPEDANCES AND ISOLATION RESISTORS

The normalized isolation resistor, $\tilde{R}_n^+ = \frac{R_n}{Z_0}$ values and normalized characteristic impedances, $\tilde{Z}_n^{\pm} = \frac{Z_n}{Z_{03}}$ of cascaded transmission lines,[2,3] are expressed in empirical polynomial formulations obtained using regression methods. The polynomial formulations for second-, third- and fourth-order cascaded power dividers are presented in ***Table 1***.

BROADBAND S-PARAMETERS CALCULATION

The multi-section Wilkinson power divider/combiner can be modeled by separating the power splitter into two half-symmetry circuits in which the vertical resistors are terminated by open and short circuits, respectively, as shown in ***Figure 2***.[4]

Based on the even-mode circuit (see Figure 2a), multiplication of the ABCD matrices is performed sequentially from section N down to

section 1, ensuring that the final matrix accurately reflects the cascading behavior of the network as in ***Equation 1***:

$$\begin{bmatrix} A_e & B_e \\ C_e & D_e \end{bmatrix} = \begin{bmatrix} A_{e,N} & B_{e,N} \\ C_{e,N} & D_{e,N} \end{bmatrix} \cdot \begin{bmatrix} A_{e,\wedge N-1h} & B_{e,\wedge N-1h} \\ C_{e,\wedge N-1h} & D_{e,\wedge N-1h} \end{bmatrix} \cdots\cdots \begin{bmatrix} A_{e,1} & B_{e,1} \\ C_{e,1} & D_{e,1} \end{bmatrix}$$
$$= \begin{bmatrix} \cos\wedge\theta_N h & jZ_{e,N}\sin\wedge\theta_N h \\ j\dfrac{\sin\wedge\theta_N h}{Z_{e,N}} & \cos\wedge\theta_N h \end{bmatrix} \cdot \begin{bmatrix} \cos\wedge\theta_{N-1} h & jZ_{e,N-1}\sin\wedge\theta_{N-1} h \\ j\dfrac{\sin\wedge\theta_{N-1} h}{Z_{e,N-1}} & \cos\wedge\theta_{N-1} h \end{bmatrix} \cdots\cdots \begin{bmatrix} \cos\wedge\theta_1 h & jZ_{e,1}\sin\wedge\theta_1 h \\ j\dfrac{\sin\wedge\theta_1 h}{Z_{e,1}} & \cos\wedge\theta_1 h \end{bmatrix} \quad (1)$$

where the electrical length (θ_n) of the n^{th} section microstrip line is expressed in ***Equation 2***:

$$0_n = \frac{2\pi f\sqrt{\varepsilon_{eff,n}}}{c} l_n, \text{ for } n = 1, 2, \ldots, N \quad (2)$$

where $\varepsilon_{eff,n}$ and l_n (quarter-wavelength, $\lambda/4$) represent the effective relative permittivity and the physical length of the n^{th} section microstrip line, respectively. These parameters can be determined using ***Equations 3***[5,6] and ***4***. The speed of light (c) = 299,792,458 m/sec and f_c is the center operating frequency.

$$l_n = \frac{c}{4f_c\sqrt{\varepsilon_{eff\_n}}} \quad (3)$$

$$\varepsilon_{eff,n} = \begin{cases} \left(\dfrac{\varepsilon_r + 1}{2} + \dfrac{\varepsilon_r - 1}{2}\left[\dfrac{1}{\sqrt{1 + 12\dfrac{h}{w_n}}} + 0.04\left(1 - \dfrac{w_n}{h}k^2\right)\right] \text{ for } \dfrac{w_n}{h} \# 1\right. \\ \left.\dfrac{\varepsilon_r + 1}{2} + \dfrac{\varepsilon_r - 1}{2}\left(\dfrac{1}{\sqrt{1 + 12\dfrac{h}{w_n}}}\right) \text{ for } \dfrac{w_n}{h} > 1\right. \end{cases} \quad (4)$$

The even-mode impedances, $Z_{e,n} = \grave{Z}_{e,n} \times Z_0$ in Equation (1) are derived using polynomial formulas provided in Table 1. The corresponding cascaded odd-mode ABCD matrices in Figure 2b can be written as shown in ***Equation 5***:

$$\begin{bmatrix} A_o & B_o \\ C_o & D_o \end{bmatrix} = \begin{bmatrix} A_{o,N} & B_{o,N} \\ C_{o,N} & D_{o,N} \end{bmatrix} \begin{bmatrix} A_{o,\wedge N-1h} & B_{o,\wedge N-1h} \\ C_{o,\wedge N-1h} & D_{o,\wedge N-1h} \end{bmatrix} \cdots\cdots \begin{bmatrix} A_{o,1} & B_{o,1} \\ C_{o,1} & D_{o,1} \end{bmatrix}$$
$$= \left\{ \begin{bmatrix} \cos\theta_N & jZ_{o,N}\sin\theta_N \\ \left(\dfrac{\cos\theta_N}{\left(\frac{R_N}{2}\right)} + j\dfrac{\sin\theta_N}{Z_{o,N}}\right) & \left(\cos\theta_N + \dfrac{jZ_{o,N}\sin\theta_N}{\left(\frac{R_N}{2}\right)}\right) \end{bmatrix} \begin{bmatrix} \cos\theta_{N-1} & jZ_{o,N-1}\sin\theta_{N-1} \\ \left(\dfrac{\cos\theta_{N-1}}{\left(\frac{R_{N-1}}{2}\right)} + j\dfrac{\sin\theta_{N-1}}{Z_{o,N-1}}\right) & \left(\cos\theta_{N-1} + \dfrac{jZ_{o,N-1}\sin\theta_{N-1}}{\left(\frac{R_{N-1}}{2}\right)}\right) \end{bmatrix} \right\}$$
$$\left\{ \cdots\cdots \begin{bmatrix} \cos\theta_1 & jZ_{o,1}\sin\theta_1 \\ \left(\dfrac{\cos\theta_1}{\left(\frac{R_1}{2}\right)} + j\dfrac{\sin\theta_1}{Z}\right) & \left(\cos\theta_1 + \dfrac{jZ_{o,1}\sin\theta_1}{\left(\frac{R_1}{2}\right)}\right) \end{bmatrix} \right\} \quad (5)$$

Since the two split microstrip transmission lines are significantly far apart, there is no coupling effect between them. As a result, the odd-mode impedance is equal to the even-mode impedance as shown in ***Equation 6***:

$$Z_{o,n} = Z_{e,n}, \text{ for } n = 1, 2, \ldots, N \quad (6)$$

The characteristic impedance (Z_0) is typically equal to 50 Ω. Based on Equations 1 and 5, the even and odd modes of the reflection coefficients (Γ_e and Γ_o) and the even-mode transmission coefficient (T_e) are simplified in ***Equations 7***, ***8*** and ***9***:[7]

$$\Gamma_e = \frac{A_e\wedge 2Z_0 h + B_e - C_e\wedge 2Z_0 h\wedge Z_0 h - D_e Z_0}{A_e\wedge 2Z_0 h + B_e + C_e\wedge 2Z_0 h\wedge Z_0 h + D_e Z_0} \quad (7) \qquad \Gamma_0 = \frac{B_o - D_o Z_o}{B_o + D_o Z_o} \quad (8) \qquad T_e \frac{2\wedge 2Z_0 h}{A_e\wedge 2Z_0 h + B_e + C_e\wedge 2Z_0 h\wedge Z_0 h + D_e Z_0} \quad (9)$$

The explicit analytical expressions for A_e, B_e, C_e, D_e, B_o and D_o for second-, third- and fourth-order cascaded Wilkinson power dividers are provided in ***Table 2***. From Equations 7 and 8, the total reflection coefficients (S_{11}, S_{22} and S_{33}) at Ports 1, 2 and 3 are given by ***Equations 10***, ***11*** and ***12***:

$$S_{11} = \Gamma_e \quad (10)$$

$$S_{22} = \frac{k\Gamma_e + \Gamma_o}{1 + k} \quad (11)$$

$$S_{33} = \frac{\Gamma_e + k\Gamma_o}{1 + k} \quad (12)$$

TABLE 2

ABCD PARAMETER EXPRESSIONS FOR SECOND-, THIRD- AND FOURTH-ORDER WILKINSON POWER DIVIDERS

N		ABCD Parameters
2	Even	$A_e = \cos(\theta_1)\cos(\theta_2) - \frac{Z_{e1}\sin(\theta_1)\sin(\theta_2)}{Z_{e2}}$
		$B_e = j[Z_{e1}\sin(\theta_1)\cos(\theta_2) + Z_{e2}\cos(\theta_1)\sin(\theta_2)]$
		$C_e = j\left[\frac{\sin(\theta_1)\cos(\theta_2)}{Z_{e1}} + \frac{\cos(\theta_1)\sin(\theta_2)}{Z_{e2}}\right]$
		$D_e = \cos(\theta_1)\cos(\theta_2) - \frac{Z_{e2}\sin(\theta_1)\sin(\theta_2)}{Z_{e1}}$
	Odd	$B_o = -\frac{2Z_{o1}Z_{o2}\sin(\theta_1)\sin(\theta_2)}{R_1} + j[Z_{o1}\sin(\theta_1)\cos(\theta_2) + Z_{o2}\cos(\theta_1)\sin(\theta_2)]$
		$D_o = \left\{\begin{array}{l}\cos(\theta_1)\cos(\theta_2) - \frac{Z_{o1}\sin(\theta_1)\sin(\theta_2)}{Z_{o2}} - \frac{4Z_{o1}Z_{o2}\sin(\theta_1)\sin(\theta_2)}{R_1R_2} \\ +2j\left[\frac{Z_{o1}\sin(\theta_1)\cos(\theta_2)}{R_2} + \frac{Z_{o2}\cos(\theta_1)\sin(\theta_2)}{R_2} + \frac{Z_{o1}\sin(\theta_1)\cos(\theta_2)}{R_1}\right]\end{array}\right\}$
3	Even	$A_e = \left\{\begin{array}{l}\cos(\theta_1)\left[\cos(\theta_2)\cos(\theta_3) - \frac{Z_{e3}\sin(\theta_2)\sin(\theta_3)}{Z_{e2}}\right] \\ -\frac{\sin(\theta_1)}{Z_{e1}}[Z_{e2}\sin(\theta_2)\cos(\theta_3) + Z_{e3}\cos(\theta_2)\sin(\theta_3)]\end{array}\right\}$
		$B_e = \left\{\begin{array}{l}j\cos(\theta_1)[Z_{e2}\sin(\theta_2)\cos(\theta_3) + Z_{e3}\cos(\theta_2)\sin(\theta_3)] \\ +jZ_{e1}\sin(\theta_1)\left[\cos(\theta_2)\cos(\theta_3) - \frac{Z_{e3}\sin(\theta_2)\sin(\theta_3)}{Z_{e2}}\right]\end{array}\right\}$
		$C_e = \left\{\begin{array}{l}j\cos(\theta_1)\left[\frac{\sin(\theta_2)\cos(\theta_3)}{Z_{e2}} + \frac{\cos(\theta_2)\sin(\theta_3)}{Z_{e3}}\right] \\ +j\frac{\sin(\theta_1)}{Z_{e1}}\left[\cos(\theta_2)\cos(\theta_3) - \frac{Z_{e2}\sin(\theta_2)\sin(\theta_3)}{Z_{e3}}\right]\end{array}\right\}$
		$D_e = \left\{\begin{array}{l}\cos(\theta_1)\left[\cos(\theta_2)\cos(\theta_3) - \frac{Z_{e2}\sin(\theta_2)\sin(\theta_3)}{Z_{e3}}\right] \\ -Z_{e1}\sin(\theta_1)\left[\frac{\sin(\theta_2)\cos(\theta_3)}{Z_{e2}} + \frac{\cos(\theta_2)\sin(\theta_3)}{Z_{e3}}\right]\end{array}\right\}$
	Odd	$B_o = b_1\left[\cos(\theta_1) + j\frac{2Z_{o1}\sin(\theta_1)}{R_1}\right] + b_2[jZ_{o1}\sin(\theta_1)]$

where

$$b_1 = Z_{o3}\sin(\theta_3)\left[j\cos(\theta_2) - \frac{2Z_{o2}\sin(\theta_2)}{R_2}\right] + jZ_{o2}\cos(\theta_3)\sin(\theta_2)$$

$$b_2 = \cos(\theta_2)\cos(\theta_3) + Z_{o3}\sin(\theta_3)\left[j\frac{2\cos(\theta_2)}{R_2} - \frac{\sin(\theta_2)}{Z_{o2}}\right]$$

and

$$D_o = d_1\left[\cos(\theta_1) + j\frac{2Z_{o1}\sin(\theta_1)}{R_1}\right] + d_2[jZ_{o1}\sin(\theta_1)]$$

TABLE 2 CONTINUED

ABCD PARAMETER EXPRESSIONS FOR SECOND-, THIRD- AND FOURTH-ORDER WILKINSON POWER DIVIDERS

where

$$d_1 = \left\{\begin{array}{l}\left[\cos(\theta_2) + j\frac{2Z_{o2}\sin(\theta_2)}{R_2}\right]\left[\cos(\theta_3) + j\frac{2Z_{o3}\sin(\theta_3)}{R_3}\right] \\ +Z_{o2}\sin(\theta_2)\left[j\frac{2\cos(\theta_3)}{R_3} - \frac{\sin(\theta_3)}{Z_{o3}}\right]\end{array}\right\}$$

$$d_2 = \left\{\begin{array}{l}\left[j\frac{\sin(\theta_2)}{Z_{o2}} + \frac{2\cos(\theta_2)}{R_2}\right]\left[\cos(\theta_3) + j\frac{2Z_{o3}\sin(\theta_3)}{R_3}\right] \\ +\cos(\theta_2)\left[j\frac{\sin(\theta_3)}{Z_{o3}} + \frac{2\cos(\theta_3)}{R_3}\right]\end{array}\right\}$$

4 Even

$$A_e = \cos(\theta_1)\left\{\begin{array}{l}\cos(\theta_2)\left[\cos(\theta_3)\cos(\theta_4) - \frac{Z_{e4}\sin(\theta_3)\sin(\theta_4)}{Z_{e3}}\right] \\ -\sin(\theta_2)\left[\frac{Z_{e3}\cos(\theta_4)\sin(\theta_3) + Z_{e4}\cos(\theta_3)\sin(\theta_4)}{Z_{e2}}\right]\end{array}\right\}$$

$$-\frac{\sin(\theta_1)}{Z_{e1}}\left\{\begin{array}{l}\cos(\theta_2)\left[Z_{e3}\cos(\theta_4)\sin(\theta_3) + Z_{e4}\cos(\theta_3)\sin(\theta_4)\right] \\ +Z_{e2}\sin(\theta_2)\left[\cos(\theta_3)\cos(\theta_4) - \frac{Z_{e4}\sin(\theta_3)\sin(\theta_4)}{Z_{e3}}\right]\end{array}\right\}$$

$$B_e = j\cos(\theta_1)\left\{\begin{array}{l}\cos(\theta_2)\left[Z_{e3}\cos(\theta_4)\sin(\theta_3) + Z_{e4}\cos(\theta_3)\sin(\theta_4)\right] \\ +Z_{e2}\sin(\theta_2)\left[\cos(\theta_3)\cos(\theta_4) - \frac{Z_{e4}\sin(\theta_3)\sin(\theta_4)}{Z_{e3}}\right]\end{array}\right\}$$

$$+jZ_{e1}\sin(\theta_1)\left\{\begin{array}{l}\cos(\theta_2)\left[\cos(\theta_3)\cos(\theta_4) - \frac{Z_{e4}\sin(\theta_3)\sin(\theta_4)}{Z_{e3}}\right] \\ -\frac{\sin(\theta_2)}{Z_{e2}}\left[Z_{e3}\cos(\theta_4)\sin(\theta_3) + Z_{e4}\cos(\theta_3)\sin(\theta_4)\right]\end{array}\right\}$$

$$+j\frac{\sin(\theta_1)}{Z_{e1}}\left\{\begin{array}{l}\cos(\theta_2)\left[\cos(\theta_3)\cos(\theta_4) - \frac{Z_{e3}\sin(\theta_3)\sin(\theta_4)}{Z_{e4}}\right] \\ -Z_{e2}\sin(\theta_2)\left[\frac{\cos(\theta_4)\sin(\theta_3)}{Z_{e3}} + \frac{\cos(\theta_3)\sin(\theta_4)}{Z_{e4}}\right]\end{array}\right\}$$

$$D_e = \cos(\theta_1)\left\{\begin{array}{l}\cos(\theta_2)\left[\cos(\theta_3)\cos(\theta_4) - \frac{Z_{e3}\sin(\theta_3)\sin(\theta_4)}{Z_{e4}}\right] \\ -Z_{e2}\sin(\theta_2)\left[\frac{\cos(\theta_4)\sin(\theta_3)}{Z_{e3}} + \frac{\cos(\theta_3)\sin(\theta_4)}{Z_{e4}}\right]\end{array}\right\}$$

$$-Z_{e1}\sin(\theta_1)\left\{\begin{array}{l}\cos(\theta_2)\left[\frac{\cos(\theta_4)\sin(\theta_3)}{Z_{e3}} + \frac{\cos(\theta_3)\sin(\theta_4)}{Z_{e4}}\right] \\ +\frac{\sin(\theta_2)}{Z_{e2}}\left[\cos(\theta_3)\cos(\theta_4) - \frac{Z_{e3}\sin(\theta_3)\sin(\theta_4)}{Z_{e4}}\right]\end{array}\right\}$$

TABLE 2 CONTINUED

ABCD PARAMETER EXPRESSIONS FOR SECOND-, THIRD- AND FOURTH-ORDER WILKINSON POWER DIVIDERS

Odd

$$B_o = b_1\left[\cos(\theta_1) + j\frac{2Z_{o1}\sin(\theta_1)}{R_1}\right] + b_2[jZ_{o1}\sin(\theta_1)]$$

where

$$b_1 = \left\{Z_{o4}\sin(\theta_4)\left[j\cos(\theta_3) - \frac{2Z_{o3}\sin(\theta_3)}{R_3}\right] + jZ_{o3}\cos(\theta_4)\sin(\theta_3)\right\} \times \left[\cos(\theta_2) + j\frac{2Z_{o2}\sin(\theta_2)}{R_2}\right] + \left\{\left[\cos(\theta_3)\cos(\theta_4) + jZ_{o4}\sin(\theta_4)\right] \times \left[j\frac{\sin(\theta_3)}{Z_{o3}} + \frac{2\cos(\theta_3)}{R_3}\right] \times jZ_{o2}\sin(\theta_2)\right\}$$

and

$$b_2 = \cos(\theta_2)\left\{\cos(\theta_3)\cos(\theta_4) + Z_{o4}\sin(\theta_4)\left[j\frac{2\cos(\theta_3)}{R_3} - \frac{\sin(\theta_3)}{Z_{o3}}\right]\right\} + \left[j\frac{\sin(\theta_2)}{Z_{o2}} + \frac{2\cos(\theta_2)}{R_2}\right]\left\{\begin{matrix}Z_{o4}\sin(\theta_4)\left[j\cos(\theta_3) - \frac{2Z_{o3}\sin(\theta_3)}{R_3}\right] + \\ jZ_{o3}\cos(\theta_4)\sin(\theta_3)\end{matrix}\right\}$$

$$D_o = d_1\left[\cos(\theta_1) + j\frac{2Z_{o1}\sin(\theta_1)}{R_1}\right] + d_2[jZ_{o1}\sin(\theta_1)]$$

Where

$$\begin{aligned} d_1 = {} & \left[\cos(\theta_2) + j\frac{2Z_{o2}\sin(\theta_2)}{R_2}\right]\left\{\begin{matrix}\left[\cos(\theta_3) + j\frac{2Z_{o3}\sin(\theta_3)}{R_3}\right]\left[\cos(\theta_4) + j\frac{2Z_{o4}\sin(\theta_4)}{R_4}\right] \\ +Z_{o3}\sin(\theta_3)\left[j\frac{2\cos(\theta_4)}{R_4} - \frac{\sin(\theta_4)}{Z_{o4}}\right]\end{matrix}\right\} \\ & + jZ_{o2}\sin(\theta_2)\left\{\begin{matrix}\left[j\frac{\sin(\theta_3)}{Z_{o3}} + \frac{2\cos(\theta_3)}{R_3}\right]\left[\cos(\theta_4) + j\frac{2Z_{o4}\sin(\theta_4)}{R_4}\right] \\ +\cos(\theta_3)\left[j\frac{\sin(\theta_4)}{Z_{o4}} + \frac{2\cos(\theta_4)}{R_4}\right]\end{matrix}\right\} \end{aligned}$$

$$\begin{aligned} d_2 = {} & \cos(\theta_2)\left\{\begin{matrix}\left[j\frac{\sin(\theta_3)}{Z_{o3}} + \frac{2\cos(\theta_3)}{R_3}\right]\left[\cos(\theta_4) + j\frac{2Z_{o4}\sin(\theta_4)}{R_4}\right] \\ +\cos(\theta_3)\left[j\frac{\sin(\theta_4)}{Z_{o4}} + \frac{2\cos(\theta_4)}{R_4}\right]\end{matrix}\right\} \\ & + \left[j\frac{\sin(\theta_2)}{Z_{o2}} + \frac{2\cos(\theta_2)}{R_2}\right]\left\{\begin{matrix}\left[\cos(\theta_3) + j\frac{2Z_{o3}\sin(\theta_3)}{R_3}\right]\left[\cos(\theta_4) + j\frac{2Z_{o4}\sin(\theta_4)}{R_4}\right] \\ +Z_{o3}\sin(\theta_3)\left[j\frac{2\cos(\theta_4)}{R_4} - \frac{\sin(\theta_4)}{Z_{o4}}\right]\end{matrix}\right\} \end{aligned}$$

Where k represents the coupling factor between Port 2 and Port 3.

The total transmission coefficients (S_{12} and S_{13}) are calculated using Equation 9 as shown in ***Equations 13*** and ***14***:

$$S_{12} = \frac{kT_e}{1+k} \quad (13)$$

$$S_{13} = \frac{T_e}{1+k} \quad (14)$$

The isolation coefficients (S_{32} and S_{23}) between the output ports can be determined using ***Equations 15*** and ***16***:

$$S_{32} = \frac{k\hat{}\Gamma_e - \Gamma_o h}{1+k} \quad (15)$$

$$S_{23} = \frac{\Gamma_e - \Gamma_o}{1+k} \quad (16)$$

CIRCUIT DIMENSIONS PREDICTION

The width w_n and length l_n (quarter-wavelength, $\lambda/4$) of the n^{th} section microstrip transmission line in the Wilkinson power divider can be determined using Equation 3[6,7] and ***Equation 17***:

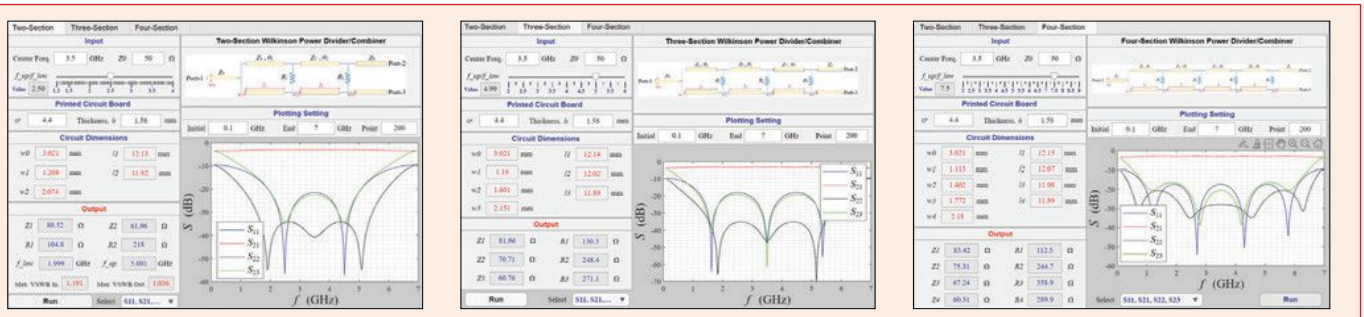

Fig. 3 MATLAB GUI for second- (a), third- (b) and fourth- (c) order Wilkinson power divider CAD.

$$w_n = \begin{cases} \dfrac{8h\exp(A)}{\exp(2A)-2} & \text{for } \frac{w_n}{h} < 2 \\ \dfrac{2h}{\pi}\{B-1-\ln(2B-1)+\dfrac{\varepsilon_r-1}{2\varepsilon_r}\left[\ln(B-1)+.039-\dfrac{0.61}{\varepsilon_r}\right]\} & \text{for } \frac{w_n}{h} > 2 \end{cases} \quad (17)$$

Where A and B are given by ***Equations 18*** and ***19***:

$$A = \frac{Z_n}{60}\sqrt{\frac{\varepsilon_r+1}{2}}+\frac{\varepsilon_r-1}{\varepsilon_r+1}\{0.23+\frac{0.11}{\varepsilon_r}\} \quad (18)$$

$$B = \frac{377\pi}{2Z_n\sqrt{\varepsilon_r}} \quad (19)$$

Here, Z_n (= $Z_{e,n}$) represents the characteristic impedance of the n^{th} section microstrip line, and the subscript n = 1, 2, …, N. The parameters ε_r and h denote the dielectric constant and thickness of the printed-circuit board substrate, respectively. Once the values of w_n are obtained from Equation 17, the corresponding length, l_n of the n^{th} section wavelength microstrip line can be determined using Equation 3. The effective relative permittivity, $\varepsilon_{eff,n}$ of the n^{th} section microstrip line is given by Equation 4.

GRAPHICAL USER INTERFACE (GUI) FOR CAD

A simple GUI for the CAD tool has been developed using MATLAB's built-in App Designer feature. The GUI consists of three tabs, each dedicated to the calculation of second-, third- and fourth-order Wilkinson power dividers (see ***Figure 3***). Users need to input only a few key parameters, including f_c, Z_0, f_U/f_L, ε_r and h. Once entered and the 'Run' button is clicked, the tool generates the dimensions (w_n and l_n) of each microstrip transmission line section, the impedances (Z_n) of each microstrip section, the appropriate values of isolation resistors (R_n) and a broadband plot of the S-parameters for performance analysis. This intuitive interface simplifies the design process, making it efficient and user-friendly.

VALIDATION

Three power dividers/combiners are used as examples to validate this study, with their reliability and accuracy compared against commercial simulation tools, including Advanced Design Systems (ADS) and the Computer Simulation Technology (CST) 2D schematic tool. The specifications of these power dividers/combiners (f_U/f_L) are listed in ***Table 3*** along with transmission line impedances (Z_n) and isolation resistors (R_n) calculated using the design formulas provided in Table 1.

Once Z_n is determined, it is substituted into Equations 3 and 17 to compute l_n and w_n of the microstrip transmission lines for the power dividers on an FR-4 substrate with ε_r = 4.4 and h = 1.58 mm designed for a center frequency of 3.5 GHz (see ***Table 4***).

In this work, the S-parameters of the designed power dividers/combiners are derived using Equations 10 through 16 and the ABCD parameters listed in Table 2. Meanwhile, S-parameters obtained from commercial simulators are based on the isolation resistors (R_n) and circuit dimensions provided in Tables 3 and 4.

For an equal split Wilkinson power divider/combiner (k = 1), the relations $S_{12}=S_{13}$, $S_{23}=S_{32}$ and $S_{22}=S_{33}$ hold. Therefore, the comparison between S-parameter results from this work and the commercial simulators focuses on S_{11}, S_{22}, S_{12} and S_{23} (see ***Figures 4*** through ***6***). The trends of the $|S_{11}|$ and $|S_{12}|$ graphs show good agreement between the analytical approach in this study and the results from commercial simulations.

TABLE 3

PREDICTED IMPEDANCES AND ISOLATION RESISTORS BASED ON THE GIVEN RATIO F_U/F_L

N	f_U/f_L	Isolation Resistors (Ω)				Transmission Line Impedance (Ω)			
		R_1	R_2	R_3	R_4	Z_1	Z_2	Z_3	Z_4
2	2.5	104.8	218	-	-	80.52	61.96	-	-
3	5.0	130.4	248.5	271.0	-	81.94	70.71	60.77	-
4	7.5	112.5	244.5	358.7	290.1	83.43	75.31	67.24	60.31

TABLE 4

CIRCUIT DIMENSIONS OF THE WILKINSON POWER DIVIDER/COMBINER

N	Width, w (mm)					Length, l (mm)			
	w_0	w_1	w_2	w_3	w_4	l_1	l_2	l_3	l_4
2	3.021	1.208	2.074	-	-	12.13	11.92	-	-
3	3.021	1.160	1.601	2.15	-	12.14	12.02	11.89	-
4	3.021	1.113	1.402	1.772	2.181	12.15	12.07	11.98	11.89

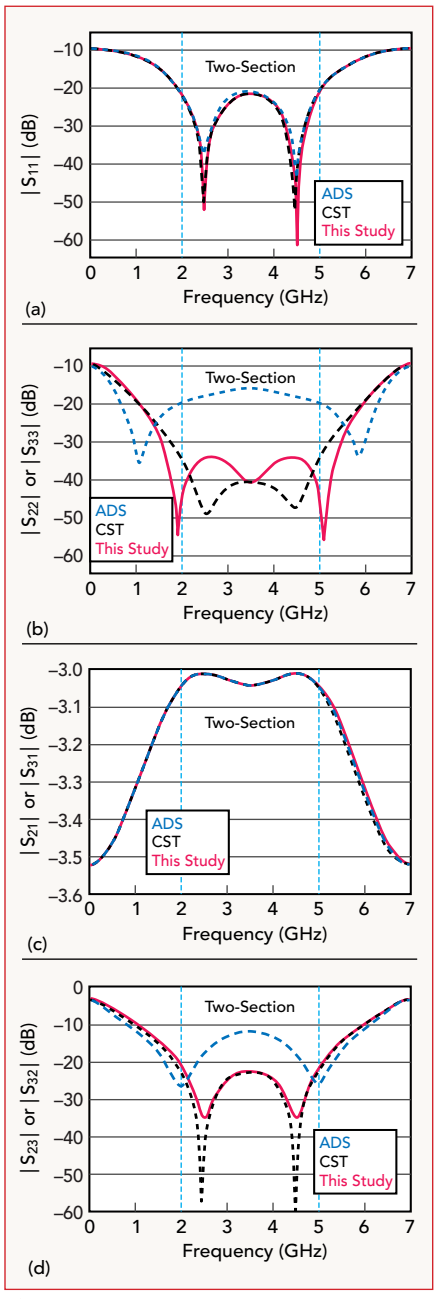

Fig. 4 Two-section Wilkinson power divider: $|S_{11}|$ (a), $|S_{22}|$ or $|S_{33}|$ (b), $|S_{21}|$ or $|S_{31}|$ (c) and $|S_{23}|$ or $|S_{32}|$ (d).

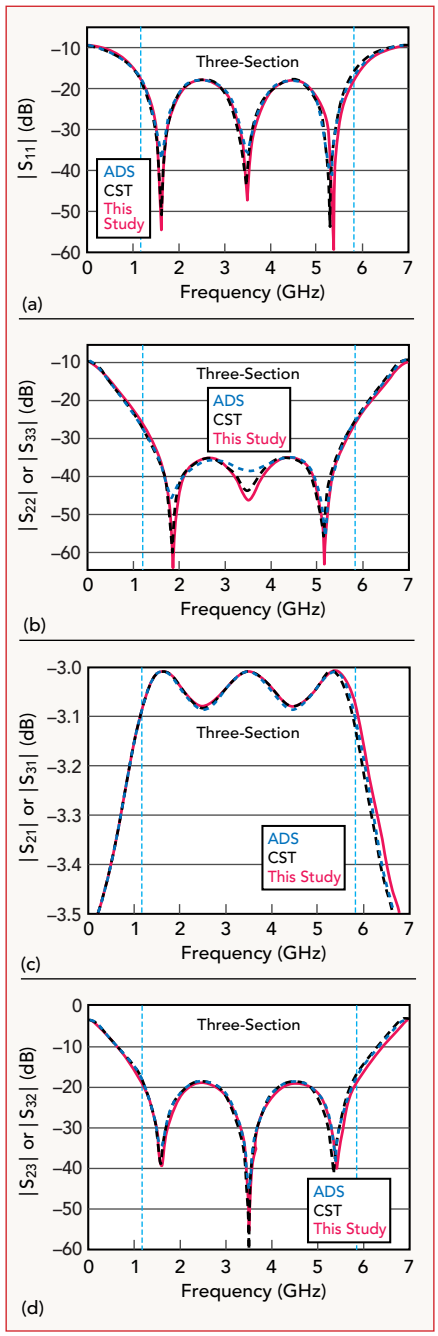

Fig. 5 Three-section Wilkinson power divider: $|S_{11}|$ (a), $|S_{22}|$ or $|S_{33}|$ (b), $|S_{21}|$ or $|S_{31}|$ (c) and $|S_{23}|$ or $|S_{32}|$ (d).

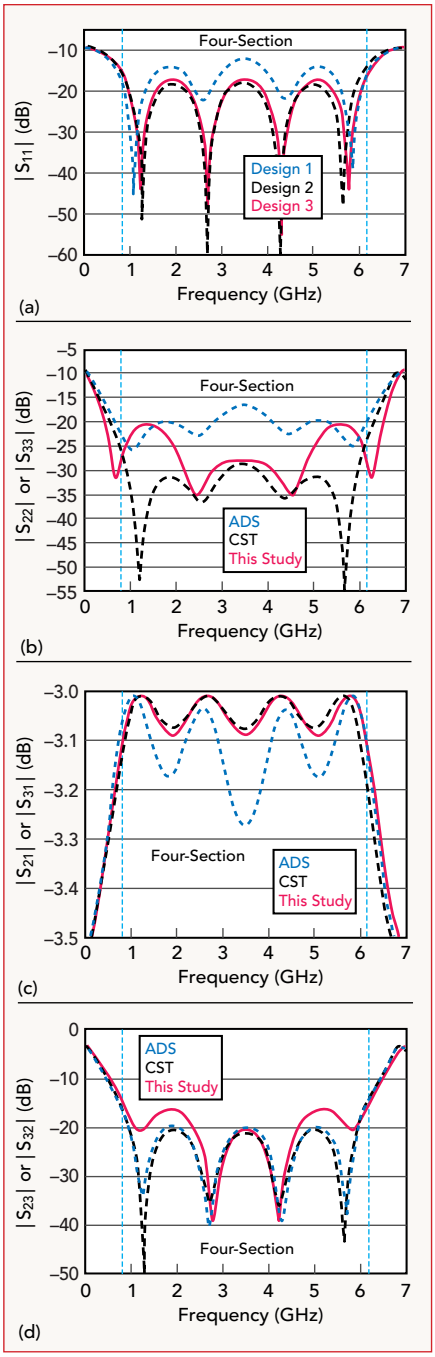

Fig. 6 Four-section Wilkinson power divider: $|S_{11}|$ (a), $|S_{22}|$ or $|S_{33}|$ (b), $|S_{21}|$ or $|S_{31}|$ (c) and $|S_{23}|$ or $|S_{32}|$ (d).

A slight deviation is observed, however, in the $|S_{22}|$ and $|S_{23}|$ graphs. This discrepancy may be attributed to variations in the installation position and split length of the isolation resistors; in this work, the isolation resistor position and split length are assumed to be independent.

CONCLUSION

A simple CAD tool for designing cascaded Wilkinson power dividers/combiners has been developed using an analytical approach. This enables the accurate plotting of broadband S-parameter performance, a feature rarely found in basic power divider CAD tools. The calculated S-parameters show close agreement with results from well-known commercial ADS and CST simulators. ■

References

1. E. J. Wilkinson, "An N-Way Hybrid Power Divider," *IRE Transactions on Microwave Theory and Techniques*, Vol. 8, No. 1, January 1960, pp. 116–118.
2. S. B. Cohn, "A Class of Broadband Three-Port TEM-Mode Hybrids," *IEEE Transactions on Microwave Theory and Techniques*, Vol. 16, No. 2, February 1968, pp. 110–116.
3. H. Howe, *Stripline Circuit Design*, Artech House, Norwood, Mass., 1974, pp. 94–110.
4. Y. Wu, Y. Liu and Q. Xue, "An Analytical Approach for a Novel Coupled-Line Dual-Band Wilkinson Power Divider," *IEEE Transactions on Microwave Theory and Techniques*, Vol. 59, No. 2, October 2011, pp. 286–294.
5. E. O. Hammerstad, "Equations for Microstrip Circuit Design," *European Microwave Conference Proceedings*, September 1975, pp. 268–272.
6. D. M. Pozar, *Microwave Engineering*, Fourth Edition, Wiley, 2011.
7. R. B. Ekinge, "A New Method of Synthesizing Matched Broad-Band TEM-Mode Three-Ports," *IEEE Transactions on Microwave Theory and Techniques*, Vol. 19, No. 1, January 1971, pp. 81–88.